Max-Planck-Institut für Meteorologie
Max Planck Institute for Meteorology

DMS cycle in the ocean-atmosphere system and its response to anthropogenic perturbations

Silvia Kloster

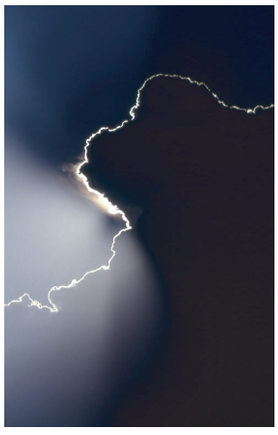
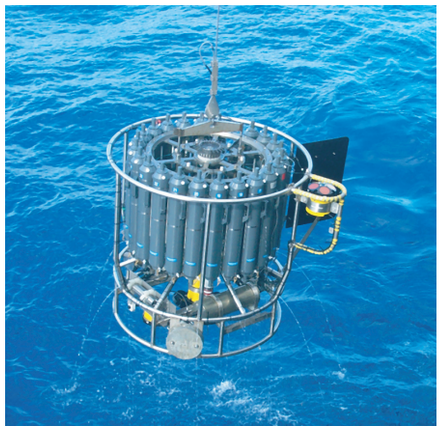


Berichte zur Erdsystemforschung 19/2006

Reports on Earth System Science

Hinweis

Die Berichte zur Erdsytemforschung werden vom Max-Planck-Institut für Meteorologie in Hamburg in unregelmäßiger Abfolge herausgegeben.

Sie enthalten wissenschaftliche und technische Beiträge, inklusive Dissertationen.

Die Beiträge geben nicht notwendigerweise die Auffassung des Instituts wieder.

Die "Berichte zur Erdsystemforschung" führen die vorherigen Reihen "Reports" und "Examensarbeiten" weiter.

Notice

The Reports on Earth System Science are published by the Max Planck Institute for Meteorology in Hamburg. They appear in irregular intervals.

They contain scientific and technical contributions, including Ph. D. theses.

The Reports do not necessarily reflect the opinion of the Institute.

The "Reports on Earth System Science" continue the former "Reports" and "Examensarbeiten" of the Max Planck Institute.

Anschrift / Address

Max-Planck-Institut für Meteorologie
Bundesstrasse 53
20146 Hamburg
Deutschland

Tel.: +49-(0)40-4 11 73-0
Fax: +49-(0)40-4 11 73-298
Web: www.mpimet.mpg.de

Layout:

Bettina Diallo, PR & Grafik

Titelfotos:
vorne:
Christian Klepp - Jochem Marotzke - Christian Klepp
hinten:
Clotilde Dubois - Christian Klepp - Katsumasa Tanaka

Berichte zur Erdsytemforschung 19/2006

Der DMS-Zyklus im Ozean-Atmosphären-System und dessen Resonanz auf anthropogene Störungen

DMS cycle in the ocean-atmosphere system and its response to anthropogenic perturbations

Dissertation zur Erlangung des Doktorgrades der Naturwissenschaften
im Fachbereich Geowissenschaften der Universität Hamburg
vorgelegt von

Silvia Kloster
aus Wilhelmshaven

Hamburg 2006

Reports on Earth System Science 19/2006

ISSN 1614-1199

Silvia Kloster
Max-Planck-Institut für Meteorologie
Bundesstrasse 53
20146 Hamburg
Germany

Als Dissertation angenommen
vom Fachbereich Geowissenschaften der Universität Hamburg

auf Grund der Gutachten von
Prof. Dr. Hartmut Graßl
und
Dr. Johann Feichter

Hamburg, den 6. Februar 2006
Professor Dr. Helmut Schleicher
Dekan des Fachbereiches Geowissenschaften

ISSN 1614-1199

DMS cycle in the ocean-atmosphere system and its response to anthropogenic perturbations

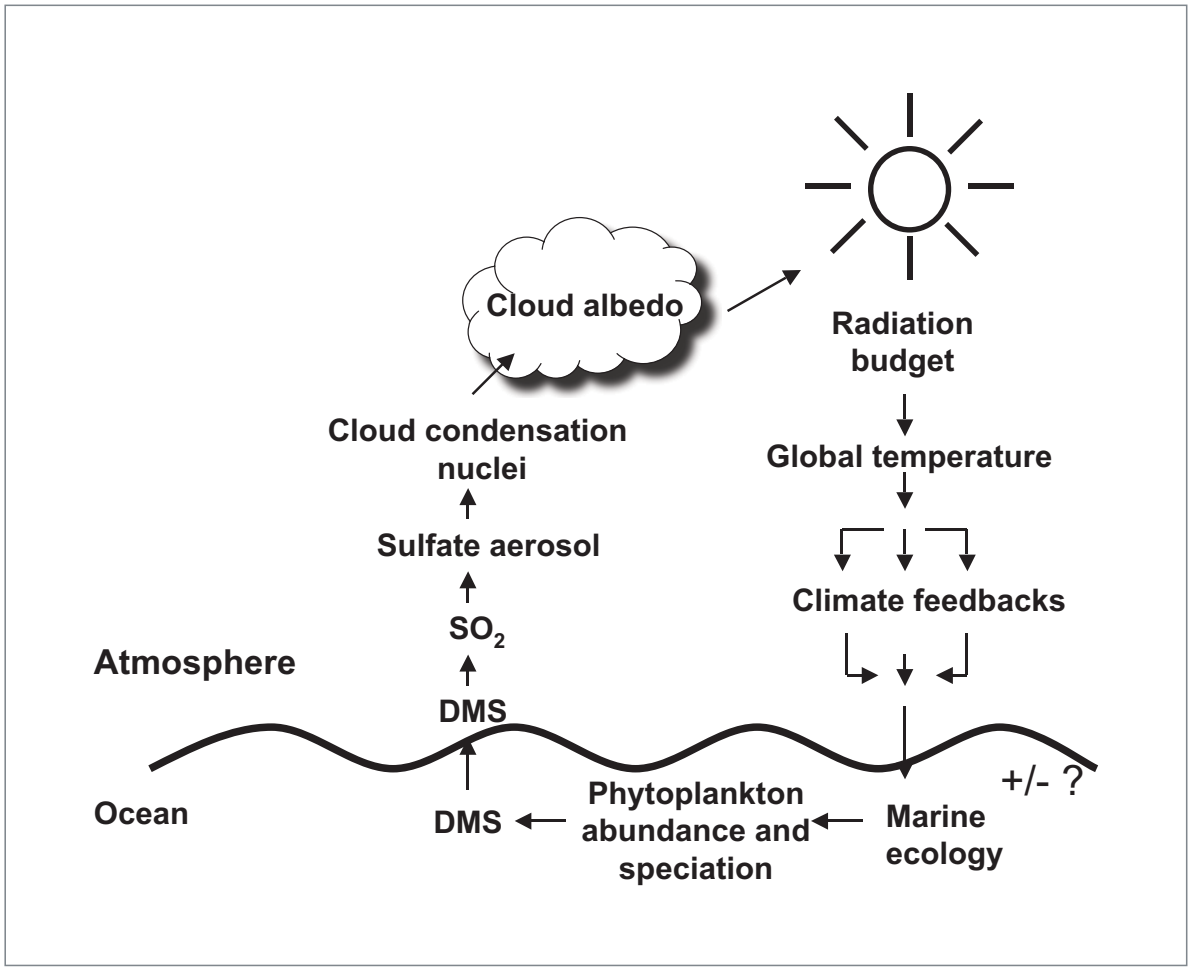

Silvia Kloster

Hamburg 2006

Contents

Abstract

Dimethylsulfide (DMS) is the main biogenic sulfur compound in the atmosphere. DMS is mainly produced by the marine biosphere and plays an important role in the atmospheric sulfur cycle. It has been proposed that DMS is linked to the global climate through a negative biogeochemical feedback cycle stabilizing the Earth against global warming. This so-called CLAW hypothesis initiated extensive research and improved the understanding of many aspects of the biogeochemical sulfur cycle. However, the overall magnitude and even the sign of this feedback cycle are still open questions in present-day research.
The objectives of this work are to study the DMS cycle in the ocean and atmosphere and to investigate its response to anthropogenic perturbations. The novelty of this study is the coupling of the relevant components. A global coupled ocean-atmosphere circulation model was established with a fully coupled prognostic treatment of DMS in the ocean, its flux into the atmosphere, and the resulting sulfur concentrations in the atmosphere. The DMS cycle in the ocean is linked to plankton dynamics simulated in the marine biogeochemistry model HAMOCC5, which is embedded in an ocean general circulation model (MPI-OM). The atmospheric model ECHAM5 is extended by the microphysical aerosol model HAM, treating the sulfur chemistry in the atmosphere and the evolution of the microphysically internally- and externally mixed aerosol population.
In order to evaluate the established modeling system, a climatological mean simulation was performed and compared to available measurements. Thereby, aerosol and aerosol-precursor emissions were set to conditions representative for the year 2000. The simulated global annual mean DMS sea surface concentration is 1.8 nmol l^{-1}. The DMS emission amounts to 28 Tg(S) yr^{-1}, resulting in a DMS burden of the atmosphere of 0.077 Tg(S), and a DMS lifetime of 1.0 days. DMS contributes 25% to the global annually averaged SO_2 column burden and 27% to the SO_4^{2-} column burden. The global distribution of DMS sea surface concentrations compares reasonably well with measurements. In the marine biological active season SO_4^{2-} surface concentrations are overestimated in regions were DMS is the main SO_4^{2-} precursor. As the DMS sea surface concentrations are in agreement with the observations, the most likely explanation is a missing chemical reaction mechanism in the atmosphere preventing the formation of SO_4^{2-} from DMS oxidation.
The response of the DMS cycle to global warming was investigated in a transient climate simulation from 1860 to 2100. The results were analyzed in terms of simulated changes between the periods 1861–1890 and 2061–2090. The global annual mean DMS sea surface concentration and DMS flux decrease by 10% in a warmer climate. Thereby, the response to global warming is largely driven by changes in the ocean dynamics, such as an enhanced ocean stratification causing a reduction in marine net primary production and a decrease in the DMS production in the ocean. The DMS burden in the atmosphere is reduced by 3%, owing to a 7% longer lifetime of DMS in the atmosphere in a warmer climate. The simulated decrease in the DMS emission and atmospheric DMS concentrations in a warmer climate is in contrast to the proposed negative feedback in the CLAW hypothesis, in which increasing DMS emissions in a warmer climate constitute a key mechanism.

Zusammenfassung

Dimethylsulfid (DMS) ist die bedeutendste Schwefelspezies aus biogenen Quellen und nimmt eine wichtige Rolle im Atmosphären-Schwefelkreislauf ein. Die Hauptquelle von DMS stellt die marine Biosphäre dar. Es wurde postuliert, dass DMS das Klima beeinflusst und dabei eine regulierende Rolle einnimmt. Diese regulierende Rolle von DMS beruht auf einem negativen Rückkopplungseffekt, welcher die Erde gegen eine globale Erwärmung stabilisieren kann. Diese Hypothese wird oft als CLAW-Hypothese zitiert. Sie initiierte eine Vielzahl wissenschaftlicher Studien, die zu dem heutigen Verständnis vieler Aspekte des biogeochemischen Schwefelkreislaufes beigetragen haben. Trotzdem ist es bis heute nicht gelungen weder die Stärke noch das Vorzeichen dieses Rückkopplungseffektes zu bestimmen.
Die Zielsetzung dieser Arbeit ist es, den DMS-Kreislauf im Ozean und in der Atmosphäre zu simulieren sowie die Wechselwirkung mit einer globalen Klimaerwärmung abzuschätzen. Zu diesem Zweck wurde ein globales Ozean-Atmosphären-Modell entwickelt, welches sowohl die Produktion von DMS im Ozean als auch die resultierende Emission und die daraus resultierenden Schwefelkonzentrationen in der Atmosphäre berechnet. Die DMS-Produktions- und Zerfallsprozesse im Ozean werden mit der im marinen Biogeochemie-Modell HAMOCC5 simulierten Planktondynamik verknüpft. HAMOCC5 ist dabei ein Bestandteil des globalen Ozean-Zirkulationsmodells MPI-OM. Das Atmosphärenmodell ECHAM5 wird in einer um das Aerosolmodell HAM erweiterten Form verwendet, welches die Schwefelchemie der Atmosphäre und die Entwicklung mikrophysikalischer, intern und extern gemischter Aerosolpopulationen umfasst.
Für eine Evaluierung des entwickelten Modellsystems wurde eine Klimasimulation durchgeführt und mit vorhandenen Messungen verglichen. Dabei wurden für das Jahr 2000 repräsentative Aerosol- und Aerosolvorläuferemissionen verwendet. Die simulierte globale DMS-Konzentration im Oberflächenwasser des Ozeans beträgt im Jahresmittel 1,8 nmol l^{-1}. Die DMS Emission beläuft sich auf 28 Tg(S) yr^{-1} und führt zu einer DMS-Gesamtmasse in der Atmosphäre von 0,077 Tg(S) bei einer Verweildauer von 1,0 Tagen. DMS trägt dabei zu 25% zur absoluten SO_2 - Masse und zu 27% zur absoluten SO_4^{2-} - Masse in der Atmosphäre bei. Die simulierte globale Verteilung der DMS-Konzentration im Oberflächenwasser des Ozeans ist in Übereinstimmung mit den Messdaten. Dagegen überschätzt das Modell in Gebieten mit einem hohen Beitrag von DMS an der SO_4^{2-} - Masse die gemessenen SO_4^{2-} Bodenkonzentrationen in der biologisch aktiven Jahreszeit. Da die DMS-Konzentrationen im Oberflächenwasser des Ozeans mit den Messdaten gut übereinstimmen, ist die wahrscheinlichste Erklärung für diese Überschätzung eine nicht berücksichtigte Reaktion in der Atmosphäre, die eine Bildung von SO_4^{2-} durch die DMS-Oxidation verhindert.
Um die Rolle des DMS-Kreislaufes in einem wärmeren Klima zu untersuchen, wurde eine transiente Klimasimulation für die Jahre 1860 bis 2100 durchgeführt. Hauptsächlich wurden die Änderungen zwischen den beiden Perioden 1861–1890 und 2061–2090 betrachtet. Sowohl die globale DMS-Konzentration der Meeresoberfläche als auch die DMS Emission sind in einem global wärmeren Klima um 10% im Jahresmittel verringert. Diese Verringerung wird hauptsächlich von Änderungen in der Ozeandynamik verursacht. So

bewirkt ein wärmeres Klima eine stärkere Stratifizierung des Ozeans, was wiederum den Nährstofftransport in die obersten Ozeanschichten stark vermindert. Weniger Nährstoffe reduzieren die marine biologische Primärproduktion und verringern somit die DMS-Produktion im Ozean. Die DMS-Gesamtmasse in der Atmosphäre wird um 3% vermindert, was auf eine Zunahme der Verweildauer in einem wärmeren Klima um 7% zurückzuführen ist. Eine Abnahme der DMS-Emissionen und der DMS-Gesamtmasse in der Atmosphäre in einem wärmeren Klima steht im Gegensatz zu dem angenommenen negativen Rückkopplungseffekt der CLAW-Hypothese, in der ein wichtiger Mechanismus die Zunahme der DMS-Emission in einem wärmeren Klima darstellt.

Chapter 1

Introduction

The Earth system comprises physical, biological, chemical, and human components. Complex feedback processes within the Earth system are hypothesized to arise a self-regulating system which maintains conditions that allow for the habitability of life on Earth (Lovelock et al., 1972). Feedback processes are highly important for the understanding and prediction of the climate change caused by anthropogenic perturbations. Their treatment is causing the largest uncertainties in the assessments of the climate response to anthropogenic forcing.
A process is called a feedback when its result affects the process-initiating mechanism thereby intensifying (positive feedback) or reducing (negative feedback) the strength of the process. Feedback processes in the Earth's climate system can involve physical climate processes (physical feedback) or biological, geological, or chemical processes (biogeochemical feedback). One possible negative biogeochemical feedback has been proposed by Charlson et al. (1987). This feedback mechanism operates by coupling the marine biosphere, the ocean, and the atmosphere through the marine biogenic sulfur compound dimethylsulfide (DMS, CH_3SCH_3).
This chapter outlines the concept of the DMS associated feedback. It separates between the DMS cycle in the ocean, the oceanic DMS emission, and the DMS cycle in the atmosphere. Connections to other physical and biological processes are addressed and recent results in global modeling approaches of the DMS cycle in the ocean and the DMS cycle in the atmosphere are summarized. Finally, the objectives of this study are defined and an outline of the thesis is given.

1.1 The DMS-cloud albedo feedback

A negative biogeochemical feedback process has been proposed by Charlson et al. (1987). It involves marine phytoplankton, sulfate aerosol formation, and cloud albedo, as illustrated in Figure 1.1. This feedback is often referred to as the CLAW hypothesis after the names of its four authors (Charlson, Lovelock, Andreae and Warren).
DMS is produced by phytoplankton and is the most abundant chemical form in which the ocean releases gaseous sulfur. Current estimates of the global marine DMS emissions range from 16 up to 54 Tg(S) yr^{-1} (Kettle and Andreae, 2000). A minor source of DMS

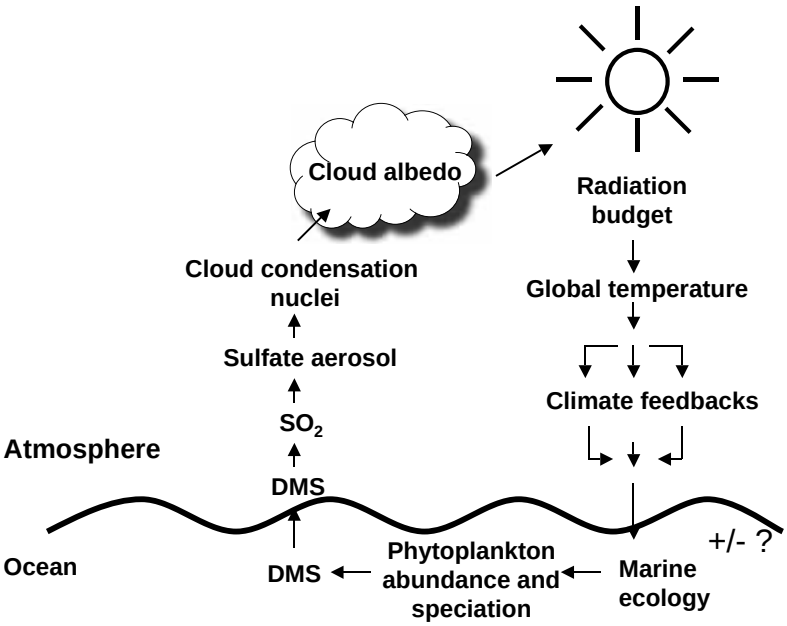

Figure 1.1: CLAW hypothesis: The DMS-cloud albedo feedback after Charlson et al. (1987).

is the terrestrial biosphere, including emissions from soils (0.05 Tg(S) yr^{-1} (Spiro et al., 1992)) and vegetation (0.86 Tg(S) yr^{-1} (Spiro et al., 1992)). Other sulfur emissions are SO_2 emissions from anthropogenic sources (60–100 Tg(S) yr^{-1} for 1985 (Benkovitz et al., 1996)), from volcanoes (6–20 Tg(S) yr^{-1} (Andres and Kasgnoc, 1998)), and from biomass burning (1–6 Tg(S) yr^{-1} for 1990 (Spiro et al., 1992)). In the Southern Hemisphere, where anthropogenic sulfur emissions are low, DMS is the major sulfur source (Gondwe et al., 2003).
In the atmosphere, DMS is oxidized to SO_2. SO_2 itself reacts with OH to produce SO_4^{2-} which can nucleate to sulfate aerosol particles. Sulfate aerosol particles influence the radiation budget of the atmosphere either directly by the scattering of solar radiation (direct aerosol effect, e.g. Ångstroem (1962)) or indirectly by acting as cloud condensation nuclei (CCN), modifying cloud properties and the hydrological cycle. Indirect effects are initiated by an extra supply of cloud condensation nuclei (CCN). Increases in CCN number concentrations lead to a formation of smaller cloud droplets for a constant liquid water path which in turn increases the cloud albedo (cloud albedo effect, (Twomey, 1974, 1977)). Another consequence is that the formation of smaller cloud droplets inhibits precipitation development, thereby increasing the cloud lifetime (cloud lifetime effect, Albrecht (1989)). Both changes in cloud albedo and cloud lifetime result in global temperature and radiative perturbations. These are potentially affecting the productivity of the marine biosphere

and hence the concentration of oceanic DMS and subsequently its emission into the atmosphere which closes the proposed feedback loop. Charlson et al. (1987) proposed that this feedback is negative and can stabilize the Earth against global climate warming by assuming that a warmer climate leads to an increase in the DMS production in the ocean. They assume that an increase in oceanic DMS production increases DMS emissions and raises atmospheric DMS concentrations. This enhances the formation of sulfate aerosol particles and the number concentration of CCNs. A greater abundance of CCNs could then lead to brighter and longer lived clouds. This optical depth enhancement is expected to cool the Earth surface resulting in a negative feedback process.
Charlson et al. (1987) state in their hypothesis that several factors can cause a change in DMS emissions in a warmer climate:

- Reduced sea ice coverage will increase the area available for gas exchange.
- Ecological changes can alter the abundance of phytoplankton species which efficiently produce DMS.
- Changes in the wind fields affect the DMS flux.
- Assuming from observations that the DMS production is highest in tropical regions, increasing sea surface temperatures might enhance DMS production.

However, the oceanic and atmospheric processes involved in this multistep feedback mechanism are more complex. Many key issues in this feedback process are still poorly understood, in particular the processes which regulate the DMS seawater concentration (Andreae and Crutzen, 1997; Liss et al., 1997; Gabric et al., 2001; Vézina, 2004). Traditionally, the DMS cycles in the atmosphere and in the ocean have been assessed independently. As a consequence, it has not been possible to assess the strength of the proposed feedback or even to anticipate if this feedback is negative (stabilizing) or positive (intensifying), since it is not known yet if in a warmer climate DMS emissions would increase or decrease. However, significant progress has been made in the last years to understand many of the mechanisms involved.

1.2 DMS cycle in the ocean

The major processes of the DMS cycle in the ocean are illustrated in Figure 1.2. Enzymatic decomposition of dimethylsulfonium propionate (DMSP) is the primary source of DMS in seawater with DMSP being released from phytoplankton by a variety of mechanisms. The biological function of DMSP and especially of its degradation to DMS is still not clear. It has been suggested that the physiological function of DMSP is related to maintaining intracellular osmotic pressure (Vairavamurthy et al., 1985). Other suggested physiological functions of DMSP in marine algae are that it may act as a cryoprotectant (Kirst et al., 1991; Stefels, 2000) and serves as an antioxidant system (Sunda et al., 2002).

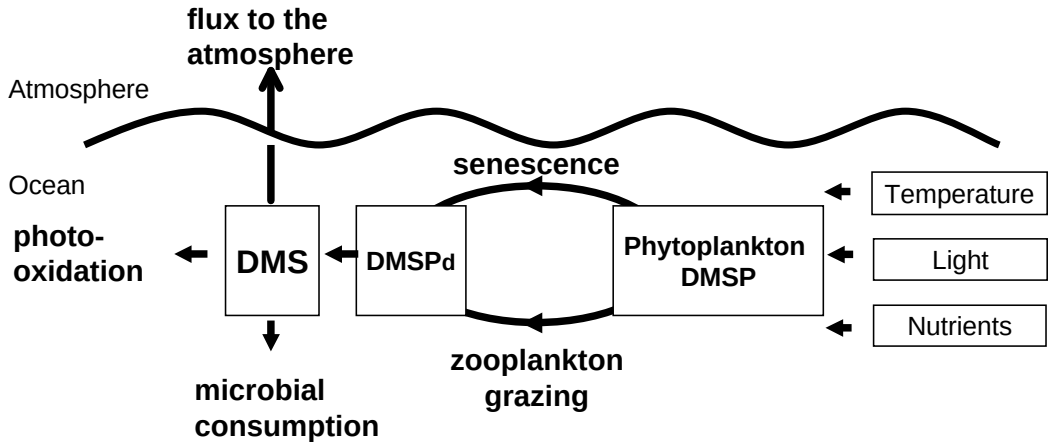

Figure 1.2: Schematic of the DMS cycle in the ocean.

DMSP is widespread among taxa but seems to be particularly abundant in specific groups, including coccolithophorids, like Emiliania huxleyi. Other groups, like the diatoms, are generally poor producers of DMSP (Keller et al., 1989).
Among other factors, DMSP release into the water is assumed to be controlled by phytoplankton senescence (Nguyen et al., 1990; Kwint and Kramer, 1995), viral lysis of phytoplankton cells (Malin et al., 1998), and zooplankton grazing (Dacey and Wakeham, 1986). Dissolved DMSP is degraded to DMS via enzymatic cleavage carried out by algal or bacterial DMSP lyase (Steinke et al., 2002; Yoch et al., 1997). A large fraction of DMSP is consumed by bacteria and does not lead to the production of DMS (Kiene, 1996). Kiene et al. (2000) hypothesized that the sulfur-demand of bacteria determines the proportion of DMSP that is processed through this demethylation pathway, rather than being converted by enzymatic degradation to DMS.
Consumption by bacteria is the major sink for DMS in seawater (Kiene and Bates, 1990; Dacey and Wakeham, 1986). Chemical oxidation of DMS to dimethyl sulfoxide (DMSO) in seawater and ventilation to the atmosphere contribute only a minor part to the total DMS removal in seawater (e.g. Shooter and Brimblecombe, 1989; Kieber et al., 1996; Bates et al., 1994; Gabric et al., 1993). Consequently, there is a potential for a substantially higher DMS sea-air flux under different climatic conditions.
As DMS is produced by phytoplankton, the DMS production is largely controlled by plankton dynamics which in turn are linked to the ocean dynamics. Sunlight and nutrients are the primary factors regulating phytoplankton growth. Light attenuates very rapidly with depth in the ocean, thus phytoplankton growth takes only place in the upper part of the ocean (euphotic zone) where insolation is sufficient for photosynthesis (primary production). The mixed layer depth (MLD) of the ocean determines the supply of nutrients into the euphotic zone, but also the mixing of phytoplankton itself is important for primary production. The shallower MLD in spring in high latitudes, due to the warming of the surface waters, keeps phytoplankton in the euphotic zone and initiates primary

production. Most of the phytoplankton in the euphotic zone is grazed by zooplankton and the nutrients comprising their biomass are remineralized within the upper surface layers of the ocean. However, a part of the primary production is exported out of the euphotic zone (export production), either trough the settling of dead cells and fecal matter (detritus) or through oceanic advection. Sinking detritus remineralizes and brings nutrients into the deep sea. Upwelling of deep water brings nutrients back into the euphotic zone and closes the so-called biological pump of the ocean.
Several attempts were made to correlate DMS sea surface concentrations with other biological quantities such as chlorophyll α concentrations (Kettle et al., 1999). Mainly the fact that DMSP intracellular concentrations vary widely between different phytoplankton species eliminates such simple empirical relationships (Keller et al., 1989). Therefore, DMS sea surface concentrations can be only assessed by marine biological model approaches accounting for the plankton dynamics in the ocean.

1.3 DMS sea air exchange

DMS sea-air fluxes may vary by orders of magnitude in space and time. The sea-air flux can be estimated from

$$F = k_w \ (C_w - C_a * K_H^{-1}) \tag{1.1}$$

which is the product of the air-sea gradient (DMS sea surface concentration, C_w, minus atmospheric DMS concentration, C_a), corrected by the solubility constant, K_H, and a generally empirically determined exchange rate, k_w. DMS exhibits a strong concentration gradient across the air-sea interface, resulting in an ever present DMS flux out of the ocean.
Even when the DMS sea surface concentrations are known, it remains difficult to calculate the DMS flux because of the uncertainties of the exchange rate across the water surface (Wanninkhof, 1992). The exchange rate is usually parameterized as a function of temperature and wind speed based on laboratory and lake tracer experiments (e.g. Wanninkhof, 1992; Wanninkhof and McGillis, 1999; Liss and Merlivat, 1986; Nightingale et al., 2000; McGillis et al., 2000; Zemmelink et al., 2002), although the physical nature of the exchange rate remains poorly understood. A common parameterization of the exchange rate is of the form

$$k_w = a \ U^x Sc^n \tag{1.2}$$

where Sc is the dimensionless Schmidt number (ratio of the kinematic viscosity of water and the molecular diffusivity of the gas) and U the 10m wind speed. The Sc exponent, n, characterizes the surface conditions (smooth water surface or rough water surface). Estimates of the wind speed exponent, x, range from a linear to a cubic behavior in U (Liss and Merlivat (1986) and Wanninkhof and McGillis (1999), respectively). The coefficient, a, varies by a factor of 2 between the two most commonly applied parameterizations, Liss and Merlivat (1986) and Wanninkhof (1992), and by a factor of 3 between parameterizations that are based on direct measurements of the exchange rate (Zemmelink et al., 2002). According to Nightingale et al. (2000), the uncertainties in the global DMS flux associated with uncertainties in the exchange rate are approximately 50%.

1.4 DMS cycle in the atmosphere

It is well-established that OH and NO_3 react with DMS in the atmosphere and that SO_2 and methane sulfonic acid (MSA) are among the major reaction products of DMS oxidation (e.g. Capaldo and Pandis, 1997; Seinfeld and Pandis, 1998). Additional stable reaction products are dimethyl sulfoxide (DMSO) and dimethyl sulfone ($DMSO_2$). However, many aspects of the DMS oxidation in the atmosphere are poorly understood (e.g. Campolongo et al., 1999; Andreae and Crutzen, 1997). For example, halogen oxide radicals (e.g. BrO, IO, ClO) are also known to react with DMS in the atmosphere, but the importance of these reactions is still very uncertain (Sayin and McKee, 2004).
A key link in the proposed feedback between DMS and climate is the nucleation of DMS derived sulfuric acid into new particles and eventually the formation of new cloud condensation nuclei (Charlson et al., 1987). However, particle formation due to the nucleation of DMS derived sulfuric acid in the marine boundary layer is still under debate (Yoon and Brimblecombe, 2002).
Only a fraction of SO_2 derived from DMS oxidation is further oxidized by OH to form SO_4^{2-} which can nucleate homogeneously or condenses onto existing particles, another fraction is oxidized in clouds and forms SO_4^{2-} which condenses onto existing particles, the rest is deposited. In the remote marine boundary layer, where DMS is the main precursor for SO_4^{2-} the condensation of SO_4^{2-} onto sea salt aerosols suppresses the efficiency of the nucleation of sulfuric acid. Measurements indicate that a significant fraction of the conversion of DMS derived SO_2 to sulfate occurs on or in sea-salt particles over the ocean and therefore does not lead to new particle production (Clegg and Toumi, 1998). Therefore, changes caused by increasing wind speed leading to higher DMS emissions but also higher sea salt emissions might not necessarily lead to higher sulfate aerosol particle nucleation rates. Direct evidence for the contribution of SO_2 derived from DMS oxidation to CCN production is provided by measurements over the South Atlantic, at Cape Grim, and at Amsterdam Island which show a strong correlation between DMS emission, the concentration of total aerosol particles, and CCN (Putaud et al., 1993; Andreae et al., 1995, 1999; Ayers and Gillett, 2000). Such findings are by no means generally applicable. Several investigators found no or only sporadic correlation between DMS and non sea salt sulfate, CN or CCN (Bates et al., 1992; Berresheim et al., 1993).
Box-model studies and observations in the clean marine boundary layer (MBL) have highlighted that aerosol number concentrations in the MBL are strongly influenced by the entrainment of aerosols from the free troposphere (Capaldo et al., 1999; Raes, 1995; Bates et al., 1998). Based on these findings, Shaw et al. (1988) proposed an alternative climate stabilizing feedback loop, which incorporates biogenic sulfur pumped from the MBL into the free troposphere by deep convection where it nucleates to sulfate aerosol particles. These free troposphere sulfate aerosol particles are entrained back into the MBL where they influence cloud albedo by serving as CCN. An increase in the sea surface temperature leads to an increased frequency and intensity of convection thereby increasing the formation of free tropospheric sulfate aerosol particles. This leads to a higher CCN number concentration, a higher cloud albedo, and subsequently a reduced sea surface temperature which in turn leads to reduced convection. This negative feedback mecha-

nism results solely from changes in convective transport and does not require the marine biosphere to increase DMS emissions in response to climate warming as proposed in the CLAW hypothesis.

1.5 Connections to other biological and physical processes

Many of the proposed mechanisms in the CLAW hypothesis are linked to other biological and physical processes which are likely to change under changing climatic conditions. A wide range of factors is known to influence DMS production in the ocean. Iron for example is one nutrient that affects DMS production. In situ iron fertilization experiments have revealed an influence of iron enrichment on DMS concentrations. Turner et al. (1996) found an increase in DMS sea surface concentration by a factor of 3.5 in the IronEx II iron enrichment experiment. They speculate that iron entrainment stimulates the synthesis of DMSP in phytoplankton. The primary source of oceanic iron is the deposition of mineral dust aerosols from the atmosphere onto the ocean's surface. Changes in climate will alter the aeolian dust input (Tegen et al., 2004) which may alter the DMSP content of phytoplankton cells. Additionally, the iron surface concentration has a direct impact on the planktonic productivity by limiting phytoplankton growth in some oceanic regions (most prominent in the 'high nitrate-low chlorophyll regions' such as the equatorial Pacific Ocean (Coale et al., 1996) and the Southern Ocean (Boyd et al., 2000)). Sunda et al. (2002) demonstrated that intracellular DMSP concentrations dramatically increase under conditions of acute oxidative stress such as exposure to high levels of ultraviolet radiation. This response may also provide a feedback via the DMS production in response to anthropogenic forcing, because solar ultraviolet radiation will change as a consequence of the observed changes in stratospheric ozone concentrations (Harder et al., 1995).
The response of oceanic biota to climate change is a possible shift in the species composition of phytoplankton (Orr et al. (2005), Bopp et al. (2005)). This has an impact on DMS production from phytoplankton as the DMSP content of phytoplankton cells differs markedly between different phytoplankton groups (Keller et al., 1989).
Anthropogenic activities change aerosol and aerosol precursor emissions (IPCC, 2001). Stier et al. (2004) showed in a global microphysical aerosol modeling study that specific emission changes cause changes in aerosol cycles of other components, confirming a microphysical coupling between the different aerosol cycles. To account for these effects, sulfate aerosol particles derived from DMS oxidation have to be studied as a part of the complex global aerosol system.
A range of physical processes has a direct impact on the DMS cycle both in the atmosphere and in the ocean. For example, changes in the ocean stratification caused by climate change will influence marine productivity (Denman et al. (1996), Cox et al. (2000), Bopp et al. (2001), Boyd and Doney (2002), Sarmiento et al. (2004)). Changes in the wind speed will directly affect the DMS emissions into the atmosphere. In the atmosphere, changes in oxidant concentrations, caused by changes in anthropogenic emissions and global warming (Johnson et al., 1999; Gauss et al., 2003), will alter the oxidative

capacity of the atmosphere and therefore the DMS oxidation efficiency (Pham et al., 2005).

1.6 Global modeling

DMS and its oxidation products in the atmosphere are short-lived species. Therefore, it is necessary to resolve the temporal and spatial distribution of the DMS sea surface concentration on a global scale to investigate its impact on the climate system. The following section gives an overview of recently developed DMS sea surface concentration climatologies. Some of these climatologies rely on empirical descriptions and were applied in climate change simulations.

1.6.1 DMS climatologies

Several studies focused on building up climatologies of the global distribution of DMS in the sea surface water. Belviso et al. (2004a) compared seven recently developed global DMS monthly climatologies (Kettle et al., 1999; Kettle and Andreae, 2000; Anderson et al., 2001; Aumont et al., 2002; Simó and Dachs, 2002; Chu et al., 2003; Belviso et al., 2004b). The studies of Kettle et al. (1999), Kettle and Andreae (2000), Anderson et al. (2001), and Simó and Dachs (2002) all rely on the Kettle et al. (1999) database which consists of almost 16,000 DMS sea surface measurements. Kettle et al. (1999) and Kettle and Andreae (2000) derived monthly mean maps on a 1° by 1° basis from the database by a complex interpolation and extrapolation procedure in regions where no data were available. Anderson et al. (2001) and Simó and Dachs (2002) used only the data points out of the Kettle et al. (1999) database with concurrent chlorophyll α and DMS sea surface measurements, which reduces the amount of data points to around 2600. Anderson et al. (2001) extended the resulting database by information about incoming light and nutrient abundance to derive a simple empirical relationship between DMS, chlorophyll α, light, and nutrients. Simó and Dachs (2002) extended the concurrent DMS and chlorophyll α measurements by information about the mixed layer depth (MLD) to derive a two equation algorithm which calculates the DMS sea surface concentration from the MLD and the chlorophyll α concentration. Aumont et al. (2002) and Belviso et al. (2004b) used a prognostic nonlinear parameterization to compute DMS sea surface concentrations from chlorophyll α concentrations together with an index of the community structure of marine phytoplankton. Their DMS parameterization was derived from data taken at several DMS surveys carried out in various areas of the Atlantic Ocean, the Mediterranean Sea, and the Indian part of the Southern Ocean. Aumont et al. (2002) applied estimated values for the trophic state and the chlorophyll α concentration from an ocean carbon cycle model to predict DMS sea surface concentration. Belviso et al. (2004b) applied the chlorophyll α concentration derived from SeaWIFS (Sea-viewing Wide Field-of-view Sensor) data. Only the approach of Chu et al. (2003) is based on a prognostic biogeochemical formulation for DMS production and DMS removal in the ocean based on the regional work of Gabric et al. (1993). Comparing these climatologies, Belviso et al. (2004a) found relative uncertainties

for the zonal and annual mean differences ranging from 50% in the tropical and temperate regions to nearly 100% in high latitudes.

1.6.2 DMS emission response to climate change calculated in global climate models

Several modeling studies have attempted to model the DMS gas exchange between atmosphere and ocean based on prescribed DMS sea surface concentrations. Most global model studies used the Kettle and Andreae (2000) climatology (e.g. Boucher and Pham, 2002; Jones et al., 2001; Berglen et al., 2004; Gondwe et al., 2003; Rotstayn and Lohmann, 2002). Up to now, none of the global atmospheric model studies included a description of the DMS cycle in the ocean. Therefore, the response of the DMS emission to climate change could be only assessed through changes in the sea-air exchange rate which varies with wind speed and temperature. Penner et al. (2001) showed a small increase in DMS emissions between 2000 and 2100 (from 26.0 Tg(S) yr^{-1} to 27.7 Tg(S) yr^{-1}) using a constant DMS sea surface concentration field (Kettle et al., 1999) together with a constant monthly climatological ice cover. The gas exchange rates were calculated interactively in the simulation, based on wind speed and sea surface temperature. However, DMS sea surface concentrations are controlled by marine biology, which is affected by variables such as solar irradiance, temperature, and ocean dynamics. These variables are likely to vary under changing climatic conditions.
Only recently the response of DMS sea surface concentration to global warming has been studied in global ocean models based on empirical relationships. Bopp et al. (2003) applied the DMS formulation given by Aumont et al. (2002) in a transient climate simulation, assuming a 1% increase in atmospheric CO_2 concentrations per year. They find a small increase in the global annual DMS flux (+2%) with considerable large spatial variability up to the year 2080 (equivalent to an atmospheric CO_2 doubling). Bopp et al. (2004) introduced these changes of the DMS flux in an atmospheric model, which includes a sulfur chemistry scheme, and calculated the response of the radiative forcing. They find a radiative perturbation resulting from DMS induced changes in the cloud albedo of -0.05 Wm^{-2} representing only a small negative feedback on global warming. The DMS algorithm given by Simó and Dachs (2002) was used by Gabric et al. (2004) to calculate DMS emissions for present-day conditions and climate conditions equivalent to a tripling of atmospheric CO_2 concentrations. In a warmer climate they find an increase in the DMS flux of 14%, predominantly caused by a decrease of the MLD in the high latitudes of the Southern Hemisphere. This result is a consequence of their assumption that DMS concentrations are inversely correlated with the MLD. However, whether this assumption is still valid under changing climate conditions is questionable. Factors like changes in the nutrient supply (either from modifications in upwelling or Aeolian deposition) or changes in the phytoplankton species composition are not taken into account in their study.

1.7 Objectives and outline of this thesis

The aim of this work is to study the DMS cycle in the ocean and in the atmosphere and its response to anthropogenic perturbations. As the DMS climate interactions are governed by multicompartment (atmosphere, ocean, biogeochemistry) feedback processes, a comprehensive global modeling system including the ocean, the marine biogeochemistry, the atmosphere, and the aerosol system has been established. Production and consumption of DMS are simulated in the ocean as part of the marine biogeochemistry model HAMOCC5. Embedded in the global ocean general circulation model MPI-OM, HAMOCC5 includes a biological production scheme simulating plankton dynamics on a global scale. Processes taken into account are DMS production by phytoplankton, DMS consumption by bacteria, photo-oxidation of DMS into DMSO, and the DMS flux into the atmosphere. Parameters which are undetermined are derived from a fit of the simulated DMS sea surface concentrations to observed DMS sea surface concentrations reported in the Kettle and Andreae (2000) database. The simulated oceanic DMS flux into the atmosphere is then passed to the atmosphere model (ECHAM5). The atmosphere model includes a sulfur chemistry scheme and an aerosol microphysics model (HAM) which calculate the atmospheric concentrations of DMS, SO_2 in-cloud and gas phase oxidation to SO_4^{2-}, the distribution of in-cloud formed SO_4^{2-} and the condensation of gas-phase formed SO_4^{2-} on pre-existing particles, as well as the formation of sulfate aerosol particles. Besides sulfate, the aerosol model treats the major global aerosol compounds: black carbon, particulate organic mass, sea salt, and mineral dust. Sea salt and mineral dust emissions are calculated interactively in the model. This provides the means to apply this model for long-term climate change simulations including the effects of varying dust depositions, caused by climate change, on the marine biogeochemistry and on DMS emissions. For the transient simulation the cloud-microphysical scheme includes the nucleation of could droplets which is parameterized depending on the aerosol number concentration, size distribution and vertical velocity (Lohmann et al., 1999).
To assess the role of DMS in the climate system, it is essential to treat the DMS cycle interactively in the ocean-atmosphere system because the proposed DMS-climate feedback is a multi-compartment feedback. This is the first time that the DMS cycle in the ocean and in the atmosphere are simulated in a consistent coupled model setup.

The major objectives of this study are to:

- Establish a modeling system of the DMS cycle in the ocean and in the atmosphere which simulates realistically and dynamically consistent DMS sea surface concentrations, DMS emissions, and DMS concentrations in the atmosphere.

  A climatological mean simulation is performed and evaluated with available measurements. Up to now it is not possible to measure the DMS flux into the atmosphere directly. However, the treatment of DMS in the ocean and in the atmosphere provides the means to evaluate the simulated DMS flux into the atmosphere. To overcome the lack of DMS measurements in the atmosphere, SO_4^{2-} measurements

in regions where DMS is the main precursor are taken into account.

- Investigate the response of the DMS sea surface concentration, the DMS fl-x, and the DMS concentration in the atmosphere to climate change caused by increasing anthropogenic activities.

  The coupled model setup has been applied in a transient climate simulation attempting to simulate the period from 1860 to 2100 with increasing greenhouse gas concentrations and aerosol and aerosol precursor emissions. The results are analyzed in terms of changes in the biological production and subsequent changes in the DMS production in the ocean, DMS sea surface concentration, DMS emission, and DMS concentration in the atmosphere. The main question addressed here is whether a warmer climate leads to an increase or a decrease in DMS emissions. This is the most uncertain link in the CLAW hypothesis. The prognostic formulation of the DMS cycle in the ocean enables us to investigate this key link.

The thesis is organized as follows: in Chapter 2 the modeling system is introduced. Results of a climatological mean simulation are presented and discussed in Chapter 3 (these results are published in Biogeosciences (Kloster et al., 2006)[1]). Perturbations in DMS quantities based on results of a transient climate simulation are presented in Chapter 4 (these results have been submitted to Global Biogeochemical Cycles[2]). Chapter 5 concludes the major findings and Chapter 6 gives an outlook on future work and challenges.

[1] published as: S. Kloster, J. Feichter, E. Maier-Reimer, K.D. Six, P. Stier and P. Wetzel, DMS cycle in the marine ocean-atmosphere system - a global model study, *Biogeosciences, 3, 29-51, 2006.*

[2] submitted as: S. Kloster, J. Feichter, E. Maier-Reimer, E. Roeckner, P. Stier, P. Wetzel, K.D. Six and M. Esch, Response of DMS in the ocean and atmosphere to global warming, to *Global Biogeochem. Cycles.*

Chapter 2

Model description

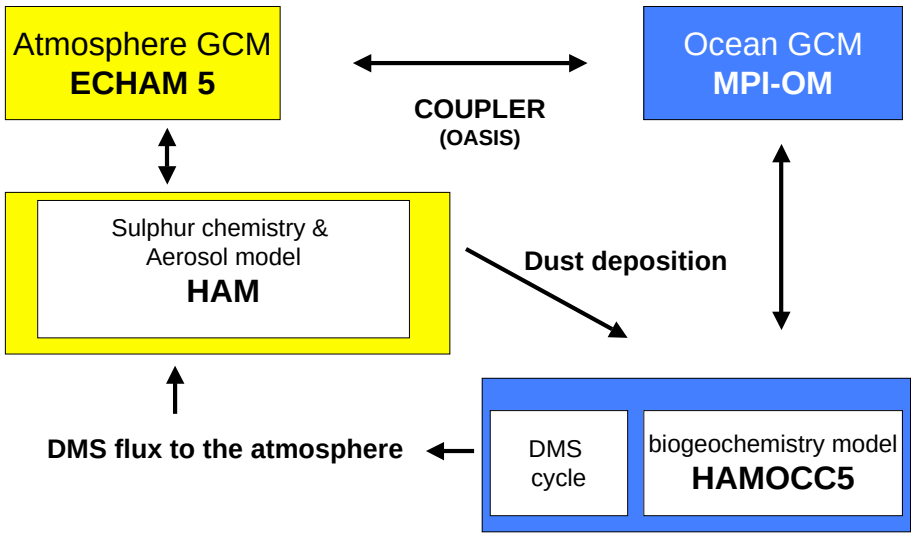

Figure 2.1: Schematic overview of the model setup applied in this study.

The model used in the experiment is a coupled atmosphere-ocean general circulation model (AOGCM). The AOGCM consists of sub-models which correspond to the atmosphere (ECHAM5) and the ocean (MPI-OM). The atmospheric model includes a microphysical aerosol model (HAM) which simulates the evolution of a microphysically interacting internally- and externally mixed aerosol population as well as their size-distribution and chemical composition. Embedded in the ocean model is a marine biogeochemistry model (HAMOCC5) which has been extended by a formulation of the DMS cycle in the ocean. A schematic overview of the model setup is given in Figure 2.1. The individual model

components are described in the following sections.

2.1 The MPI-OM general circulation model

The ocean component is the Max-Planck-Institute ocean model (MPI-OM) (Marsland et al., 2003). MPI-OM is a z-coordinate global general circulation model based on the primitive equations for a Boussinesq-fluid on a rotating sphere. The transport is computed with a total variation diminishing (TVD) scheme (Sweby, 1984). It includes parameterizations of sub-grid scale mixing processes like isopycnal diffusion of the thermohaline fields, eddy induced tracer transport following Gent et al. (1995), and a bottom boundary slope convection scheme. The model treats a free surface and a state of the art sea ice model with viscous-plastic rheology and snow (Hibler, 1979). The model works on a curvilinear orthogonal C-grid. In this study, we use a nominal resolution of 1.5 ° at the equator with one pole located over Greenland and the other over Antarctica. In the vertical, the model has 40 levels with level thickness increasing with depth. Eight layers are located within the upper 90 m and 20 layers within the upper 600 m.

2.2 The marine biogeochemistry model HAMOCC5

The marine biogeochemistry component is the Hamburg Oceanic Carbon Cycle Model (HAMOCC5) (Maier-Reimer et al., 2005; Six and Maier-Reimer, 1996; Maier-Reimer, 1993). HAMOCC5 simulates the biogeochemical tracers in the oceanic water column and the sediment. The model is coupled online to the circulation and diffusion of the MPI-OM ocean model and runs with the same time step and resolution. Figure 2.2 shows a schematic overview of the marine eco-system as simulated in HAMOCC5. The eco-system model is based on nutrients, phytoplankton, zooplankton and detritus (NPZD-type) as described in Six and Maier-Reimer (1996). In addition, new elements like nitrogen, dissolved iron and dust are accounted for and new processes like denitrification, nitrogen fixation, dissolved iron uptake and release by biogenic particles, and dust deposition and sinking are implemented as described in detail in Wetzel (2004). The dust deposition to the ocean surface is calculated online in the ECHAM5-HAM model and passed to the marine biogeochemistry model HAMOCC5 once per day. Bioavailable iron is released in the ocean surface layer immediately after deposition of dust.
Photosynthesis and zooplankton grazing are restricted to the upper 100 m of the water column (euphotic zone) where insolation is sufficient to support net productivity. Below the euphotic zone all organic matter ultimately remineralizes to nutrients. Limiting nutrients within HAMOCC5.1 are phosphate, nitrate, and iron. HAMOCC5 considers only one phytoplankton pool, but links the export of detritus to the export of calcium carbonate and particulate silicate and separates thereby indirectly between diatoms and coccolithophorids.

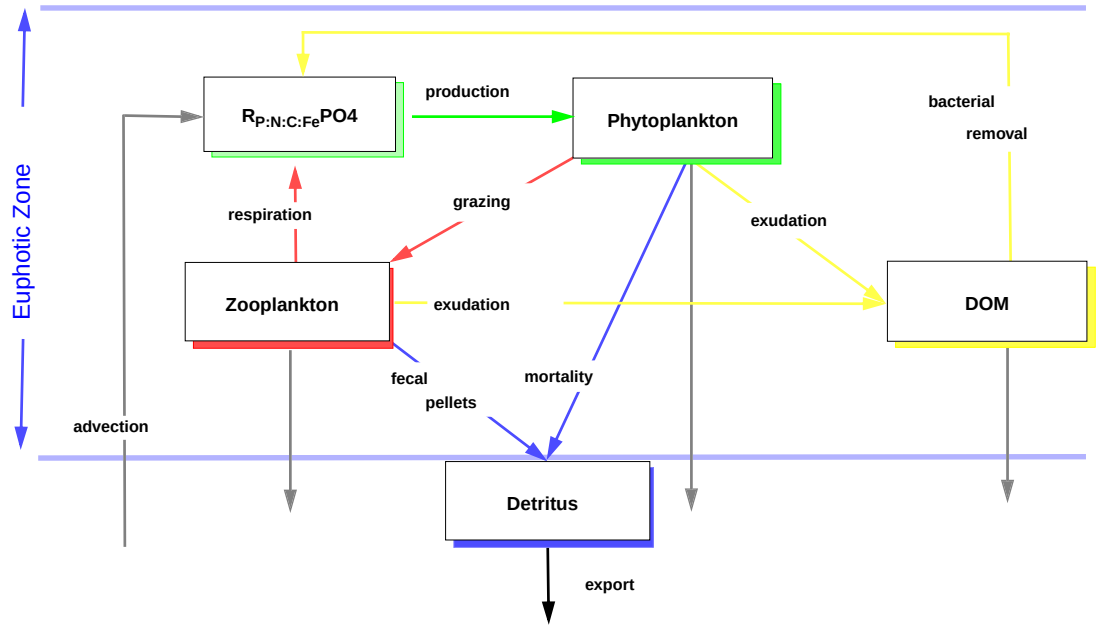

Figure 2.2: Simplified schematic overview of the marine eco-system simulated by HAMOCC5 (adapted from Maier-Reimer et al. (2005)).

2.2.1 DMS formulation in the marine biogeochemistry module HAMOCC5

The DMS formulation in HAMOCC5 is derived from the formulation originally developed for a former version of the marine biogeochemistry module (HAMOCC3.1 (Six and Maier-Reimer, 1996)).
The formulation for DMS production in the ocean assumes that DMS is produced (DMS_{prod}) when phytoplankton cells are destroyed due to senescence or grazing processes. The DMS decay occurs via consumption by bacteria (DMS_{bac}), chemical oxidation to DMSO (DMS_{UV}) and ventilation to the atmosphere (DMS_{flux}).

$$\frac{d[DMS]}{dt} = DMS_{prod} - DMS_{bac} - DMS_{UV} - DMS_{flux} \tag{2.1}$$

Here only dissolved DMS is considered. DMSP as the precursor of DMS in the ocean is not taken explicitly into account because very little is known about the processes that lead to the reduction of DMSP to DMS (Kiene et al., 2000). Moreover, only few measurements of DMSP concentrations in the ocean are available which makes an evaluation not feasible.
HAMOCC5 was developed to simulate the carbon chemistry in the ocean. To simulate the vertical alkalinity distribution, it separates between the export of particulate silicate and calcium carbonate ($export_{sil}$ and $export_{CaCO_3}$, respectively). The resulting vertical alkalinity distribution compares well with available measurements (Wetzel et al., 2005; Wetzel, 2004). By separating the export into the export of calcium carbonate and the export of

silicate, HAMOCC5 distinguishes indirectly between the two phytoplankton groups: the diatoms which form opal frustels and the coccolithophorids which build skeletons made of calcium carbonate. It is assumed that fast growing diatoms consume nutrients as long as silicate is available. Therefore, the export of organic carbon is linked to silicate until silicate is depleted in the ocean. After depletion of silicate the phytoplankton growth is carried out by coccolithophorids, resulting in the export of calcium carbonate. The simulated ratio of calcium carbonate to organic carbon export is tuned to be 0.06 on global average in order to simulate a realistic alkalinity distribution (Wetzel, 2004; Sarmiento et al., 2002). This distinction between diatoms and coccolithophorids is important, as they are known to differ markedly in terms of their cellular DMSP content, and hence their ability for producing DMS (Keller et al., 1989). The distinction between silicate and calcium carbonate export is utilized to simulate the DMS production as follows:

$$DMS_{prod} = f(T) * (k_{psi} * export_{sil} + k_{pcc} * export_{CaCO_3}) \tag{2.2}$$

k_{psi} and k_{pcc} are the respective scaling factors defined in Table 2.1. The function f(T) accounts for the observed temperature dependence of intracellular DMSP concentrations. Under low temperature conditions, e.g. in polar regions, the DMSP content in phytoplankton cells is higher than under temperate conditions (Baumann et al., 1994). This effect is parameterized as follows:

$$f(T) = (1 + \frac{1}{(T + k_{pt})^2}) \tag{2.3}$$

with T in ° C. k_{pt} scales the temperature dependency (Table 2.1).
The DMS destruction processes are formulated as follows:
The destruction of DMS by photo-oxidation to DMSO depends on the solar radiation at the surface (Shooter and Brimblecombe, 1989; Brimblecombe and Shooter, 1986; Kieber et al., 1996). The incident solar radiation I_0 is attenuated in HAMOCC5 by water and phytoplankton as a function of depth (z) according to the equation:

$$I_z = I_0 * e^{-(k_w + k_{chl}) * z} \tag{2.4}$$

The attenuation coefficient for pure water is chosen to be $k_w = 0.04\ m^{-1}$. Light attenuation by phytoplankton is assumed to be a linear function of the chlorophyll concentration $k_{chl} = 0.03\ [CHL]\ m^{-1}$, with the chlorophyll concentration $[CHL]$ given in mg l^{-1}. The chlorophyll concentration is computed from the modeled phytoplankton concentration with a fixed chlorophyll to carbon ratio of 1:60. The incident surface radiation [Wm^{-2}] is calculated interactively, including the effects of clouds and aerosols, in the ECHAM5-HAM model. The decay of DMS by photo-oxidation is then formulated as follows:

$$DMS_{UV} = k_{luv} * I_z * [DMS] \tag{2.5}$$

k_{luv} is the respective scaling factor defined in Table 2.1. DMS destruction due to consumption by bacteria is assumed to be temperature dependent:

$$DMS_{bac} = k_{lb} * (T + 3.) * [DMS] * f([DMS]) \tag{2.6}$$

with T in $^\circ$ C. k_{lb} denotes the scaling factor for the consumption process by bacteria. Observations suggest that consumption by bacteria appears to be less efficient in areas with low DMS concentrations (Kiene and Bates, 1990). This variation is parameterized with a saturation function:

$$f([DMS]) = (\frac{[DMS]}{k_{cb} + [DMS]}) \tag{2.7}$$

k_{cb} is set to 10 nmol l^{-1} which ensures an almost linear behaviour for low DMS concentrations.
For the atmosphere, the most important DMS loss mechanism in seawater is the loss due to sea-air exchange. For the sea-air exchange calculation the DMS concentration in the atmosphere is neglected, as it is small compared to the DMS sea surface concentration. The DMS sea-air exchange is then formulated as follows:

$$DMS_{flux} = k_{sea-air} * [DMS] \tag{2.8}$$

$k_{sea-air}$ denotes the sea-air exchange rate. This simulation applies the formulation after Wanninkhof (1992):

$$k_{sea-air} = 0.31 * w_{10m}^2 * (\frac{Sc}{660})^{-\frac{1}{2}} \tag{2.9}$$

where w_{10} is the 10 m wind speed and Sc the Schmidt number for DMS which is calculated analogous to Saltzman et al. (1993).
The undetermined parameters (k_{psi}, k_{pcc}, k_{pt}, k_{luv}, k_{lb}) are derived from a fit of the simulated DMS sea surface concentrations to observed DMS sea surface concentrations. Kettle and Andreae (2000) compiled a database of almost 16,000 DMS sea surface concentration measurements. Thereby, the original database (Kettle et al., 1999) was updated by new measurements. The updated database is used to optimize the parameters in the proposed DMS parameterization. Therefore, the data points are distributed onto the ocean grid cells on a monthly mean basis. The DMS concentration at a grid-point is taken to be the average of the individual monthly mean measurements within the grid cell. Since the data coverage is very sparse and the partitioning into monthly means is rather arbitrary, the resulting DMS sea surface concentrations of a single grid box are extrapolated to the adjacent grid boxes and values from the adjacent months are also taken into account for the monthly splitting. Due to computational constraints it is not feasible to conduct the optimization process within the fully coupled AOGCM. To derive the DMS scaling parameters, an offline version of the ocean model (MPI-OM/HAMOCC5) forced by NCEP/NCAR reanalysis data (Kalnay et al., 1996) is used. The model setup is described in detail in Wetzel et al. (2005). From this simulation the year 1995 is arbitrarily chosen for the optimization process of the DMS scaling parameters. Periodically repeating the simulation with NCEP/NCAR forcing fields for the year 1995, global value deviation fields of the modeled DMS sea surface concentration and the DMS sea surface map, generated from the Kettle and Andreae (2000) database, are calculated. Thereby, only ocean grid boxes are taken into account with an ocean depth greater than 300 m. Regions with a shallower depth, like the North Sea, are not well captured by the model. In these regions the Kettle and Andreae (2000) database includes a disproportional high number of

Symbol	constant		Process
DMS Production			
k_{psi}	0.0136	$[S(DMS)/(Si)]$	silicate
k_{pcc}	0.1345	$[S(DMS)/(C)]$	calcium carbonate
k_{pt}	10.01	[° C]	temperature dependence
DMS Decay			
k_{luv}	0.0011	$[m^2/Wd]$	photolysis
k_{lb}	0.1728	$[d^{-1\circ}\ C^{-1}]$	bacteria

Table 2.1: Parameters for the DMS formulation in HAMOCC5. The parameters are derived from an optimization procedure of HAMOCC5 using DMS sea surface concentration measurements from the Kettle and Andreae (2000) database.

measurements. To avoid a bias in the optimization process towards these measurements, these grid boxes are excluded. A cost function is defined as the global annual sum of the deviation fields. In a series of two year runs, starting with the same initial conditions, this cost function is minimized by changing the five free parameters (k_{psi}, k_{pcc}, k_{pt}, k_{luv}, k_{lb}) of the DMS formulation sequentially by plus or minus 5%. The cost function is then calculated during every second model year. The parameters are changed along the gradient leading to a minimum of the cost function. The task of this global optimization process is to find the global minimum of the cost function. However, one cannot exclude that this optimization process leads to a local minimum, which is a general problem in optimization procedures. The resulting parameters of the optimization parameters are compiled in Table 2.1.

2.3 The ECHAM5 general circulation model

The atmospheric component is the general circulation model ECHAM5 (Roeckner et al., 2003) with the current standard resolution of 31 vertical levels on a hybrid sigma-pressure coordinate system up to a pressure level of 10 hPa. Prognostic variables are vorticity, divergence, surface pressure, temperature, water vapour, cloud water, cloud ice, cloud droplet and ice crystal number concentrations. Except for the water and chemical components, the prognostic variables are represented by spherical harmonics with triangular truncation at wavenumber 63 (T63). Physical processes and nonlinear terms are calculated on a Gaussian grid with a nominal resolution of 1.8 ° in longitude and latitude. For the advection of water vapour, cloud liquid water, cloud ice and tracer components, a flux form semi-Lagrangian transport scheme (Lin and Rood, 1996) is applied. Cumulus convection is based on the mass flux scheme after Tiedtke (1989) with modifications according to Nordeng (1994). The cloud microphysical scheme (Lohmann and Roeckner, 1996) consists of prognostic equations for cloud liquid water and cloud ice. The cloud cover is predicted with a statistical scheme including prognostic equations for the distribution moments (Tompkins, 2002). The transfer of solar radiation is parameterized after Fouquart and Bonnel (1980) and the transfer of longwave radiation after Morcrette et al.

(1998).

2.4 The HAM aerosol model

The ECHAM5 model has been extended by a complex microphysical aerosol model HAM, described in detail in Stier et al. (2005a). The aerosol spectrum is represented by the superposition of seven log-normal distributions. Each of these seven aerosol modes can be described by three moments: the aerosol number, the number median radius, and the standard deviation (the former two parameters are predicted, the latter one is prescribed). The seven modes are divided into four geometrical size classes (nucleation, Aitken, accumulation and coarse mode). Three of the modes include only insoluble compounds, four of the modes contain at least one soluble compound. The major global aerosol compounds are considered: sulfate (SU), black carbon (BC), particulate organic mass (POM), sea salt (SSA), and mineral dust (DU). HAM consists of a microphysical core model M7, an emission module, a sulfur chemistry scheme, a deposition module, and a radiation module defining the aerosol radiative properties.

The microphysical core model M7

The microphysical core M7 (Vignati et al., 2004) treats the aerosol dynamics and thermodynamics. It evolved from an earlier version M3+ which has been applied and tested in offline global chemical transport models (Wilson et al., 2001). Processes considered are coagulation within and among the modes, condensation of gas-phase sulfuric acid on the aerosol surface, the binary nucleation of sulfate, and water uptake depending on the ambient relative humidity.

Emission module

The emission of mineral dust and sea salt is calculated interactively according to the scheme of Tegen et al. (2002) and Schulz et al. (2004), respectively. DMS emissions are calculated online in the marine biosphere submodel HAMOCC5. For the other aerosol compounds, emission strengths, emission size distribution and emission height are prescribed. Considered aerosol and aerosol precursor emissions are sulfur emissions from industry, bio- and fossil-fuel use, biomass burning, and volcanoes. For the carbonaceous compounds (BC and POM) bio- and fossil-fuel use and biomass burning sources are considered. For the climatological mean simulation the emission strengths, emission size distribution and emission height are based on the AEROCOM (Aerosol Model Inter-Comparison, http://nansen.ipsl.jussieu.fr/AEROCOM) emission inventory for the year 2000 (Frank Dentener, in prep.). For the transient simulation the emission strengths are based on an inventory derived by the Japanese National Institute for Environmental Studies (NIES) following the SRES A1B storyline from 2000 on (T. Nozawa et al., pers. comm., 2004).

The chemistry scheme

The sulfur chemistry module (Feichter et al., 1996) treats DMS, SO_2 and SO_4^{2-} as prognostic variables. In the gas phase, SO_2 and DMS are oxidized by the hydroxyl radical (OH) during the day. Additionally, DMS reacts with nitrate radicals (NO_3) at night. Reaction products are SO_2 and SO_4^{2-}. Dissolution of SO_2 within cloud water is calculated according to Henry's law (e.g. Seinfeld and Pandis, 1998). In the aqueous phase, the oxidation of SO_2 by hydrogen peroxide (H_2O_2) and ozone (O_3) are considered. The oxidant concentrations are prescribed as three dimensional monthly mean fields from calculations of the MOZART chemical transport model (Horowitz et al., 2003). Gas phase produced sulfate is allowed to condensate onto pre-existing particles or to nucleate to new particles, calculated by the aerosol microphysical module M7. In-cloud produced sulfate is distributed to the available pre-existing accumulation mode and coarse mode aerosol particles according to their respective number concentration.

Deposition processes

The deposition processes, i.e. wet deposition, dry deposition, and sedimentation, are calculated online in dependence of aerosol size and composition. The dry deposition for gases is calculated according to Ganzeveld et al. (1998). For aerosols the dry deposition is calculated in dependence of the simulated aerosol radius and density. The resulting dry deposition flux is subtracted from the respective emission flux and provides the lower boundary conditions for the vertical diffusion scheme of ECHAM5. The wet deposition of tracers is calculated in dependence of the in-cloud content and the precipitation formation rate simulated in ECHAM5. For gases the in-cloud content is derived from Henry's law (Seinfeld and Pandis, 1998). For aerosols the in-cloud content is derived from prescribed scavenging ratios with lower efficiencies for the insoluble modes.

The radiation module

The radiation module calculates the aerosol optical properties explicitly from the prognosed size distribution, composition, and mixing state within the framework of the Mie theory. The optical properties are pre-calculated and supplied in a look-up table, providing the necessary input for the radiation scheme in ECHAM5 (extinction cross section, single scattering albedo, and asymmetry factor) which are then passed to the radiation scheme of ECHAM5. Only the effects of aerosols on the solar part of the spectrum are considered.

Cloud microphysics

The stratiform cloud scheme of ECHAM5 has been extended by a prognostic treatment of cloud droplet number and ice crystal number concentration. Nucleation of cloud droplets is parameterized semi-empirically in terms of the aerosol number size distribution and vertical velocity (Lin and Leaitch, 1997). Sub-grid scale vertical velocity is derived from the turbulent kinetic energy (Lohmann et al., 1999). Sink processes are parameterized in analogy to those formulated in ECHAM5 for the in-cloud liquid water content. The

cloud optical properties depend on the droplet effective radius, which is a function of the in-cloud liquid water content and cloud droplet number concentration (CDNC). These parameters control the auto-conversion rate following Khairoutdinov and Kogan (2000). Thus, this setup accounts for both the first and second indirect aerosol effects. This extended version of the stratiform cloud scheme was only applied in the transient climate simulation. However, results from the climatological simulation presented in chapter 3 use the standard ECHAM5 stratiform cloud scheme.

For this study the ECHAM5-HAM model has been extended by a technique to mark SO_2 and SO_4^{2-} attributable to DMS. This allows to isolate the fraction of DMS-derived SO_2 and SO_4^{2-}. Such quantification facilitates assessment of the contribution of aerosols from DMS oxidation. Additionally, the knowledge of the contribution of DMS to SO_4^{2-} enables us to use SO_4^{2-} concentration measurements at sites with a relatively high contribution of DMS to SO_4^{2-} for an evaluation of the atmospheric DMS cycle in the model.

2.5 The coupler OASIS

The ocean and the atmosphere models are coupled with the OASIS coupler (Valcke et al., 2003) with a coupling time step of one day. The ocean model MPI-OM passes the sea surface temperature and sea ice variables to the atmosphere through OASIS. The atmosphere model ECHAM5-HAM uses these boundary conditions for one coupling timestep and transfers the surface forcing fields through OASIS back to the ocean model. Required surface forcing fields are heat, freshwater and momentum fluxes, downward solar radiation and the 10 m wind speed. Additionally, the DMS flux to the atmosphere, calculated in HAMOCC5, is passed to the atmosphere model. The dust deposition calculated in the HAM model is passed to HAMOCC5 through OASIS. The coupled ocean-atmosphere model does not employ flux adjustments.

Chapter 3

The present-day marine and atmospheric DMS cycle

A climatological mean simulation for present-day conditions is performed and compared to available measurements both in the atmosphere and in the ocean. To overcome the lack of DMS measurements in the atmosphere, SO_4^{2-} measurements in regions where DMS is the main precursor are taken into account. A coloured tracer technique is applied to estimate the contribution of DMS derived SO_4^{2-} to the total SO_4^{2-}concentration. The results are published in this form in Biogeosciences Dissc.[1].

3.1 Simulation setup

In order to initialize the coupled atmosphere-ocean model (AOGCM), the uncoupled ocean model was integrated over thousand years to reach quasi-equilibrium state. From there on the coupled AOGCM was integrated with fixed external forcing to reach quasi-equilibrium state. From these initial conditions the simulation is started and integrated for 15 years. The results presented here are averaged over the last 10 years. The mineral dust, sea salt and DMS emissions are calculated interactively as described in the previous chapter. All other aerosol and aerosol precursor emissions are prescribed based on the AEROCOM (Aerosol Model Inter-Comparison, http://nansen.ipsl.jussieu.fr/AEROCOM) emission inventory for the year 2000 (Frank Dentener, in prep.). The emission strength for all aerosol compounds is summarized in Table 3.1.

3.2 Results

In the following sections the results of the climatological mean simulation are presented separated in an ocean and atmosphere part. The ocean part focuses on the simulated DMS sea surface concentrations and the resulting DMS flux. Additionally, DMS sea surface concentrations predicted from a simple empirical algorithm proposed by Simó and Dachs

[1]published as: S. Kloster, J. Feichter, E. Maier-Reimer, K.D. Six, P. Stier and P. Wetzel, DMS cycle in the marine ocean-atmosphere system - a global model study, *Biogeosciences, 3, 29-51, 2006.*

Species	Source	Reference	Tg yr^{-1}
DMS	Terrestial Biosphere	Pham et al. (1995)	0.3
	Marine Biosphere	HAMOCC5	27.6
SO_2	Volcanoes	Andres and Kasgnoc (1998) Halmer et al. (2002)	14.6
	Vegetation Fires	van der Werf et al. (2003)	2.1
	Industry, Fossil-Fuel, Bio-Fuels	Cofala et al. (2005)	54.2
Total sulfur			99.0
BC	Vegetation Fires	van der Werf et al. (2003)	3.0
	Fossil-Fuel and Bio-Fuels	Bond et al. (2004)	4.7
Total BC			7.7
POM	Vegetation Fires	van der Werf et al. (2003)	34.7
	Biogenic	Guenther et al. (1995)	19.1
	Fossil-Fuel and Bio-Fuels	Bond et al. (2004)	12.5
Total POM			66.3
SSA	Wind driven	Schulz et al. (2004)	5868.6
DU	Wind driven	Tegen et al. (2002)	1060.6

Table 3.1: Aerosol and aerosol precursor emissions used in the HAM model. Global annual mean in Tg yr^{-1} and Tg(S) yr^{-1} for sulfuric species.

(2002) are introduced and compared to DMS sea surface concentrations simulated within the marine biogeochemistry model HAMOCC5. In the atmosphere part the main focus is the evaluation of the simulated DMS concentration in the atmosphere.

3.3 Ocean

A detailed description of the simulated ocean and biochemical mean state of MPI-OM/HAMOCC5 is given in Wetzel (2004). On average, the simulated global net primary production is 24 GtC $year^{-1}$. The export production, defined as the part of the net primary production that is transported out of the euphotic zone, amounts to 5 GtC $year^{-1}$. This is on the low end of model and observational estimates (Oschlies, 2002). The global annual averaged export of calcium carbonate is 0.27 GtC $year^{-1}$, which leads to a rain ratio (the ratio of calcium carbonate to organic carbon in export production) of 0.06 on average. This ratio lies within current estimates (Sarmiento et al., 2002) and leads to a realistic alkalinity distribution. Wetzel (2004) shows that the model is able to reproduce chlorophyll distribution from the SeaWIFS Satellite, except for the coastal regions, where shelf processes and riverine input of nutrients are not captured by the global model. Additionally, the model tends to simulate higher chlorophyll concentrations in the Southern Ocean and in the subtropical gyres than derived from satellite observations. Wetzel (2004) concludes that this might be predominantly a result of the modeled ocean dynamic with too strong vertical mixing in the Southern Ocean and a too weak down-

welling in the subtropical gyres.
A novel feature of the coupled model used in this study, is that dust deposition fields are calculated interactively in the atmospheric model and passed once per day to the ocean, instead of prescribing the dust deposition from climatological mean fields. This provides the means to apply this model for longterm climate change simulations including the effects of varying dust depositions, caused by climate change, on the marine biogeochemistry and on the DMS sea surface concentration. Assuming an iron content in dust of 3.5% we simulated an annual global mean iron deposition flux of 666 Gmol(Fe) yr^{-1}, whereas 204 Gmol(Fe) yr^{-1} are deposited to the ocean surface. The iron deposition onto the ocean surface lies within the range used in other global marine biogeochemistry studies (Fung et al. (2000): 118 Gmol(Fe) yr^{-1}, Aumont et al. (2003): 149.7 Gmol(Fe) yr^{-1}, Archer and Johnson (2000): 131.7 - 487.4 Gmol(Fe) yr^{-1}). The wide range given in the global iron deposition rates highlights the uncertainties in the iron content of dust particles, as in the magnitude and the size variation of the dust emission into and deposition from the atmosphere.
In the following section we will focus on the simulated DMS sea surface concentrations and compare our results to measurements as well as to a recently developed DMS algorithm by Simó and Dachs (2002).

3.3.1 DMS in the ocean

HAMOCC5 simulates a global total DMS production of 351 Tg(S) yr^{-1}. The loss of DMS in the ocean proceeds mainly via the consumption by bacteria (294 Tg(S) yr^{-1}). The DMS flux into the atmosphere (28 Tg(S) yr^{-1}) accounts for 8% of the global DMS removal in the ocean, the photo-oxidation (31 Tg(S) yr^{-1}) for 9%. The relative rates of the decay processes are not well constrained through measurements, in particular on a global scale. Archer et al. (2002) found a DMS flux equivalent to 10% of the DMS production in a six day Lagrangian experiment conducted in the northern North Sea. DMS removal by bacterial consumption accounted for the majority of the DMS removal (62-82% for surface levels and 98% for subsurface levels). Similar findings are reported for the Eastern Tropical Pacific where measurements show a 3 to 430 times faster removal of DMS by biological consumption than by the DMS flux into the atmosphere (Kiene and Bates, 1990) and for the North East Pacific where biological consumption accounted for 67% of the total DMS consumption and the DMS flux into the atmosphere accounted for only a small fraction (1%) of the DMS loss (Bates et al., 1994). The simulated annual mean decay rates are in accordance with these findings. However, for an evaluation of the simulated production and decay processes more measurements are needed.

The simulated seasonal mean sea surface concentrations of DMS are shown in Figure 3.1. The predicted DMS concentrations show high values throughout the year, generally exceeding 1-2 nmol l^{-1}, in the biological active upwelling zones like the equatorial Pacific Ocean, or in the upwellings off Peru and Angola. The subtropical gyres in both hemispheres show low DMS sea surface concentrations. The polar oceans (North Pacific, North Atlantic and Southern Ocean) feature high DMS concentrations in the respective summer season with values up to 20 nmol l^{-1} in the Southern Ocean.

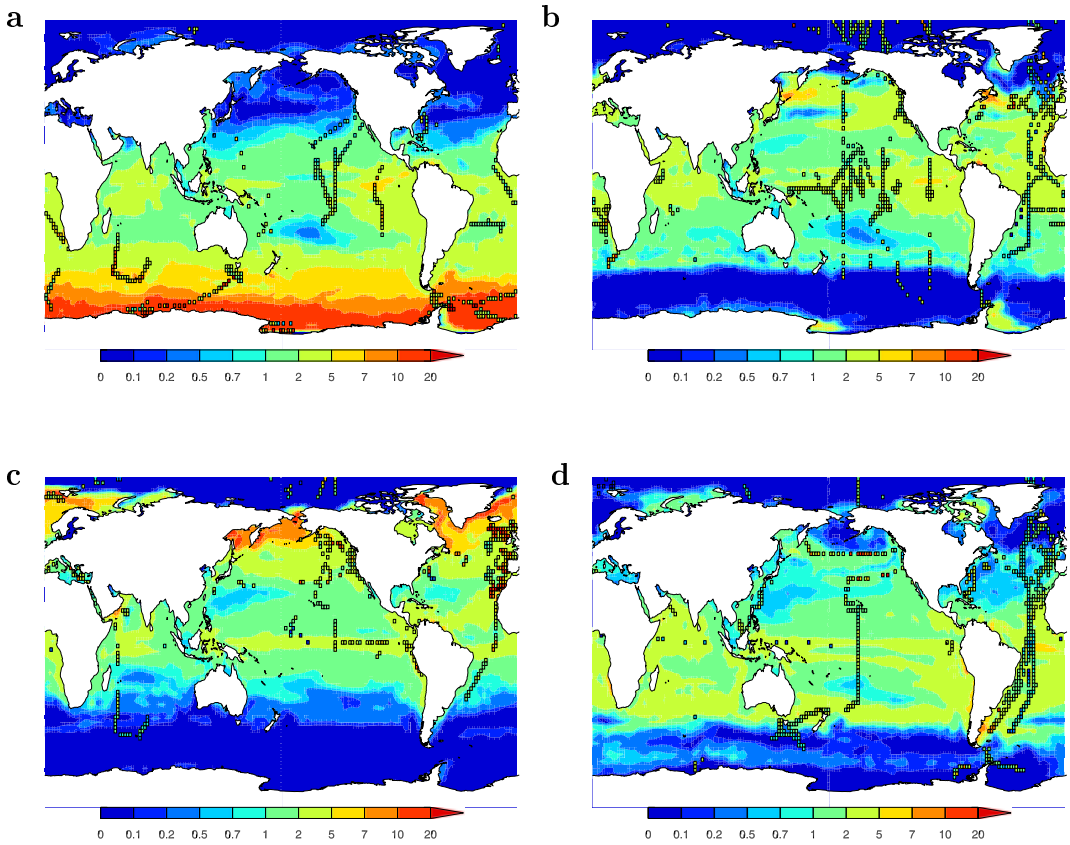

Figure 3.1: Modeled seasonal mean DMS sea surface concentration. a: Mean for December, January, February; b: Mean for March, April, May; c: Mean for June, July, August; d: Mean for September, November, December. Overlaid grid boxes are ocean data points given in the Kettle and Andreae (2000) database (data points where the ocean depth is below 300 m are excluded) gridded onto the model grid. Units are nmol l^{-1}.

The predicted annual global mean DMS sea surface concentration lies with 1.8 nmol l^{-1} within the range of annual mean concentrations from recently published DMS climatologies (Kettle et al. (1999): 2.1 nmol l^{-1}, Kettle and Andreae (2000): 2.0 nmol l^{-1}, Anderson et al. (2001): 2.6 nmol l^{-1}, Aumont et al. (2002): 1.7 nmol l^{-1}, Simó and Dachs (2002): 2.3 nmol l^{-1}, Chu et al. (2003): 1.5 nmol l^{-1}, Belviso et al. (2004b): 1.6 nmol l^{-1}; global numbers taken from Belviso et al. (2004a)).
Figure 3.2a compares the percentage frequency distribution of the DMS sea surface concentration with the percentage frequency distribution of measurements as given in the Kettle and Andreae (2000) database. The data points of the Kettle and Andreae (2000) database were distributed onto the model grid on a monthly mean basis and only corresponding model values are taken into account. Data points where the ocean depth is less than 300 m are excluded. Values with DMS sea surface concentrations higher than 20 nmol l^{-1} are not shown. The measurements show 32 data points with DMS sea surface

concentrations higher than 20 nmol l^{-1}, in the simulation we find 25 values. The percentage frequency distribution shows a good agreement between model and observations. The percentage frequency distributions show highest values for low DMS sea surface concentrations, whereas the observations exhibit a maximum of 1.0 to 1.5 nmol l^{-1} and the simulation for 1.5 to 2.0 nmol l^{-1}. Moderate DMS sea surface concentrations (2.5 to 5.5 nmol l^{-1}) are less frequent in the simulation than in the observations. For higher DMS sea surface concentrations (10 nmol l^{-1} and higher) both the model and the observations show a very low frequency with less than 1%. Overall the model tends to underestimate DMS sea surface concentrations in the moderate DMS regimes, but it captures the high frequency of low DMS sea surface concentrations and the low frequency of the high DMS sea surface concentrations. Since the Kettle and Andreae (2000) database was used for the optimization of the model parameters the comparison might be misleading. For an independent evaluation we compare the simulation with the updated version of the Kettle and Andreae (2000) database (Global Surface Seawater Dimehylsulfide (DMS) Database, available at http://saga.pmel.noaa.gov/dms/) which has been extended by additional 12,866 DMS sea surface measurements from 10 different measurement campaigns. Compared to the Kettle and Andreae (2000) database the data coverage of the additional measurements is sparser. By gridding the measurement data points onto the model grid, only 572 grid boxes are assigned to an annual mean DMS sea surface concentration value, whereas the Kettle and Andreae (2000) data points cover 2301 grid boxes. The percentage frequency distribution is displayed in Figure 3.2b. Similar to the Kettle and Andreae (2000) database the observations show the highest frequency for DMS sea surface concentrations in the range 1.0 to 1.5 nmol l^{-1} and the simulation in the range 1.5 to 2.0 nmol l^{-1}. The agreement for moderate DMS sea surface concentrations (2.5 to 5.5 nmol l^{-1}) is reasonably well, whereas higher DMS sea surface concentrations are less frequent in the simulation.

Monthly latitudinal profiles of the model results, the Kettle and Andreae (2000) database data and the DMS sea surface climatology from Kettle and Andreae (2000) are compared in Figure 3.3. Only data points where the ocean depth is above 300 m are used. As DMS is a product of marine biological activity, the DMS sea surface concentration has large seasonal variations. This is especially pronounced in the high latitudes where DMS concentrations peak in the Southern Hemisphere in December and in the Northern Hemisphere in June. The amplitude of the seasonal variation is lower in the model than in the Kettle and Andreae (2000) climatology. However, the climatology in this region is based only on a few data points. In the tropics the modeled DMS sea surface concentrations stay almost constant with 2-3 nmol l^{-1} throughout the year. This value is confirmed by measurements in these latitudes and present as well in the Kettle and Andreae (2000) climatology. Overall the model simulates the observed DMS sea surface concentrations reasonably well.

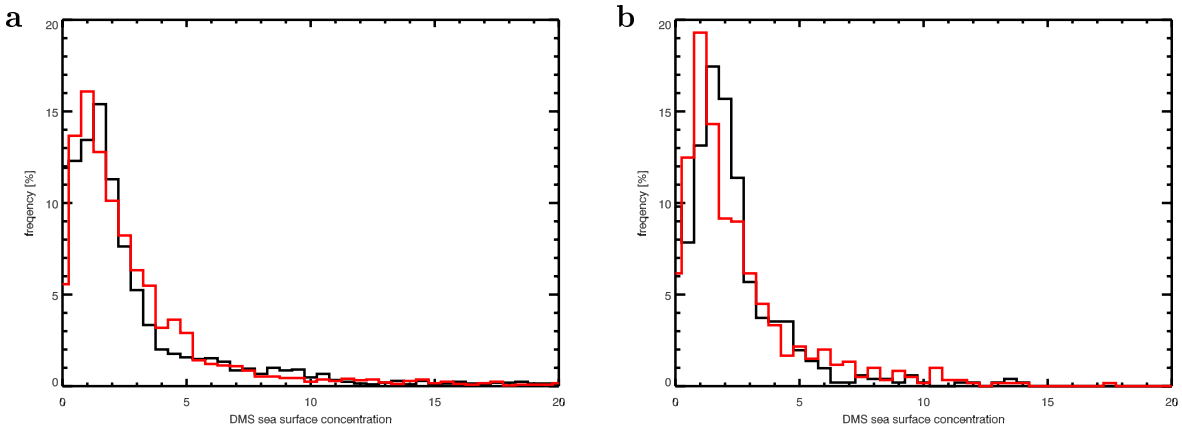

Figure 3.2: Frequency distribution of simulated and measured DMS sea surface concentrations. a) Measurements from the Kettle and Andreae (2000) database. b) Measurements obtained from http://saga.pmel.noaa.gov/dms/, excluding the measurements of the Kettle and Andreae (2000) database. The measurements are gridded onto the model grid. The simulated distribution is shown in black, the measured distribution in red. Data points with an ocean depth greater than 300 m are excluded.

3.3.2 DMS concentration predicted from mixed layer depth and chlorophyll α

Simó and Dachs (2002) developed a two equation algorithm to predict DMS sea surface concentrations using chlorophyll α surface concentration (CHL) and the mixed layer depth (MLD) of the ocean. Our model setup allows to apply the proposed algorithm to the simulated MLD and sea surface chlorophyll α concentration. We compare the resulting DMS sea surface concentration to the one given in Simó and Dachs (2002) using climatological input fields and to the one simulated within the marine biogeochemistry model. The DMS algorithm is formulated by Simó and Dachs (2002) as follows:

$$DMS = -ln(MLD) + 5.7, \qquad CHL/MLD < 0.02 \tag{3.1}$$

$$DMS = 55.8(CHL/MLD) + 0.6, \qquad CHL/MLD \geq 0.02 \tag{3.2}$$

The units of MLD are m, of CHL are mgm^{-3}, and of DMS sea surface concentrations are nmol l^{-1}. The algorithm is based on the assumption of Simó and Pedrós-Alió (1999) that vertical mixing plays a major role in controlling the production of DMS in the sea surface layers. They found that DMS is quantitatively related to the ratio of chlorophyll α and MLD, leading to high DMS concentrations not only associated with high chlorophyll α concentrations but also with moderate chlorophyll α concentrations and a concurrent shallow MLD. They explained this relation with the fact that a shallow mixing tends to favor phytoplankton blooms of taxa with a high DMSP cell content. Simó and Dachs (2002) derived global monthly DMS sea surface concentrations using a global monthly climatology for the MLD (Samuel and Cox' GFDL Global Oceanographic Data Set Atlas, available at http://dss.ucar.edu/datasets/ds279.0/) and chlorophyll α concentrations

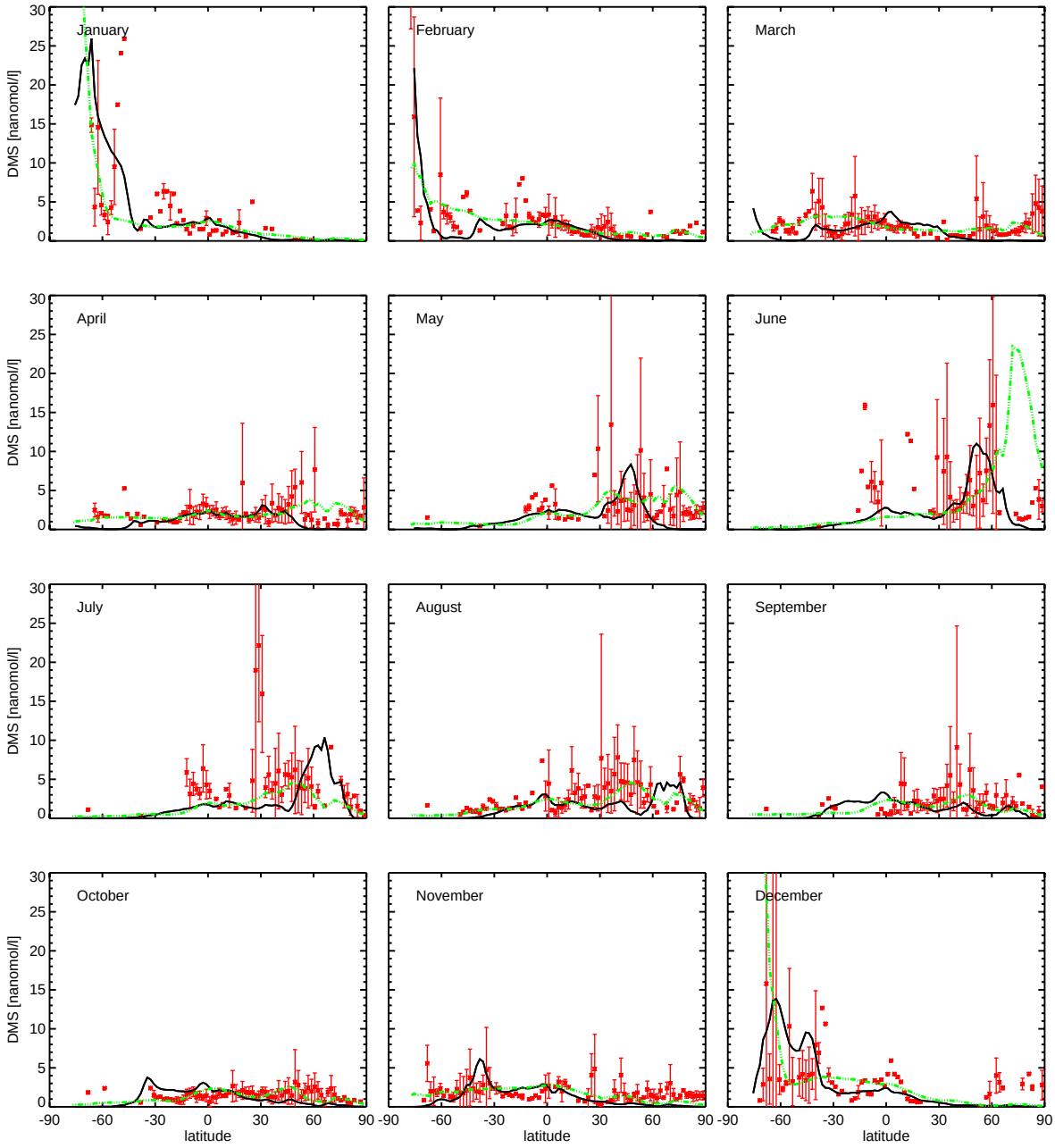

Figure 3.3: Zonally averaged profiles of DMS sea surface concentrations for all months. The black line represents the zonal average of the modeled DMS sea surface concentration, the green line the zonal average of the Kettle and Andreae (2000) DMS sea surface climatology. The red symbols represent the zonally averaged ocean data points given in the Kettle and Andreae (2000) database (data points where the ocean depth is below 300 m are excluded) gridded onto the model grid. Where more than one ocean grid box is present, the standard deviation is given by the red vertical line. Units are nmol l^{-1}.

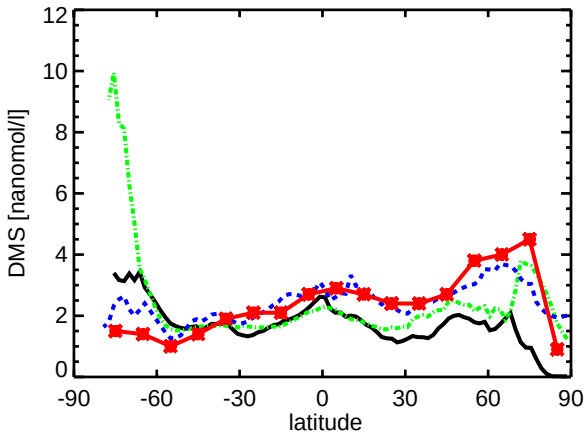

Figure 3.4: Zonal annual means of sea surface DMS for the Simó and Dachs (2002) algorithm using the simulated MLD and chlorophyll α concentrations (dashed blue line), resulting concentrations from the simulation using the marine biogeochemistry model HAMOCC5 (black line), annual mean DMS sea surface concentrations averaged over 10 ° latitudinal bands given in Simó and Dachs (2002) using climatological MLD and chlorophyll α concentrations from SeaWiFS (red stars) and for the Kettle and Andreae (2000) climatology (dotted green line). Units are nmol l^{-1}.

from SeaWiFS averaged over the period September 1997 to November 2000. The MLD is equally defined by the density criterion as in our simulation (depth where $\Delta\sigma_t = 0.125$ relative to the surface). We applied the proposed relationship using the simulated MLD and chlorophyll α concentrations. In about 80% of the total ocean surface, the ratio CHL/MLD is < 0.02 and Equation 3.1 applies. If the MLD exceeds 298 m, Equation 3.1 predicts negative DMS values. This is the case for 9% of the total ocean surface. We excluded these values. A monthly mean MLD deeper than 298 m is simulated in the winter months in the North Atlantic and in the Southern Ocean. This is consistent with observations and also present in the Samuel and Cox MLD climatology, whereas here only 2% of the ocean surface shows a monthly mean MLD deeper than 298 m. Figure 3.4 shows the resulting zonal annual mean DMS sea surface concentrations compared to the concentrations obtained from our simulation, the concentrations from Simó and Dachs (2002) using climatological input fields and the concentrations from the Kettle and Andreae (2000) climatology. The DMS sea surface concentration derived from the Simó and Dachs (2002) algorithm with simulated MLD and chlorophyll α concentration is comparable to the one derived by Simó and Dachs (2002) using a MLD climatology and chlorophyll α concentrations from SeaWiFS. Discrepancies occur in the high latitudes where during the summer months high chlorophyll α concentrations persist and predominantly Equation 3.2 applies. The DMS sea surface concentration resulting from the simulated MLD and chlorophyll α concentration is higher in the southern high latitudes and slightly lower in the northern high latitudes. The lower values in the northern high latitudes are caused by a simulated deeper mixed layer depth compared to the Samuel and Cox climatology.

For the southern high latitudes high simulated chlorophyll α concentrations lead to high DMS sea surface concentrations. The simulated chlorophyll α concentrations are slightly higher than the satellite estimates and probably overestimated by the model (Wetzel, 2004). However, particularly in the high latitudes the climatological fields comprise large uncertainties which are caused by a sparse data coverage for the MLD and by frequent cloud contamination for the satellite derived chlorophyll α concentration.
The simulated DMS sea surface concentration using the DMS formulation introduced in the marine biogeochemistry model HAMOCC5 results in distinct different zonal annual mean concentration variations compared to DMS sea surface concentration derived with the Simó and Dachs (2002) algorithm. Particularly in the Northern Hemisphere our simulation results in significantly lower DMS sea surface concentrations which are in agreement with the measurements given in the Kettle and Andreae (2000) database and present as well in the DMS sea surface climatology from Kettle and Andreae (2000). Both show a minimum in the DMS sea surface concentration around 30 ° N which is not captured with the Simó and Dachs (2002) algorithm. Discrepancies are highest in the northern high latitudes. In the late summer, with moderate chlorophyll α concentrations in the northern high latitudes, the Simó and Dachs (2002) algorithm predominately relies on the MLD only. This results in a broadening of the summer maximum leading to high annual mean DMS sea surface concentration in this region. The Kettle and Andreae (2000) climatology shows as the Simó and Dachs (2002) algorithm high DMS sea surface concentrations in the northern high latitudes. The high values in the climatology are probably caused by the inclusion of DMS measurements from the North Sea region. We excluded these datapoints for the optimization of our DMS formulation. The remaining measurements mainly show DMS sea surface concentrations around 1-2 nmol l^{-1} (see Figure 3.3) which is consistent with our simulation.

3.3.3 DMS sea-air exchange

As described in section 2.2.1 we use the DMS sea-air exchange parameterization according to Wanninkhof (1992) using the 10 m wind speed and the sea surface temperature provided by the atmospheric model ECHAM5 to calculate the DMS flux interactively in the model. The resulting global annual mean DMS flux is 28 Tg(S) yr^{-1}. Estimates of the global DMS flux differ widely depending mainly on the used DMS sea surface climatology, sea-air exchange parameterization, and wind speed data, ranging from 16 Tg(S) yr^{-1} up to 54 Tg(S) yr^{-1} (see e.g. Kettle and Andreae (2000) for a review). Kettle and Andreae (2000) calculated a global DMS flux between 27 and 32 Tg(S) yr^{-1} with their DMS sea surface climatology applying the same sea-air exchange parameterization (Wanninkhof, 1992) and four different combinations of data sets for the wind speed and sea surface temperature. Our simulated global annual mean DMS flux is in agreement with their findings. Figure 3.5 displays the global distribution of the annual mean DMS flux into the atmosphere. The distribution of the DMS flux is closely related to the DMS sea surface distribution (c.f. Figure 3.1). High DMS fluxes persist in regions with high DMS sea surface concentrations, such as the equatorial Pacific and Atlantic Ocean and in high

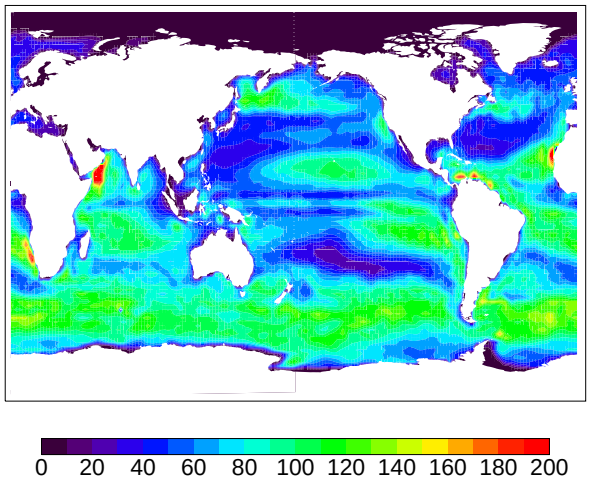

Figure 3.5: Annual mean DMS flux into the atmosphere. Units are mg(S) m^{-2} yr^{-1}.

wind speed regions, e.g. the broad band with elevated DMS emissions in the Southern Ocean between 40 ° and 60 ° S.

3.4 The atmospheric sulfur cycle

Global budgets

Table 3.2 summarizes the characteristics of the global DMS and sulfur budgets. Globally, the DMS emission flux is 28 Tg(S) yr^{-1}. The highest emissions are simulated in the Southern Hemisphere (17.6 Tg(S) yr^{-1}). Compared to the total SO_2 source resulting from SO_2 emissions from anthropogenic sources, wildfires and volcanic eruptions as prescribed from the AEROCOM emission scenario and SO_2 resulting from DMS oxidation, DMS accounts for 30% of the total sulfur source (14% in the Northern Hemisphere and 67% in the Southern Hemisphere). Globally, 84% of the DMS is removed via oxidation by OH radicals. This ratio is close to the one reported in other studies using similar DMS reaction mechanisms (Berglen et al. (2004): 73%, Chin et al. (2000): 88%, Pham et al. (1995): 86%). Oxidation by NO_3 is more important in the Northern Hemisphere (8.7%) than in the Southern Hemisphere (6.5%). The annual global mean DMS burden is with 0.08 Tg(S) in agreement with other studies (Chin et al. (2000): 0.07 Tg(S), Koch et al. (1999): 0.06 Tg(S), Pham et al. (1995): 0.05 Tg(S)) as is the lifetime with 1.0 days (Chin et al. (2000): 2.0 days, Koch et al. (1999): 1.9 days, Pham et al. (1995): 0.9 days). The chemical conversion is the major sink for SO_2 (78%). The dry deposition accounts for only 18% of the total removal. This is low compared to other studies, as already pointed out by Stier et al. (2005a). The serial resistance dry deposition scheme used here results in significantly lower SO_2 dry deposition fluxes compared to other studies (Ganzeveld et al., 1998). The low dry deposition sink results in a high yield of SO_4^{2-} from the chemical conversion of SO_2 into SO_4^{2-}. SO_4^{2-} is mainly wet deposited (95%). Dry

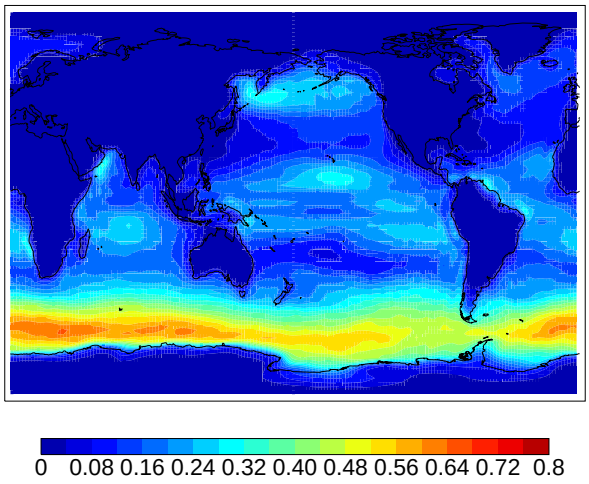

Figure 3.6: Annual mean DMS column burden. Units are mg(S) m^{-2}.

deposition accounts for 3% and sedimentation for 2% of the total SO_4^{2-} removal.

3.4.1 DMS in the atmosphere

The annual global distribution of the DMS burden is displayed in Figure 3.6. Highest burdens persist in the Southern Hemisphere, in particular around 60 ° S. This agrees with the high DMS flux simulated in this region. Additionally, DMS experiences a longer lifetime in the Southern Hemisphere compared to the Northern Hemisphere (1.15 days compared to 0.78 days, respectively). In the industrialized Northern Hemisphere, high NO_3 levels ensure a steady oxidation of DMS even during nighttime when OH concentrations are zero. About 88% of DMS emitted in the Southern Hemisphere is oxidized by OH and 12% by NO_3. In the Northern Hemisphere, 77% is oxidized by OH and 23% by NO_3. In the Southern Hemisphere, the limited removal of DMS via NO_3 due to the low NO_3 concentrations leads to an accumulation of DMS and a higher atmospheric DMS burden compared to the Northern Hemisphere (0.056 Tg(S) compared to 0.021 Tg(S), respectively).

In Figure 3.7a simulated and observed seasonal variations of atmospheric DMS concentrations are compared at Amsterdam Island in the Southern Ocean (Sciare et al., 2000). Atmospheric DMS mixing ratios were measured on a daily basis from August 1990 to December 1999. Shown are monthly mean values. The simulated seasonal variation is in agreement with the observations. However, the summer maximum is overestimated and shifted by two months in the model. Highest concentrations are simulated in November (822 pptv), whereas the observations show a maximum in January (557 pptv). Figure 3.7b shows the simulated SO_2 concentration at Amsterdam Island compared to measurements reported by Putaud et al. (1992). The measurements were taken for the period March 1989 to January 1991. The SO_2 concentrations show a similar seasonal variation as the DMS concentrations, both in the simulation and in the measurements. The amplitude of

	SH	NH	Global
DMS			
Source [Tg(S) yr^{-1}]:			
total:	17.8	9.8	27.6
Sinks [Tg(S) yr^{-1}]:			
oxidation with OH	15.8	7.5	23.3
oxidation with NO_3	1.8	2.4	4.2
burden [Tg(S)]:	0.056	0.021	0.077
lifetime [d] :	1.15	0.78	1.02
SO_2			
Source [Tg(S) yr^{-1}]:			
total (Emission + DMS oxidation)	25.9	69.3	94.2
Sinks [Tg(S) yr^{-1}]:			
oxidation	21.6	51.7	73.3
dry deposition	2.9	14.3	17.3
wet deposition	1.4	2.2	3.6
burden[Tg(S)]:	0.19	0.41	0.60
lifetime [d] :	2.7	2.2	2.4
$SO_{4\ gas}^{2-}$			
Source [Tg(S) yr^{-1}]:			
total (SO_2 gas oxidation)	8.7	18.3	27.0
Sinks [Tg(S) yr^{-1}]:			
condensation	8.7	18.2	26.8
nucleation	0.05	0.06	0.11
wet deposition	0.02	0.02	0.04
dry deposition	0.002	0.004	0.006
burden [Tg(S)]:	0.0003	0.0004	0.0007
lifetime [d] :	0.014	0.008	0.010
SO_4^{2-}			
Source [Tg(S) yr^{-1}]:			
total (Emission + SO_2 in cloud oxidation + condensation + nucleation)	24.4	53.9	78.4
Sinks [Tg(S) yr^{-1}]:			
dry deposition	0.6	1.8	2.5
wet deposition	23.3	50.8	74.1
sedimentation	0.56	1.29	1.85
burden [Tg(S)]:	0.24	0.49	0.73
lifetime [d] :	3.64	3.32	3.42

Table 3.2: Sulfur budget: global, Northern Hemisphere (NH) and Southern Hemisphere (SH). The lifetime is calculated as the ratio of the column burden to the sum of all sources.

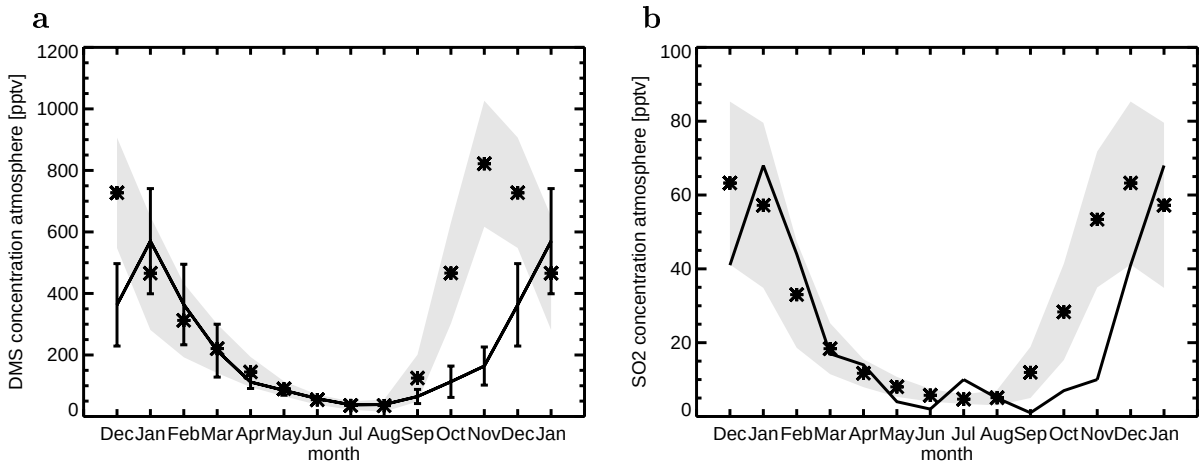

Figure 3.7: a) Atmospheric DMS on Amsterdam Island, measurements and standard deviation after (Sciare et al., 2000). b) Atmospheric SO_2 at Amsterdam Island, the measurements are reported by Putaud et al. (1992). The line represents the measurements, stars the model results. The grey shading indicates the monthly mean simulated standard deviation. Units are pptv.

the seasonal cycle which is defined by the ratio R = (average concentration for December, January and February) / (average concentration for June, July and August), is 8 for the measured as well as for the simulated SO_2 concentrations. The amplitude of the seasonal atmospheric DMS cycle is simulated equal to 9 and measured equal to 8 and is comparable to that of SO_2. The seasonal variation of the atmospheric DMS concentration at Amsterdam Island is largely driven by variations in the DMS sea surface concentration. The seasonal amplitude of the sea surface DMS is simulated equal to 9 and fits exactly the simulated seasonal cycle for DMS in the atmosphere (data not shown).

3.4.2 DMS contribution to SO_2 and SO_4^{2-} column burdens

In order to quantify the importance of DMS-derived SO_2 and SO_4^{2-}, we simulated the contribution of DMS-derived SO_2 and SO_4^{2-} to the total SO_2 and SO_4^{2-} concentration in the atmosphere. Additionally, this allows to use SO_4^{2-} concentration measurements in regions with a high DMS contribution for the evaluation of the DMS cycle.

SO_2 column burden

The spatial distribution of the total SO_2 column burden, the SO_2 column burden resulting from DMS, and the relative contribution of the DMS-derived SO_2 to the total SO_2 column burden are displayed in Figure 3.8. Shown are annual averages, averages for June, July and August and for December, January, and February. The same is shown for the SO_4^{2-}column burden in Figure 3.9. The respective global mean column burdens are sum-

marized in Table 3.3.
The global distribution of SO_2 column burdens resulting from all sources reflects the dominant anthropogenic sulfur sources in the Northern Hemisphere, most pronounced over the industrialized areas of Europe, North America, and China. The SO_2 column burden resulting from DMS emission alone highlights the strong seasonal variation of DMS in the atmosphere. The highest column burdens persist in the Southern Hemisphere for December, January, and February with values up to 1 mg(S)m^{-2} in high latitudes. The maximum in the Northern Hemisphere for June, July, and August is less pronounced. In the equatorial regions, the SO_2 column burden attributable to DMS stays almost constant throughout the year. The simulated high DMS sea surface concentration here causes a steady emission of DMS into the atmosphere and therefore a high load of SO_2 derived from DMS integrated over the atmospheric column. The relative contribution of DMS-derived SO_2 to the total SO_2 shows clearly the overwhelming role of DMS in the Southern Hemisphere during the biological active season. In December, January, and February the contribution is up to 90%.
The simulated global annual burden of SO_2 is 0.60 Tg(S), 25% of which can be attributed to DMS. Hence, DMS contributes globally less than proportional to the SO_2 column burden. The contribution of DMS to the SO_2 burden is greatest in the Southern Hemisphere (44%), whereas anthropogenic sources dominate in the Northern Hemisphere. DMS accounts for 16% of the total SO_2 column burden on the annual mean in the Northern Hemisphere. Even in the summer months (June, July, and August), when maximum DMS sea surface concentrations are simulated in the Northern Hemisphere, the contribution of DMS to the total SO_2 column burden is greatest in the Southern Hemisphere (32% compared to 17% in the Northern Hemisphere).

SO_4^{2-} column burden

The global distribution of the SO_4^{2-} column burden resulting from all sources shows highest burdens close to the main sources and the sources of its precursor SO_2 in the Northern Hemisphere (Figure 3.9). Significant export to low emission regions, for example the Middle East, North Africa, the North Pacific and the North Atlantic, occurs throughout the year. The SO_4^{2-} column burden resulting from DMS emissions alone shows almost the same distribution as the SO_2 column burden resulting from DMS. A high burden persists in the Southern Hemisphere in the summer season. The export of SO_4^{2-} into low emission regions cause a slight southward shift of the areas significantly influenced by DMS emissions. While for the SO_2 burden a contribution of DMS of 60 to 70% for December, January, and February is simulated in the equatorial regions of the Pacific and Atlantic, the contribution for SO_4^{2-} lies only between 40 to 50%.
The global annually averaged column burden of SO_4^{2-} is 0.73 Tg(S) with a DMS contribution of 27% globally. The greatest DMS contribution occurs in December, January and February with up to 37% globally and 57% in the Southern Hemisphere. The DMS contribution to the SO_4^{2-} burden lies within the same range as the DMS contribution to the SO_2 column burden. This is caused by the simulated fast chemical conversion rate of

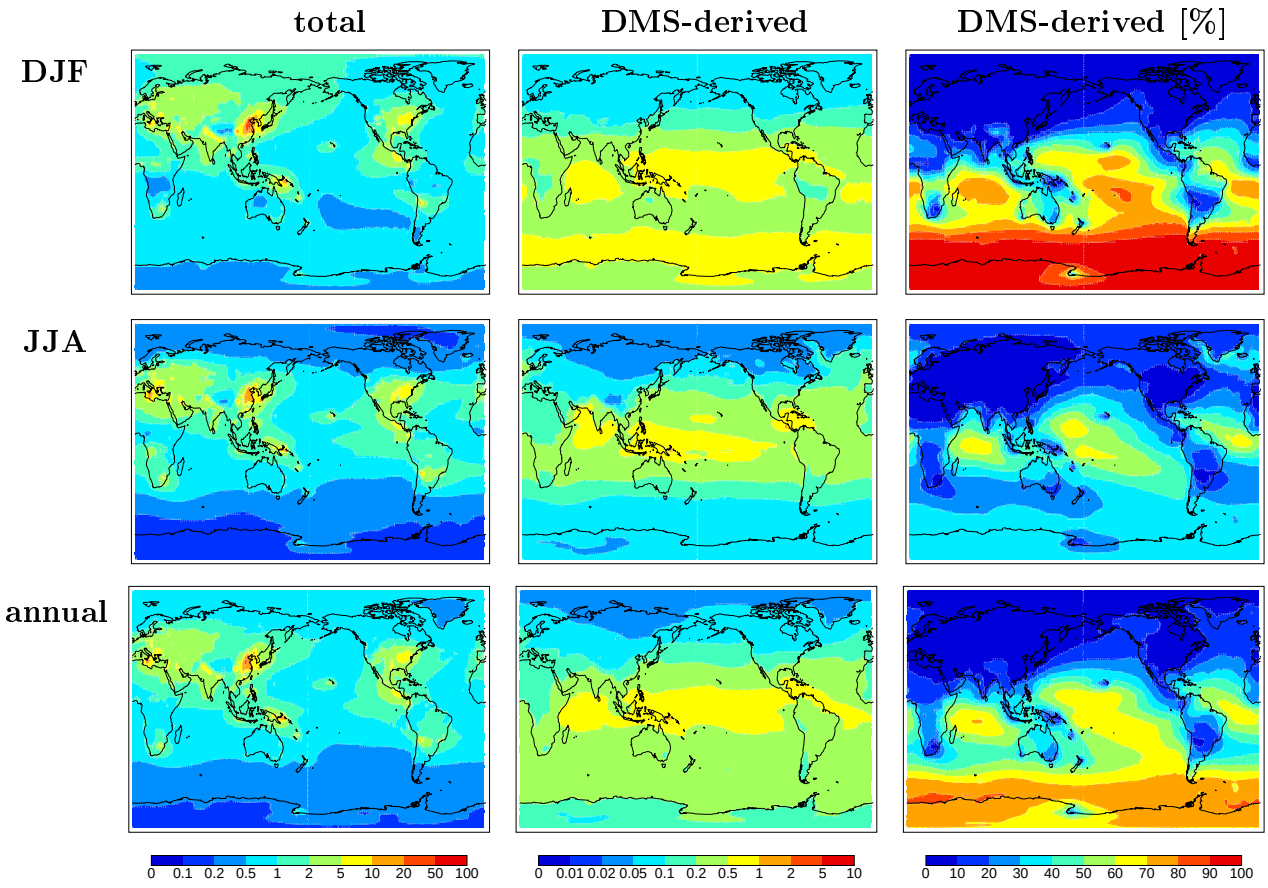

Figure 3.8: Mean column burdens of SO_2 averaged for December, January and February (DJF) and June, July and August (JJA) and annual mean values resulting from all sources (total), resulting solely from DMS (DMS-derived) and percentage of SO_2 attributable to DMS (DMS-derived [%]), respectively. Units are mg(S) m^{-2} and %, respectively.

SO_2 to SO_4^{2-}.

3.4.3 DMS-derived SO_4^{2-} in the atmosphere

The global distribution of the fraction of the SO_4^{2-} burden attributable to DMS shows the dominant role of DMS as SO_4^{2-} precursor in the Southern Hemisphere, in particular at high latitudes (Figure 3.8). A comparison of the simulated SO_4^{2-} concentrations with measurements in these remote regions therefore gives an indication of the representation of the DMS cycle in the model simulation. Several measurement networks include SO_4^{2-} surface concentration measurements. We choose the multi-annual measurements from the University of Miami network (Dennis Savoie, *pers.comm.*), as this network includes mainly measurements from remote sites. These measurements have been conducted mainly on islands or at coastal stations. The number of measurement years varies with site. The measurement locations are displayed in Figure 3.10. Red points indicate stations with a

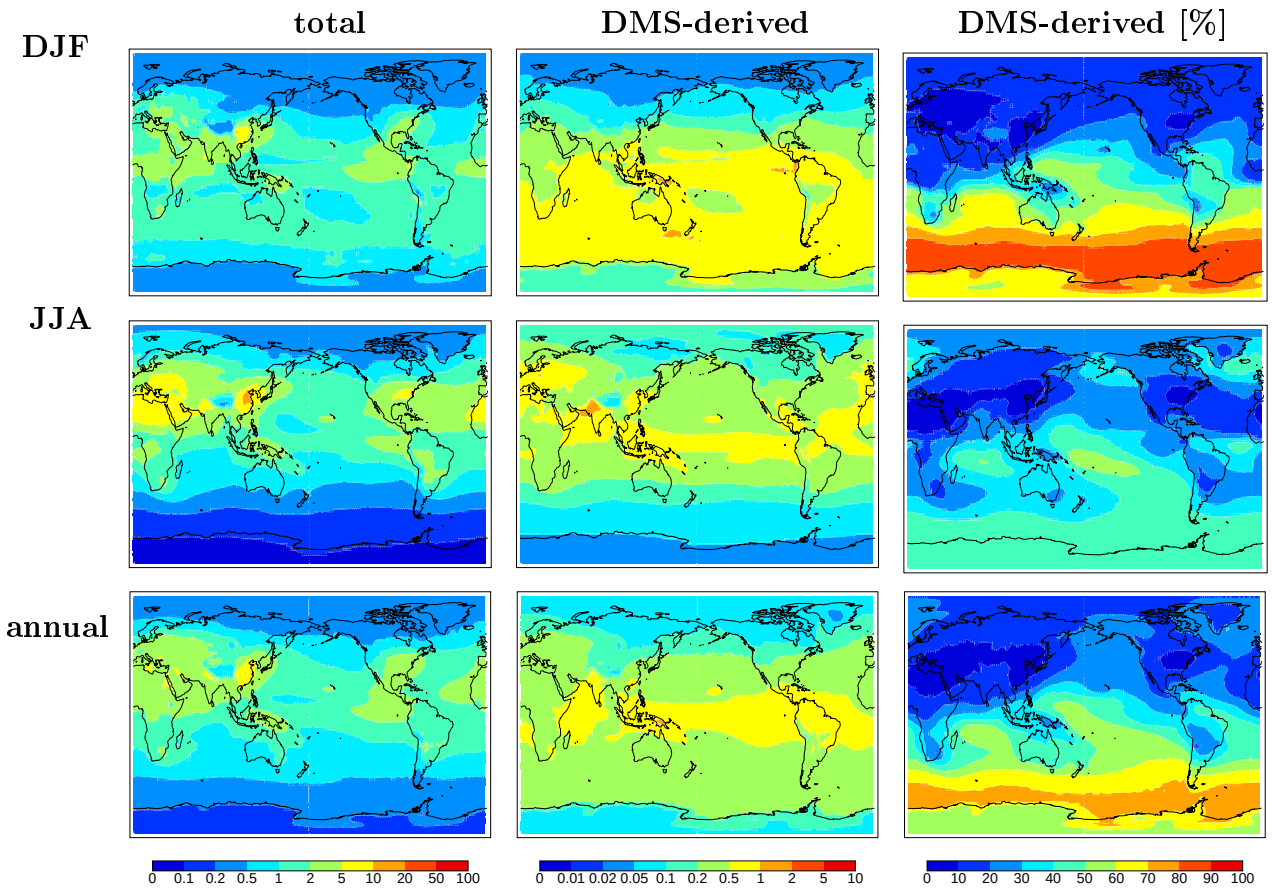

Figure 3.9: Mean column burdens of SO_4^{2-} averaged for December, January and February (DJF) and June, July and August (JJA) and annual mean values resulting from all sources (total), resulting solely from DMS (DMS-derived) and percentage of SO_4^{2-} attributable to DMS (DMS-derived [%]), respectively. Units are mg(S) m^{-2} and %, respectively.

	annual mean			December/January/February			June/July/August		
	global	NH	SH	global	NH	SH	global	NH	SH
DMS [Tg(S)]	0.077	0.021	0.056	0.151	0.013	0.137	0.048	0.032	0.016
SO_2 total [Tg(S)]	0.604	0.414	0.190	0.642	0.440	0.202	0.592	0.400	0.192
% of SO_2 from DMS	24.7	15.7	44.2	28.8	15.0	58.9	21.0	15.8	31.25
SO_4^{2-} total [Tg(S)]	0.733	0.493	0.240	0.674	0.363	0.311	0.813	0.617	0.195
% of SO_4^{2-} from DMS	26.7	17.8	45.0	37.2	20.7	56.6	21.3	17.5	33.3

Table 3.3: Annual mean column burdens of DMS, SO_2, SO_4^{2-} resulting from all sulfur sources (total) in [Tg(S)] and resulting only from DMS in [%].

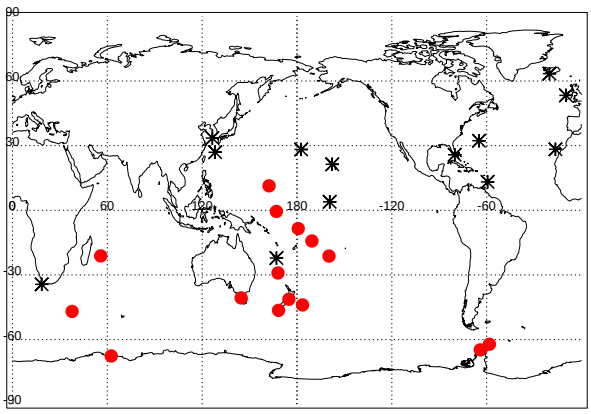

Figure 3.10: Location of the measurement sites included in the University of Miami network. Red points indicate stations with a simulated annual mean DMS contribution to SO_4^{2-}at the surface higher than 50%.

simulated annual contribution of DMS to SO_4^{2-} of more than 50% within the lowest model layer. These stations are mainly located in the Southern Hemisphere.

Figure 3.11 shows the scatter of the measured and simulated SO_4^{2-} surface concentration. Shown are monthly, annual, December, January and February, and June, July and August mean values. In addition, Table 3.4 lists the annual mean values for all measurement locations together with the relative contribution of DMS to SO_4^{2-} in the lowest model layer. Out of a total of 320 monthly mean samples, 213 (67%) agree within a factor of 2 with the measurements. The model overestimates the SO_4^{2-} surface concentrations especially for low concentrations. The lowest values reported coincide with locations where anthropogenic influences are low and where therefore the DMS contribution to SO_4^{2-} generally exceeds 50%. On the annual mean, 15 stations show a contribution of DMS abvove 50%. 9 of these stations lie within a factor of 2 within the measurement values. At the remaining stations the concentrations are all overpredicted by the model. This becomes exceedingly evident for the Southern Hemisphere summer season (mean over December, January and February) where the DMS sea surface concentration and the DMS emission are high. DMS contributions higher than 50% appear in 17 stations. For 12 stations with a contribution higher than 50%, the simulated values are a factor of 2 higher than the measured values. During the winter months (mean over June, July and August) DMS contributions higher than 50% exist for only 5 locations, 2 of which show higher simulated than measured values. In summary, for remote measurement stations the simulated SO_4^{2-} surface concentrations are in agreement with the reported measurement values. Discrepancies from the observed values are highest for locations with a high DMS contribution, in particular in the summer season of the Southern Hemisphere. Here the model overpredicts the averaged observed concentrations by a factor of 2.3. This overestimation may be caused by too high DMS emissions in these regions which are either due to too high DMS sea surface concentrations or too high sea-air exchange rates. The simulated DMS

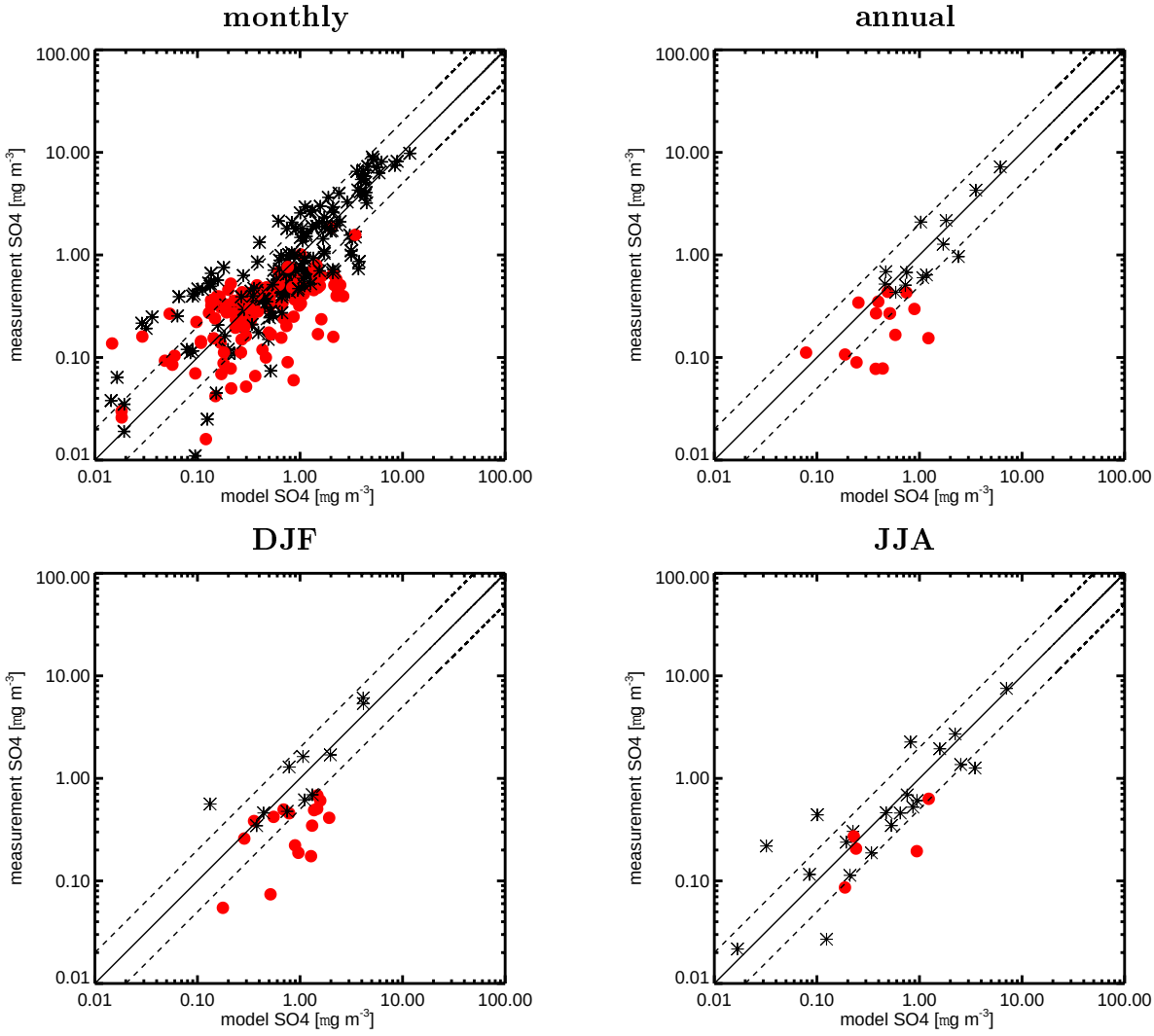

Figure 3.11: Scatter plots of measured and simulated surface aerosol mass concentration of SO_4^{2-}. Measurements are from the University of Miami network. a) Monthly mean, b) annual mean, c) mean for December, January and February, d) mean for June, July and August. Red symbols indicate a contribution of DMS to SO_4^{2-} higher than 50%. The solid line indicates the 1:1 ratio, the dashed lines the 1:2 and 2:1 ratios. Units are μg(S) m^{-3}.

sea surface concentrations in summer in the Southern High Latitudes are very high compared to other regions of the ocean. Measurements reported from these regions confirm these high concentrations in the sea surface layers. The model tends to slightly overestimate these high values. The differences lie thereby in the range of the standard deviation and only partly explain the too high simulated atmospheric SO_4^{2-} surface concentrations. The sea-air exchange rate parameterization used (Wanninkhof, 1992) leads to the highest flux compared to other existing sea-air exchange rate parameterizations (e.g. Nightingale et al., 2000; Liss and Merlivat, 1986). Differences in the DMS flux can be up to a factor of 2 (e.g. Kettle and Andreae, 2000; Boucher et al., 2003). Despite too high simulated DMS

emissions, one possible reason for the overestimated SO_4^{2-} surface concentration might be a missing reaction mechanism of DMS in the atmosphere preventing the formation of SO_4^{2-}. Several studies highlight the importance of the reaction of DMS with bromine oxide (BrO) radicals leading to the formation of DMSO (e.g. von Glasow and Crutzen, 2004; Boucher et al., 2003). This reaction mechanism is not included in our study. DMSO reacts with OH in the atmosphere, whereas the reaction products are uncertain. It has been postulated that dimethyl sulfone ($DMSO_2$) is the main oxidation product leading to the formation of methyl sulfinic acid (MSIA) and methyl sulfonic acid (MSA) (Yin et al., 1990). A 1-d model study for marine boundary layer conditions (von Glasow and Crutzen, 2004) shows that the inclusion of halogen chemistry increases the DMS destruction by about 25% in summer and 100% in winter time. The SO_2 yield from the oxidation of DMS is simulated to be lower when halogen chemistry is included. However, the lack of BrO measurements in the atmosphere makes a global assessment of the importance of the BrO oxidation difficult.

Location	Longitude	Latitude	Model annual mean [μg m^{-3}]	Measurements annual mean [μg m^{-3}]	DMS contribution to annual mean [%]
Chatham Island - New Zealand	-176.5	-43.9	0.52	0.27	59
Cape Point - South Africa	18.5	-34.3	1.08	0.60	37
Cape Grim - Tasmania	144.7	-40.7	0.89	0.30	51
Iinverargill - New Zealand	168.4	-46.4	0.49	0.44	60
Marsh - King George Island	-58.3	-62.2	0.38	0.27	52
Marion Island	37.8	-46.9	0.44	0.08	61
Mawson - Antarctica	62.5	-67.6	0.08	0.11	73
Palmer Station - Antarctica	-64.1	-64.8	0.24	0.09	63
Reunion Island	55.8	-21.2	0.40	0.35	54
Wellingtin - New Zealand	174.9	-41.3	0.75	0.43	52
Yate - New Caledonia	167.0	-22.1	0.59	0.43	45
Funafuti - Tuvalu	-179.2	-8.5	0.58	0.17	60
Nauru	166.9	-0.5	1.22	0.15	58
Norfolk Island	168.0	-29.1	0.51	0.27	55
Rarotonga - Cook Islands	-159.8	-21.2	0.19	0.11	65
American Samoa	-170.6	-14.2	0.25	0.34	64
Midway Island	-177.4	28.2	0.46	0.52	33
Oahu Hawaii	-157.7	21.3	0.73	0.51	33
Cheju - Korea	126.5	33.5	6.14	7.21	6
Hedo Okinawa - Japan	128.2	26.9	3.55	4.28	15
Fanning Island	-159.3	3.9	1.17	0.64	48
Enewetak Atoll	162.3	11.3	0.37	0.08	55
Barbados	-59.4	13.2	0.75	0.67	38
Izana Tenerife	-16.5	29.3	2.40	0.96	22
Bermuda	-64.9	32.3	1.03	2.09	22
Heimaey Iceland	-20.3	63.4	0.47	0.69	26
Mace Head - Ireland	-9.9	53.3	1.70	1.27	22
Miami	-80.2	25.8	1.82	2.17	18

Table 3.4: List of measurements sites from the University of Miami Network used in Figure 3.11.

3.5 Summary

The production of marine dimethylsulfide (DMS) and its fate in the atmosphere are simulated in a global coupled atmosphere-ocean circulation model. The processes for marine DMS production and decay are included in the representation of plankton dynamics in the marine biogeochemistry model HAMOCC5 embedded in a global ocean general circulation model (MPI-OM). The atmospheric model ECHAM5 is extended by the microphysical aerosol model HAM.
The simulated DMS sea surface concentrations generally match the observed concentrations. The model captures the seasonal variation with high DMS sea surface concentrations in high latitudes in summer. The global annual mean DMS sea surface concentration of 1.8 nmol l^{-1} lies within the range of DMS sea surface climatologies (e.g. Belviso et al., 2004a).
We apply our simulated mixed layer depth (MLD) and chlorophyll α concentration to the Simó and Dachs (2002) algorithm, to calculate DMS sea surface concentrations solely from this two quantities. The resulting zonal mean DMS sea surface distribution is comparable to the one derived by Simó and Dachs (2002) using climatological MLD fields and chlorophyll α concentrations from SeaWiFS. However, compared to the DMS sea surface concentration simulated with the biogeochemical model the Simó and Dachs (2002) algorithm results in distinct different DMS sea surface distributions. This is most pronounced in the Northern Hemisphere, with simulated values lower than the ones predicted from the Simó and Dachs (2002) algorithm.
The treatment of DMS in a coupled atmosphere-ocean model including a microphysical aerosol scheme and an atmospheric sulfur model allows to gain additional insight into the DMS representation in the model by a comparison with atmospheric DMS related measurements. The simulated DMS flux into the atmosphere is 28 Tg(S) yr^{-1} which is in the range of current estimates (e.g. Kettle and Andreae, 2000). The resulting column integrated burden of DMS in the atmosphere is 0.08 Tg(S) and the lifetime is 1.0 days. DMS contributes 30% to the total sulfur source considered in the model (sulfur emissions from fossil- and bio-fuel use, wildfires and volcanoes and sulfur from DMS oxidation). The contribution of SO_2 derived from oxidation of DMS by OH and NO_3 to the total SO_2 column burden is 25%. SO_2 is oxidized by OH in the gas phase and by H_2O_2 and O_3 in the aqueous phase to form SO_4^{2-}. 27% of the produced SO_4^{2-}can be attributed to DMS oxidation. The contribution is highest in the biologically active season in remote regions of the Southern Ocean with values up to 90%.
The comparison of SO_4^{2-} measurements and simulated SO_4^{2-} concentrations at remote sites where the contribution of DMS to SO_4^{2-} is generally high shows an overestimation of the SO_4^{2-} surface concentrations by the model, most pronounced in the biologically active season. Possible explanations are an overestimation of the DMS sea surface concentration, a too high sea-air exchange rate or a missing reaction mechanism of DMS in the atmosphere. The simulated DMS sea surface concentrations are generally in agreement with the observations. A direct validation of the DMS flux is not possible because it cannot yet be measured directly. A missing reaction of DMS in the atmosphere model is the reaction with BrO. It has been shown by several investigators that this reaction is

important in remote regions (e.g. von Glasow and Crutzen, 2004; Boucher et al., 2003). However, the concentration of BrO in the atmosphere is not well known which makes a global assessment not feasible.
The generally good agreement between model and measurements indicates that the DMS cycle in the model represents the processes governing DMS sea surface concentrations, DMS emissions and resulting atmospheric concentrations reasonably well. However, the lack of measurements of the consumption and production processes of DMS in the ocean hampers the full evaluation of the DMS formulation as a predictive tool for DMS in the atmosphere. Nevertheless, the DMS formulation applied in a coupled ocean-atmosphere model is a step forward in providing a model system to assess marine biosphere-climate feedbacks.

Chapter 4

The evolution of the DMS cycle in a transient climate simulation

In order to investigate the response of the DMS sea surface concentration, the DMS flux, and the DMS concentration in the atmosphere to climate change caused by anthropogenic perturbations the fully coupled global ocean-atmosphere model described in detail in the previous chapter was forced with the IPCC SRES A1B scenario for greenhouse gases, aerosol and aerosol precursor emissions. This chapter focuses on the response of the marine biology and the subsequent changes in the DMS emissions and DMS concentrations in the atmosphere to global warming caused by increasing anthropogenic activities. The main question is whether DMS emissions increase or decrease in a warmer climate. The results presented here have been submitted in this form to Global Biogeochem. Cycles.[1]

4.1 Simulation setup

The simulation is started from a control run using preindustrial conditions for the aerosol and aerosol precursor emissions, well-mixed greenhouse gases and ozone. Preindustrial conditions refer here to the assumed values for 1860, i.e. for the well-mixed greenhouse gases: CO_2=286.2 ppmv, CH_4=805.6 ppbv, N_2O= 276.7 ppbv, $CFC-11^*$=12.5 pptv, and $CFC-12$=0 ($CFC-11^*$ accounts for the effect of minor species, including a small contribution from natural sources). The respective emissions for the prescribed aerosol and aerosol precursors together with the interactively calculated emissions for the year 1860 are listed in Table 4.1. The model run is performed until a quasi steady state is reached, from then on the transient climate simulation is integrated until present-day conditions (simulation period: 1860-2000), and further onwards until the year 2100 following the SRES A1B scenario for the greenhouse gases as well as for the aerosol and aerosol precursor emissions.

Until 2000, the model takes into account the variation in solar irradiance according to Solanki and Krivova (2003), and influences of volcanic aerosols on the radiation by inclu-

[1] submitted as: S. Kloster, J. Feichter, E. Maier-Reimer, E. Roeckner, P. Stier, P. Wetzel, K.D. Six and M. Esch, Response of DMS in the ocean and atmosphere to global warming, to *Global Biogeochem. Cycles.*

		1860	maximum	1861–1890	2061—2090
SO_2	[Tg(S) yr^{-1}]	17.01	106.50 (2020)	19.91	49.83
BC	[Tg yr^{-1}]	1.28	30.65 (2080)	1.66	30.22
POM	[Tg yr^{-1}]	29.05	186.73 (2050)	31.39	180.57
Dust	[Tg yr^{-1}]	1171.11	-	1128.68	1203.50
Sea salt	[Tg yr^{-1}]	6295.09	-	6263.44	6252.47

Table 4.1: Aerosol and aerosol precursor emissions simulated and prescribed within the aerosol model HAM.

sion of the optical depth of volcanic aerosol above the tropopause level as estimated by Sato et al. (1993). We used the updated version available at
http://www.giss.nasa.gov/data/strataer. The well-mixed greenhouse gases are prescribed according to observations (smoothly fitted to ice core data, direct observations, and SRES values for the year 2000). Ozone is prescribed on a monthly basis in the troposphere and stratosphere following Kiehl et al. (1999). The offline monthly mean oxidant fields (OH, H_2O_2, NO_2, O_3) needed in the sulfur chemistry scheme are taken from calculations of the MOZART chemical transport model (Horowitz et al., 2003) representative for the year 2000. These fields are kept constant during the simulation period. This probably introduces an error in our simulation, as these concentrations are likely to change under changing climatic conditions and emissions. As a result of the increase in water vapour concentrations in the atmosphere in a warmer climate, chemical transport models show that the tropospheric oxidant concentrations of OH, H_2O_2, and O_3 are enhanced (e.g. Johnson et al. (1999), Gauss et al., 2003). The NO_2 emissions are slightly increasing between 2000 and 2050 (from 7.0 to 7.4 Tg(N) yr^{-1}) and are from then on reduced reaching in 2100 7.0 Tg(N) yr^{-1} according to the A1B storyline of the IPCC SRES scenario. We expect a similar variation in the atmospheric NO_2 concentrations. However, these changes are not included in our transient climate simulation. We will discuss the impact of this simplification in more detail in the summary chapter.
The aerosol and aerosol precursor emission fluxes of anthropogenic SO_2 and BC are prescribed based on an inventory derived by the Japanese National Institute for Environmental Studies (NIES) following the SRES A1B storyline from 2000 on (T. Nozawa et al., pers. comm., 2004). Sources for BC are fossil fuel combustion, domestic fuel wood consumption, agricultural waste burning, and vegetation fires. Apart from BC emissions from fossil fuel combustion and SO_2 fossil fuel emissions, which are prescribed annually, the other emissions are prescribed on a monthly mean basis. The POM emission flux is estimated from the BC emission flux using source specific emission ratios (F. Dentener, pers. comm.). The same applies to the SO_2 emissions from vegetation fires which are derived by a scaling of the BC emissions from vegetation fires. The transient evolution and the global distribution of the single emission fluxes and the resulting aerosol distributions are described in detail in Stier et al. (2005a). Here we only summarize the global annual mean emissions assumed for the preindustrial control run (assuming the emissions of the year 1860), the two periods of interest for the following analysis (1861–1890 and 2061–2090), and the year with the respective highest emissions (Table 4.1). Total SO_2

		1861–1890	2061–2090
organic carbon export	[GtC yr^{-1}]	4.23	3.71 (-12.4%)
$CaCO_3$ export	[GtC yr^{-1}]	0.257	0.260 (+0.9%)
$Si(OH)_4$ export	[Tmol(Si) yr^{-1}]	71.48	60.56 (-15.3%)

Table 4.2: Global mean simulated export productions within HAMOCC5. Values in parenthesis are percentage changes between the periods 1861–1890 and 2061–2090.

emissions (fossil fuel, volcanoes, and vegetation fires) peak at around 107 Tg(S) yr^{-1} in the year 2020. The POM emissions are dominated by the contribution from vegetation fires and peak in 2050 at 187 Tg(POM) yr^{-1}. The BC emissions show a peak later on (2080) amounting to 31 Tg(C) yr^{-1}. The interactively calculated sea salt emissions show no significant trend during the simulation period, whereas the dust emissions show an increase towards the end of the simulation period (between 1861–1890 and 2061–2090 the dust emissions are increased by around 6%).

4.2 Results

To separate the climate change signal from the interannual variability we analyse the difference between the mean state of two 30 year periods. We choose the periods 1861–1890 (19C) for preindustrial conditions and the period 2061–2090 (21C) for future conditions. We consider three aspects: First, we analyse changes in physical quantities affecting the biological production in the ocean and hence DMS sea surface concentrations and DMS emissions into the atmosphere. Second, we investigate the response of DMS sea surface concentrations and the DMS flux into the atmosphere to global warming. Third, we assess the resulting changes of DMS concentrations in the atmosphere. Finally, we summarize the findings by relating the observed changes to each other. Results are presented in terms of differences between future (21C) and pre-industrial conditions (19C). Following Roeckner et al. (2005), we test the significance of the differences by applying a non-parametric test, as the usual parametric Student's t test is only applicable for normal distributed parameters. The null hypothesis is formulated as follows: The difference (21C-19C) of any variable is within the range of variations between randomly chosen 30-year segments of a control run. In order to enlarge the sample size, not only data from the control run (100 years) are used, but also data from the detrended 20th century simulation. We estimate the distribution of differences by splitting the enlarged control sample (240 years) into 30-year periods taking the average for each period (8 means). By forming differences across all available 30-year means (n(n-1)/2)=28 differences are obtained. We then determine if the difference (21C-19C) is larger than the 95% percentile of this frequency distribution. If this is the case, we reject the null hypothesis with a risk of less than 5%.

4.2.1 Changes in the physical quantities affecting the biological production

Detailed descriptions of the atmospheric and oceanic physical mean state and the response to the global warming are presented elsewhere (e.g. Roeckner et al. (2005) focusing on changes in the atmosphere, Stier et al. (2005b) focusing on the evolution of the microphysical aerosol system, Jungclaus, J. et al. (2005) focusing on the change in the ocean circulation). Here we summarize the physical changes most relevant to future DMS sea surface concentrations and to the DMS flux into the atmosphere.
The transient evolution of the deviation of the global mean air and sea surface temperature and observed global mean temperature from the mean state 1961-1990 are shown in Figure 4.1. The warming signal observed since the late 19th century is well captured by the simulation. In the assumed IPPC SRES scenario A1B, the well-mixed greenhouse gases in the atmosphere show a strong increase from the late 19th century on, leading to a rapid increase in the global mean 2m temperature. In 2100, the global mean 2m temperature is predicted to rise by around 3.6°C compared to the mean state averaged over the period 1961-1990. The global mean sea surface temperature mirrors the rise in the global mean 2m temperature. The pattern of the sea surface temperature change shows the strongest warming, between 19C and 21C around 4°C, in the North Pacific (Figure 4.3a) and a minimum in the Southern Ocean and in the North Atlantic (due to high ocean heat uptake in areas of deep ocean mixing). Similar global warming patterns are evident in previous global climate change studies (e.g. Cubasch et al. (2001), Sarmiento et al. (2004)).

The warming of the atmosphere and ocean surface causes a melting of the sea ice. This has a direct impact on the DMS flux, which is inhibited in regions covered by sea ice. The melting accelerates during the first half of the 21th century (Figure 4.2). The annual mean sea ice areal coverage has declined by 44% around Antarctica in 21C compared to the initial state in 19C; the decline in the Arctic is even higher (-50%). In both hemispheres the summer season shows the strongest decline. In Antarctica the sea ice coverage is reduced by 70% . The summer season in the Arctic is almost ice free (-98%).
Under warmer climate conditions the 10m wind speed increases most noticeably in the central equatorial Pacific and the southern high latitudes (Figure 4.3b). The increase in the southern high latitudes combined with a decrease around 40° S is associated with a poleward shift of the storm tracks. This shift has also been observed in other global warming simulations and is related to changes in the zonal SST gradient of the Southern Hemisphere (e.g. Bengtsson et al. (2005)).

The increase in the sea surface temperature and an enhanced freshwater flux in the high latitudes induced by stronger rainfall (not shown) cause an overall reduction in the surface water density consequently enhancing the ocean stratification. The impact of increased stratification is reflected in the simulated mixed layer depth (MLD). The MLD is defined as the shallowest depth at which water density exceeds its surface value by 0.125 kg/m^3. The maximum MLD, defined as the deepest MLD of the year, decreases in most parts of the ocean (Figure 4.4a). The decline is strongest where the MLD is deep, for instance in the Southern Ocean and the North Atlantic. Only a few regions show an increase in

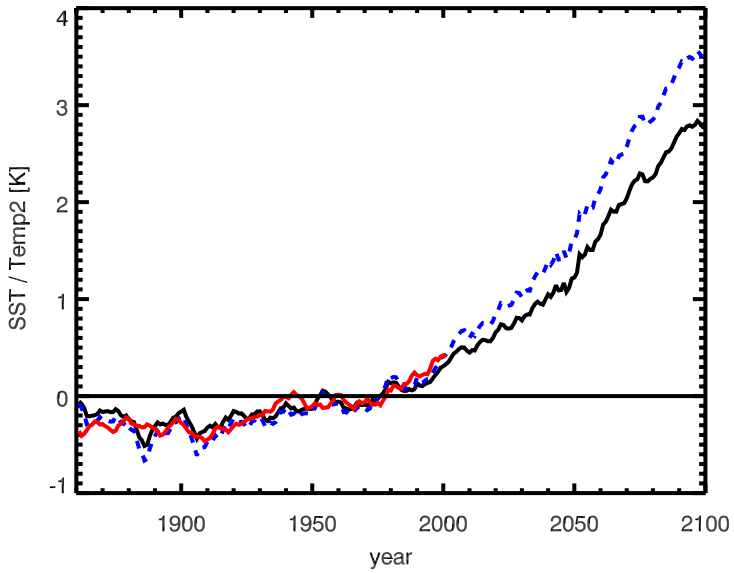

Figure 4.1: Temporal evolution of the deviation of the annual mean SST (solid black), annual mean 2m temperature (dashed blue) and observed annual mean temperatures (red line) from the mean state of 1960-1990 smoothed using a 5-year running mean. Units are [°C]. Observations are from P. D. Jones et al.: Global and hemispheric temperature anomalies - land and marine instrumental records, available at http://cdiac.ornl.gov/trends/temp/jonescru/jones.html.

the MLD. The shoaling of the maximum MLD is evident in most AOGMCs under global warming (e.g. Sarmiento et al. (2004), Manabe (1998)) and is accompanied by a reduction in the Atlantic meridional overturning circulation (19C: 22 Sv; 21C: 16 Sv). Changes in the maximum MLD greatly impact the vertical flux of nutrients into the surface ocean waters, stimulating or suppressing surface biological production (e.g. Quere et al. (2003), Bopp et al. (2001), Sarmiento et al. (2004)) and therefore influencing DMS production. The change pattern of the minimum MLD (Figure 4.4b) reflects the changes in the 10m wind speed (Figure 4.3b). An increase in the minimum MLD is found south of 50° S accompanied by a reduction between 40° and 50° S both caused by the poleward shift of the storm track region. Changes in the minimum MLD become important for the marine biology in regions where the primary production is predominantly light limited, such as in the Southern Ocean (e.g. Boyd (2002)).

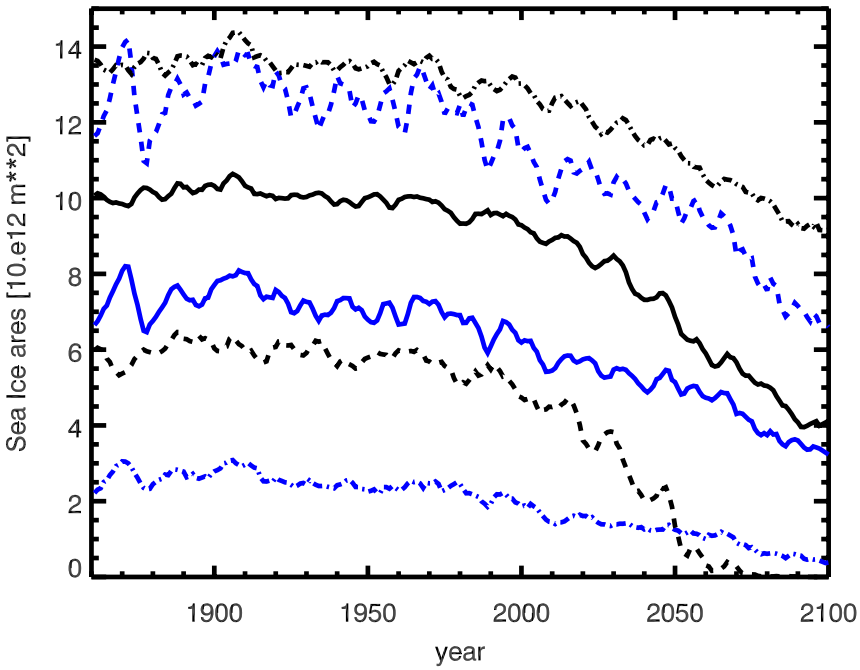

Figure 4.2: Temporal evolution of total sea ice areal coverage in the Artic (black) and Antarctic (blue) smoothed using a 5 year-running mean. Solid lines: annual mean, dashed lines: March mean, dashed-dotted line: September mean. Units are [Million km^2].

4.2.2 Response of DMS sea surface concentrations and DMS flux to climate change

The DMS sea surface concentration is controlled by the DMS production, DMS degradation, DMS emission and transport in the ocean. Simulated are the DMS production by phytoplankton, the consumption by bacteria, the photo-oxidation of DMS to DMSO in the surface waters, and the ventilation into the atmosphere. DMS production is parameterized as a function of the export of calcium carbonate and silicate. The export itself is driven by the changes in the total biological production which is influenced by the availability of nutrients, solar radiation, and, to a lesser extent, temperature (Quere et al. (2003), Bopp et al. (2001)). Before we discuss the changes in the DMS production and degradation we investigate changes in the driving factors of biological production and export in more detail.

Changes in the nutrient distribution

Limiting nutrients considered in HAMOCC5 are phosphate (PO_4), nitrate (NO_3), and iron (Fe). In general, the global warming induced stratification in the ocean reduces the

vertical transport of nutrients into the surface layers and subsequently the nutrient's surface concentrations. The surface concentration of phosphate in 21C is reduced by 6% compared to 19C (Table 4.2). The reduction for the nitrate surface concentration is of similar magnitude. The iron surface concentration is reduced by about 3%. The iron surface concentration depends, besides on the mixing into the surface layers, on the dust deposition onto the ocean surface. The explicitly simulated dust deposition increases by 6% between the periods 19C and 21C (Table 4.1). This increase is predominantly caused by higher dust emissions due to higher wind speeds in the Saharan northwestern source region and subsequent higher dust deposition into the equatorial Atlantic (not shown). This partly counteracts the reduction in sea surface iron through the shoaling of the MLD. However, as the changes in the dust deposition are largest in the equatorial Atlantic where

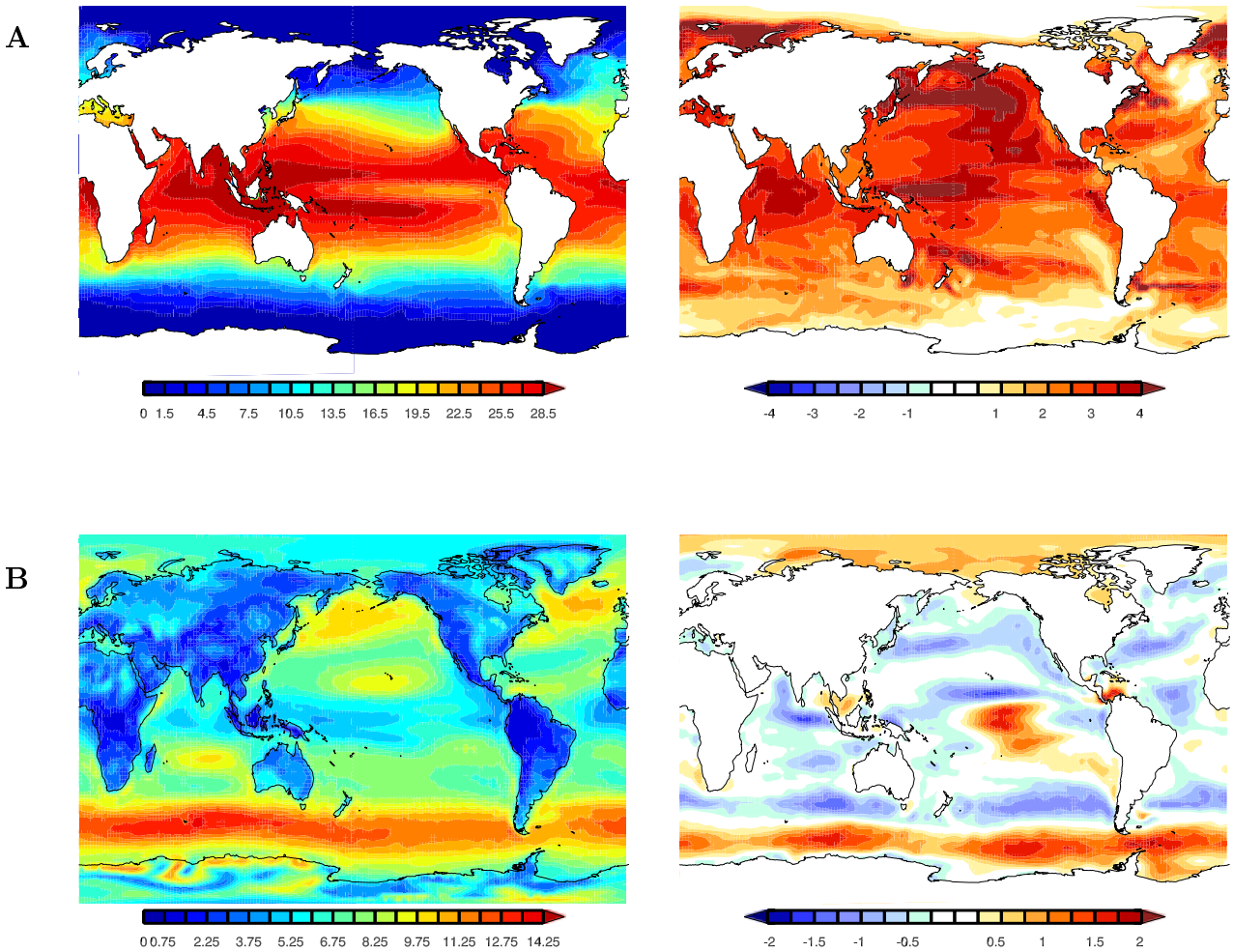

Figure 4.3: A: Annual mean sea surface temperature in [° C]. B: Annual mean 10m wind speed in [m/s]. Left-hand column: Mean values for the period 1861–1890. Right-hand column: Absolute changes between the periods 1861–1890 and 2061–2890.

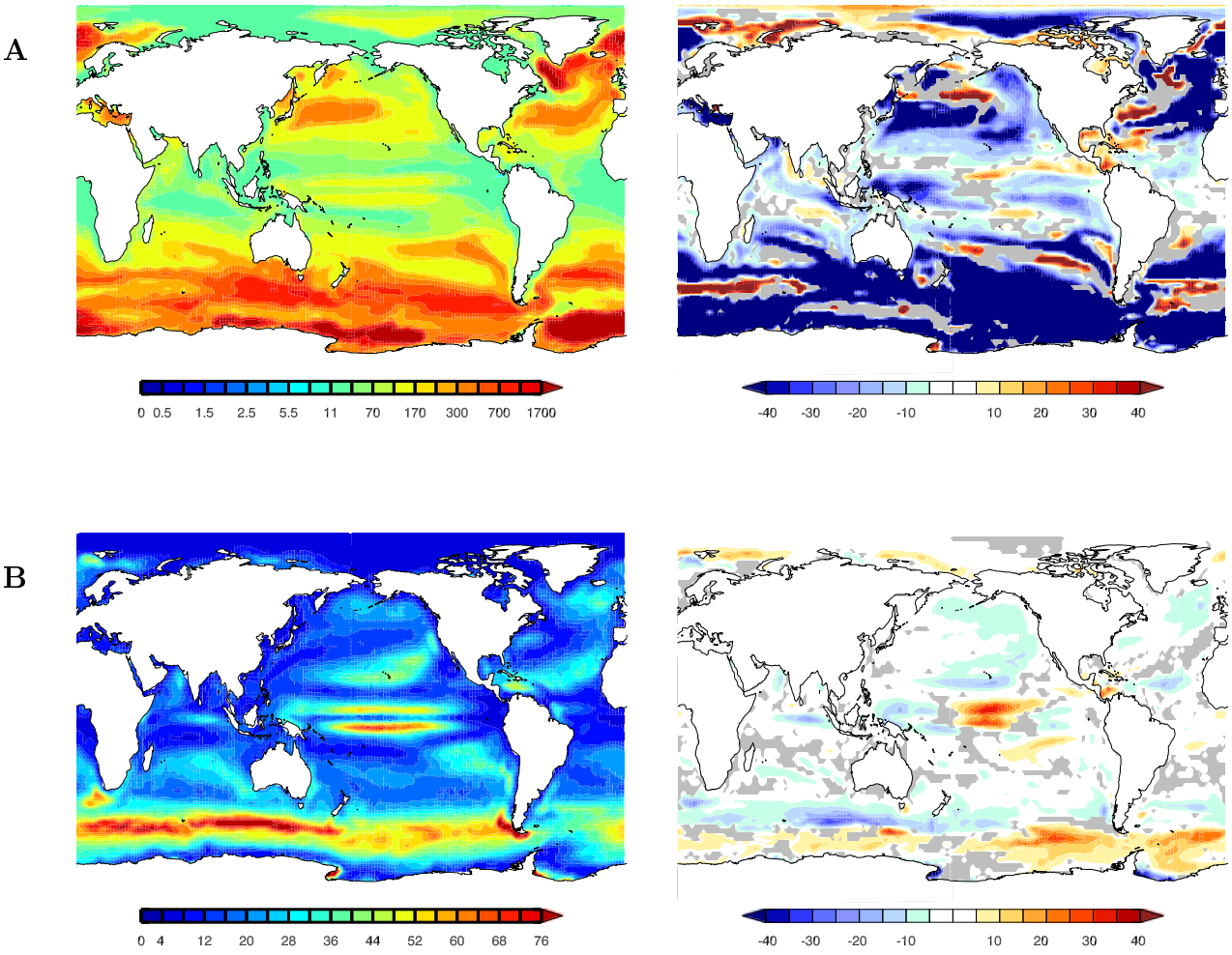

Figure 4.4: A: Maximum mixed layer depth of the year in [m]. B: Minimum mixed layer depth of the year in [m]. Left-hand column: Mean values for the period 1861–1890. Right-hand column: Absolute changes between the periods 1861–1890 and 2061–2090. Grey areas are regions where the absolute changes are below the 95% significance level.

the primary production is not limited by iron (Aumont et al., 2003) we conclude that the overall impact on the biological production and the DMS production in our simulation is only of minor importance. However, dust emissions in our simulation are calculated assuming fixed source areas and vegetation cover representative for the year 2000. Therefore, the simulated changes in the dust emissions and depositions are probably only a lower estimate. Surface silicate is reduced by 8% in the 21C period compared to 19C. The stronger reduction of silicate compared to nitrate and phosphate is caused by the different prescribed vertical penetration profiles. Generally, silicate maximum concentrations are at deeper levels than phosphate and nitrate maxima. Therefore, a reduction in the vertical mixing has a stronger effect on silicate than on phosphate or nitrate.

		1861–1890	2061–2090
phosphate	[μmol l^{-1}]	1.00	0.95 (-5.0%)
silicate	[μmol l^{-1}]	13.78	12.63 (-8.3%)
nitrate	[μmol l^{-1}]	15.60	14.82 (-5.0%)
iron	[nmol l^{-1}]	0.265	0.258(-2.6%)

Table 4.3: Global mean nutrients surface concentrations as simulated within HAMOCC5. Values in parenthesis are percentage changes between the periods 1861–1890 and 2061–2090.

The global change pattern for surface phosphate concentrations shows a strong decline in the Indian and South Atlantic Ocean caused by the stratification-induced reduced vertical mixing (Figure 4.5a). Higher surface phosphate concentrations in the period 21C compared to 19C are simulated in the North Atlantic and in the North Pacific corresponding to regions with a deepening of the maximum MLD. The South East Pacific exhibits along the coast of Peru higher phosphate surface concentrations despite a shoaling in the MLD. In this region, the sea surface temperature response to the simulated global warming is also weaker than in other regions (c.f. Figure 4.3a). This indicates that the region is characterized by an inflow of relatively cold waters from the Antarctic Circumpolar Current accompanied by a strong vertical mixing which reduces the warming signal. The transport of nutrient rich waters from the Southern Ocean into the East Pacific along the coast of Peru ensures a high supply of nutrients. In the period 21C, the model simulates less primary productivity in the Southern Ocean (between 50° and 60° S) leaving more nutrients in the surface waters compared to the period 19C (c.f. Figure 4.5b). This leads to an enhanced flow of nutrients into the southeast Pacific and explains the observed increase in the phosphate surface concentration.

Changes in the export

The changes in nutrient surface concentrations have a strong impact on the net primary production and export production. Averaged over the period 19C, the simulated export is 4.23 GtC yr^{-1}. In the period 21C, the export is reduced by 12% and amounts to 3.71 GtC yr^{-1}. Similar findings are reported by Bopp et al. (2001). Under 2xCO_2 conditions (assuming a 1% increase per year) compared to present-day conditions they find a reduced export (globally by -6%). Our simulated changes in the export are linked to changes in the net primary production (-8%), the phytoplankton concentration (-6%) and the zooplankton concentration (-14%). This is in agreement with simulations performed by Bopp et al. (2001) (net primary production: -9%, phytoplankton: -6%, zooplankton: -9%).

Changes of calcium carbonate and silicate export patterns are displayed in Figure 4.5b and 4.5c. The silicate export declines for most parts of the ocean under warmer climate conditions. The strongest decrease is simulated in the equatorial Atlantic and in the Indian Ocean coincident with the reduced phosphate surface concentration. An increase is simulated in the regions around Antarctica and in the Arctic Ocean, in the South East Pacific, and in the North Atlantic. In high latitudes, the reduced sea ice cover increases the available insolation for photosynthesis and allows phytoplankton to grow. The North

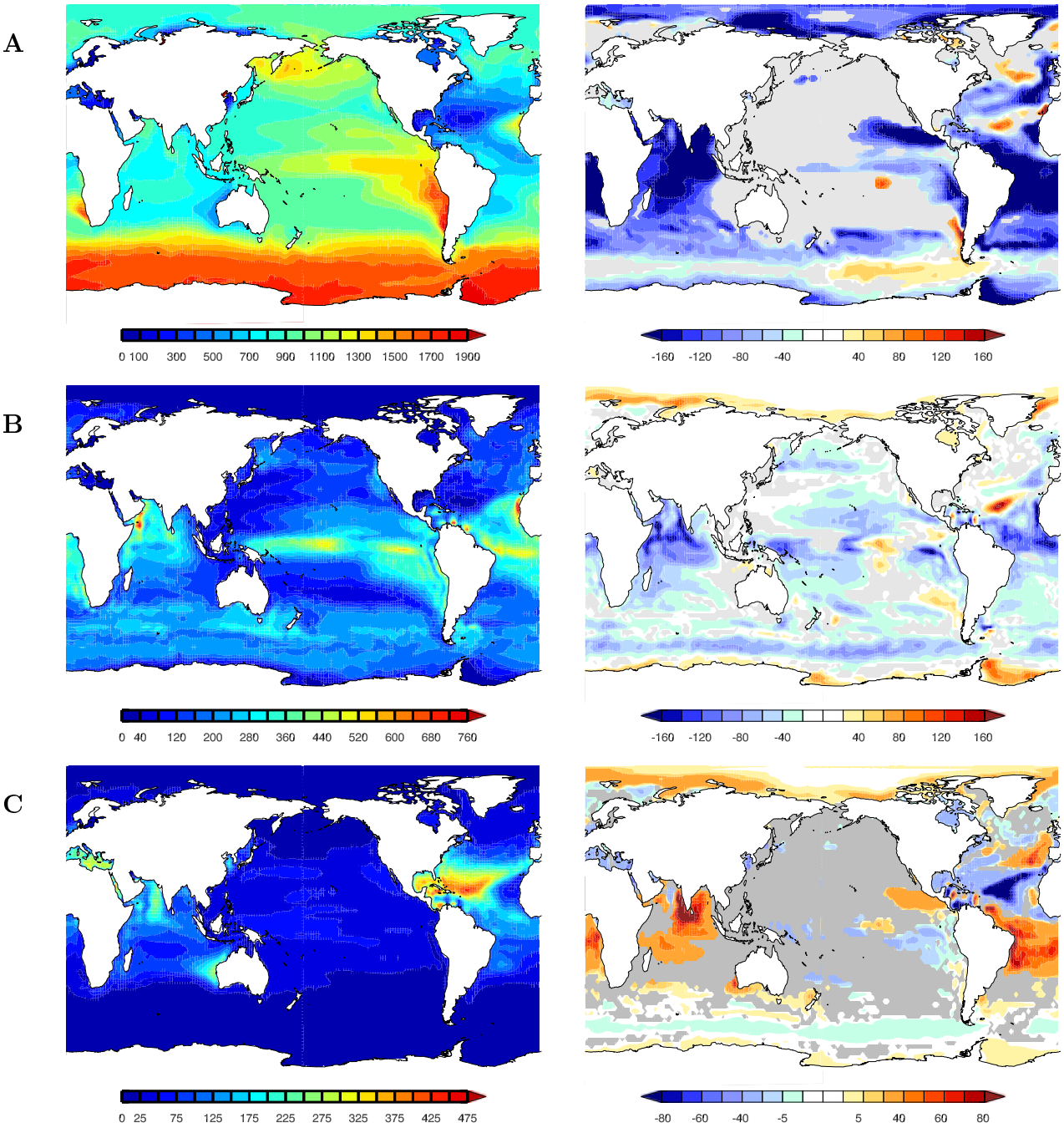

Figure 4.5: A: Annual mean surface phosphate concentration in [nmol l^{-1}]. B: Annual mean export of silicate in [mmol $(m^2 * year)^{-1}$]. C: Annual mean export of calcium carbonate in [mmol $(m^2 * year)^{-1}$]. Left-hand column: Mean values for the period 1861–1890. Right-hand column: Absolute changes between the periods 1861–1890 and 2061–2090. Grey areas are regions where the absolute changes are below the 95% significance level.

Atlantic shows higher nutrient surface concentrations and enhanced silicate export production in regions with a deeper maximum MLD under warmer climate conditions. In the South East Pacific, the higher phosphate surface concentration causes a higher biological production and subsequent a higher export production. In the zonal band between 50° and 60° S, the export of silicate is largely reduced in the 21C period compared to 19C. The difference pattern matches the simulated increase in the minimum MLD caused by increasing wind speeds (c.f. Figure 4.4b and 4.3b). In the Southern Ocean, the primary productivity is light-limited, i.e. winter mixing creates high nutrient concentrations at the upper surface which cannot be utilized until insolation increases in springtime. Then primary production takes place since the shoaling of the MLD keeps the phytoplankton in the euphotic zone. An increase in the summer time MLD results in a mixing of phytoplankton into deeper regions where insolation is much lower than in the surface levels, as light is attenuated by the water and by the phytoplankton itself (Equation 3.1). Overall, there will be significantly less light available for phytoplankton growth and this diminishes the primary productivity. The reduced maximum MLD in the Southern Ocean reduces the nutrient supply. But given the large availability of nutrients in the Southern Ocean, the deep winter mixing ensures a sufficient supply of nutrients into the surface waters even after a reduction due to global warming. Additionally, we observe a slight decrease in the solar radiative flux at the water surface (up to 10 W/m^2 on the annual mean, not shown) caused by an increase in cloud cover in the zonal band between 50° and 60° S. Combining these effects, the light conditions in the Southern Ocean are less favorable for primary production in the 21C period compared to the 19C period, whereas the surface water nutrient concentrations are almost identical. This leads to a reduced primary production and subsequently to a reduced export of silicate.
Calcium carbonate export exhibits a different anomaly pattern compared to that of silicate export (Figure 4.5c). Globally, the export increases by about 1% (Table 4.2). The regions with the strongest increase are the Indian Ocean and the South Atlantic where the silicate export shows the strongest decline. This response of calcium carbonate export is caused by the fact that coccolithophorids abundance is limited by the presence of diatoms. The simulated stronger export of calcium carbonate indicates a shift of the phytoplankton species from diatoms towards coccolithophorids in the Indian Ocean and in the South Atlantic.

Changes in the DMS production and degradation processes and resulting DMS sea surface concentrations

As the simulated DMS production is coupled to the export production of silicate and calcium carbonate, DMS production mirrors the changes in the export production. The DMS cell content in diatoms is much lower than the DMS content in coccolithophoride cells (Keller et al., 1989). Therefore, the export of calcium carbonate leads to higher DMS production than the export of silicate. A shift towards more calcium carbonate export as simulated in the Indian Ocean and the Atlantic Ocean is more than compensated by the overall reduction in the export production in these regions, leading to an overall decrease

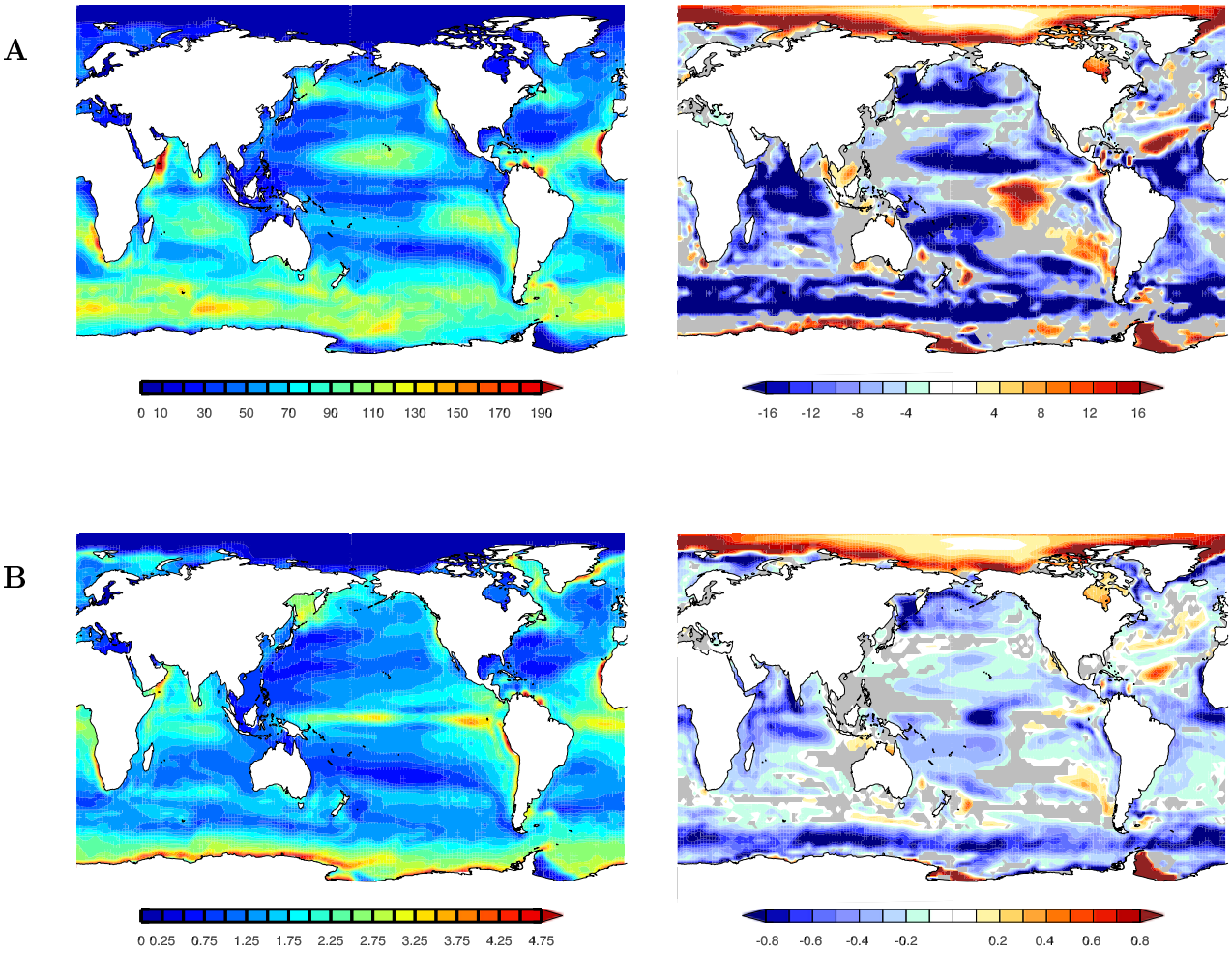

Figure 4.6: A: DMS flux into the atmosphere in [mg(S) $(m^2 * year)^{-1}$]; B: DMS sea surface concentration in [nmol l^{-1}]. Left-hand column: Mean values for the period 1861–1890. Right-hand column: Absolute changes between the periods 1861–1890 and 2061–2090. Grey areas are regions where the absolute changes are below the 95% significance level.

in the DMS sea surface concentration. Globally, the annual mean DMS production is reduced by 13% in 21C compared to 19C (Table 4.4). The DMS degradation processes show a similar decline. The photo-oxidation of DMS to DMSO is reduced by 13% and the bacterial consumption by 14%. The DMS flux into the atmosphere is reduced as well (-10%). This weaker decline of the DMS flux is predominantly caused by a higher sea air exchange rate, $k_{sea-air}$, in the 21C period compared to the 19C period (+4%). The increase in the sea air exchange rate, depending quadratically on the wind speed, is predominantly caused by an increase in the 10m wind speed (+1%) and is partly reduced by a reduction in gas solubility at higher sea-water temperatures. The global pattern of the changes in the DMS flux are displayed in Figure 4.6a. Similar to the export production,

	1861–1890	2061–2090
DMS_{prod}	327.88	283.21 (-13.6%)
DMS_{flux}	24.17	21.69 (-10.3%)
DMS_{bac}	272.39	234.16 (-14.0%)
DMS_{UV}	31.32	27.36 (-12.6%)

Table 4.4: Global mean DMS production and degradation processes as simulated within HAMOCC5. Units are [Tg(S) yr^{-1}]. Values in parenthesis are percentage changes between the periods 1861–1890 and 2061–2090.

the DMS flux is reduced in most parts of the ocean. The decrease around 60° S of the export production is partly offset by the higher wind speeds simulated for 21C compared to 19C in this region (c.f. Figure 4.3b). In the South East Pacific and in the North Atlantic, the higher DMS production in the warmer climate combined with high wind speeds in these regions results in a stronger increase in the DMS flux. Additionally, the melting of sea ice allows a DMS flux into the atmosphere in regions that were covered by sea ice in 19C.

How do these changes affect the DMS sea surface concentration? Globally, the DMS sea surface concentration is reduced by 7% in the boreal summer season (June, July and August) and by 15% in the austral summer season (December, January and February) between 19C and 21C (Table 4.4). The major DMS degradation process is the DMS consumption by bacteria. The DMS flux into the atmosphere accounts for only about 8% of the total DMS sink. Therefore, the changes in the DMS sea surface concentrations are largely driven by the changes in the DMS production and the DMS consumption by bacteria. As these processes mirror the changes in the export production, the changes in the DMS sea surface concentrations behave very similar. In most parts of the ocean, lower DMS sea surface concentrations are simulated in 21C compared to 19C.

The global mean changes for the different ocean basins are listed for the boreal summer and winter seasons for the period 19C and 21C in Table 4.5 and are displayed for the entire simulation period in Figure 4.7. In the boreal winter season, the highest DMS sea surface concentrations are simulated in the Southern Ocean (6.2 nmol l^{-1} for 19C). These high concentrations persist until the late 19th century and become then reduced by 13% in 21C compared to 19C. In the boreal summer season, the highest DMS sea surface concentrations are simulated in the North Atlantic (2.36 nmol l^{-1} for 19C). With increasing sea surface temperatures from the late 19th century on, the DMS sea surface concentration decreases and is reduced in 21C by around 11% compared to 19C.

The strongest decrease in DMS sea surface concentrations is simulated in the South Atlantic for the boreal winter season (-29%). An increase in the DMS sea surface concentration is simulated for the low productive austral winter season in the Southern Ocean (+14%). However, the austral winter DMS sea surface concentrations in the Southern Ocean are almost zero and thus the influence on the global DMS change is only of minor importance.

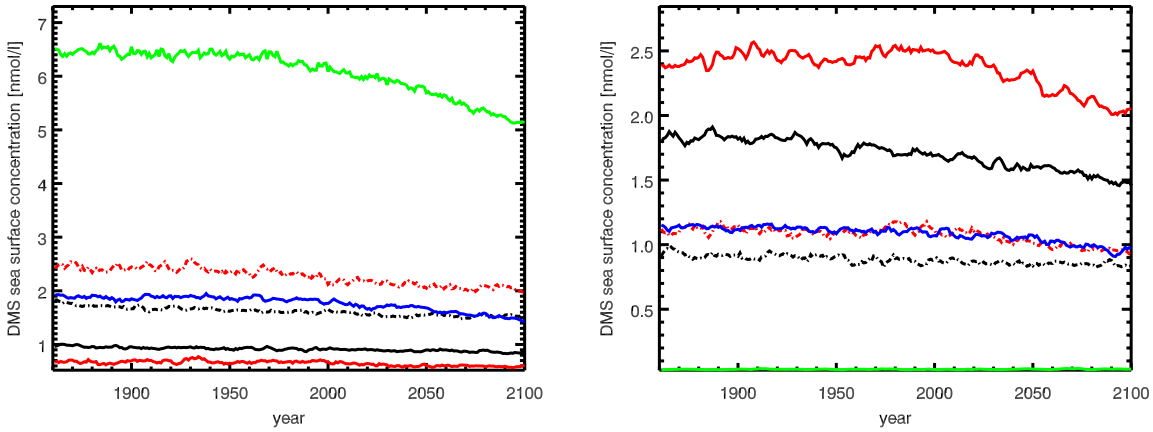

Figure 4.7: DMS sea surface concentration. Left: boreal winter season (December, January, February), right: boreal summer season (June, July, August). Black = North Pacific, black dotted = South Pacific, red = North Atlantic, red dotted = South Atlantic, green = Southern Ocean, blue = Indian Ocean. Data are smoothed using a 5-year running mean. Units are [nmol l^{-1}].

4.2.3 Response of DMS in the atmosphere

The DMS emission from the ocean represents the largest source of DMS in the atmosphere. Emissions from vegetation and soil are only of minor importance (0.3 Tg(S) yr^{-1} on the global annual mean (Pham et al., 1995)). Changes in the oceanic DMS emission will therefore have a strong impact on the atmospheric concentration of DMS. In the atmosphere DMS is mainly oxidized with OH during day-time and by NO_3 during night-time. One of the reaction products is SO_2 (Andreae and Crutzen, 1997). The pattern of the vertical integral of the DMS oxidation (Figure 4.8a) mirrors the DMS flux into the atmosphere. Regions with high DMS emissions coincide with regions of high DMS oxidation rates. The reduction in the DMS emission flux into the atmosphere causes a reduction in the total DMS oxidation in the atmosphere (c.f. Figure 4.8a and 4.6a). Re-

	DMS sea surface concentration [nmol l^{-1}]				DMS flux [Tg(S) yr^{-1}]			
	1861–1890		2061–2090		1861–1890		2061–2090	
	JJA	DJF	JJA	DJF	JJA	DJF	JJA	DJF
North Atlantic	2.36	0.77	2.12 (-10.5)	0.59 (-23.3)	4.11	1.73	3.84 (-6.7)	1.30 (-24.9)
South Atlantic	1.15	2.64	0.99 (-13.6)	1.87 (-29.1)	1.43	2.69	1.28 (-10.6)	2.09 (-22.1)
North Pacific	1.74	1.00	1.59 (-8.7)	0.89 (-11.3)	4.76	3.18	4.15 (-12.9)	3.53 (+11.4)
South Pacific	0.88	1.77	0.87 (-0.36)	1.42 (-19.6)	2.74	4.39	2.95 (+7.7)	3.74 (-14.7)
Indian Ocean	1.10	1.91	0.98 (-10.8)	1.61 (-15.7)	3.19	3.49	2.79 (-12.6)	2.80 (-19.5)
Southern Ocean	0.03	6.20	0.04 (+14.3)	5.41 (-12.7)	0.18	23.72	0.20 (+19.5)	22.22 (-6.5)
global	1.26	2.41	1.18 (-6.5)	2.06 (-14.4)	18.28	40.15	17.14 (-6.2)	36.69 (-8.6)

Table 4.5: DMS sea surface concentration and DMS flux into the atmosphere for different regions. Values in parenthesis are percentage changes between the periods 1861–1890 and 2061–2090.

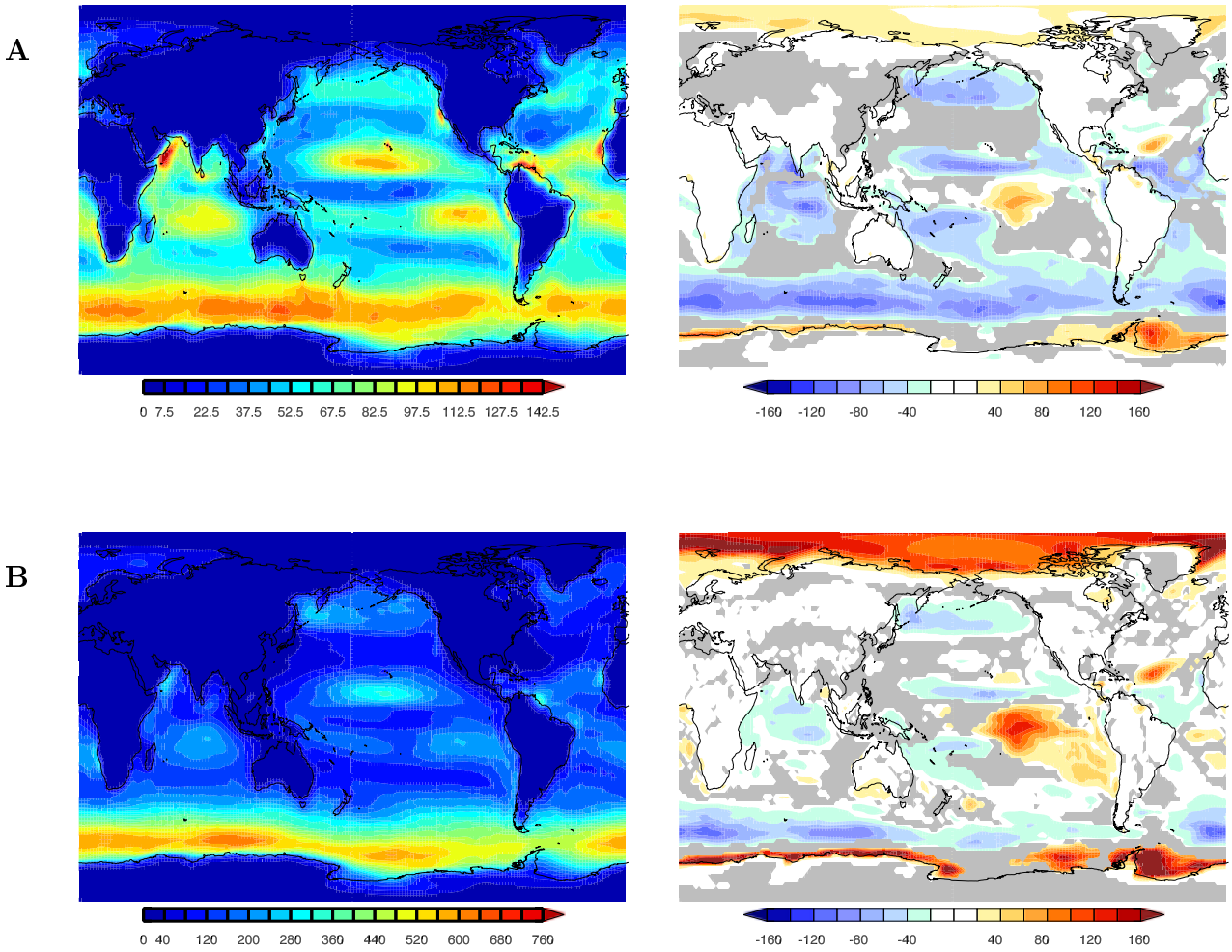

Figure 4.8: A: DMS oxidation in [mg(S) $(m^2 * year)^{-1}$]; B: Annual mean DMS burden in the atmosphere in [$\mu g\ m^{-2}$]. Left-hand column: Mean values for the period 1861–1890. Right-hand column: Absolute changes between the periods 1861–1890 and 2061–2090. Grey areas are regions where the absolute changes are below the 95% significance level.

gions with an increase in the DMS flux between the periods 19C and 21C coincide with regions where the total DMS oxidation is enhanced, for instance at high latitudes of the Southern and Northern Hemisphere. Globally, the total DMS oxidation is reduced by 10% (Table 4.6). Oxidation of DMS with NO_3 is increased in the 21C period compared to the 19C period (+3%), whereas the oxidation with OH is reduced by 13%. The oxidation with NO_3 becomes only prevalent in the polluted regions of the Northern Hemisphere during winter when OH concentrations are low. Enhanced oxidation of DMS due to the reaction with NO_3 is therefore most likely caused by an increase in the DMS emission flux in the North Pacific which amounts to 12% when averaged over December, January and February (see Table 4.5).

As the lifetime of DMS is short, the resulting DMS burden shows highest values in regions with strong DMS emissions most noticeably in the Southern Ocean (Figure 4.8b). The global change pattern of the DMS burden between the periods 19C and 21C is comparable to changes in the total DMS oxidation and the DMS flux (Figure 4.6a and 4.8a) although the magnitude of the changes is smaller. The mid and low latitudes show only a weak decrease in the DMS burden, despite a stronger reduction in the DMS flux.

Figure 4.9 shows the vertical profile of zonal mean DMS concentrations in the atmo-

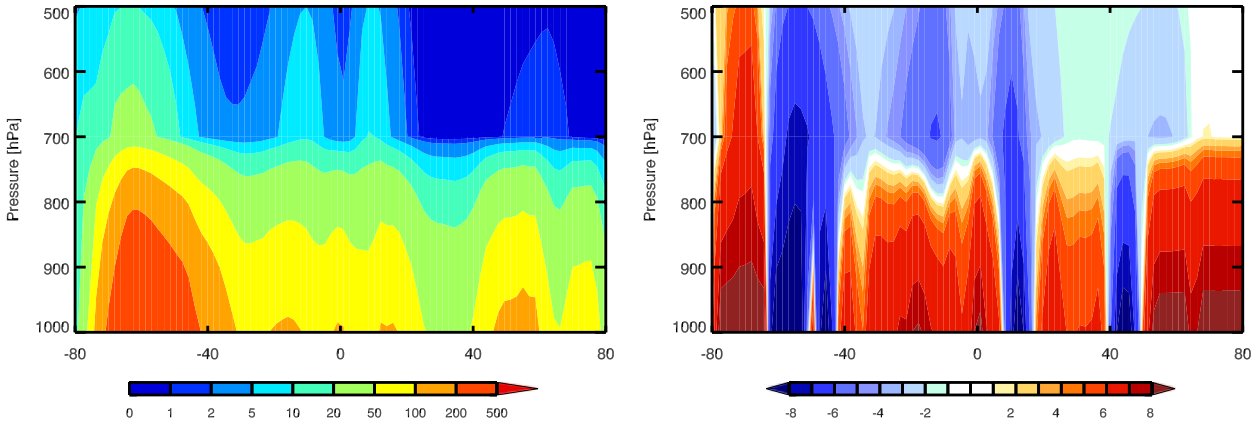

Figure 4.9: Vertical profile of the zonal annual of DMS in the atmosphere in [pptv]. Left-hand column: Mean values for the period 1861–1890. Right-hand column: Absolute changes between the periods 1861–1890 and 2061–2090.

sphere for the 19C period together with the absolute changes between the periods 19C and 21C. DMS in the atmosphere shows a strong increase in the high latitudes. This increase is caused by increasing DMS emissions in these regions. Higher DMS concentrations are also found in the lower troposphere in the mid and low latitudes in the 21C period. To a first glance this is in contrast to the simulated decrease in the DMS flux into the atmosphere in most of the mid and low latitudes (Figure 4.6a). The increasing concentrations of DMS in the atmosphere in the mid and low latitudes despite decreasing DMS emissions can be explained by a less efficient DMS oxidation (longer DMS lifetime) in the 21C period. The main oxidation mechanism is the DMS oxidation with OH. OH levels exhibit low values in the high latitude regions and lower concentrations near the surface than in the free troposphere (data not shown). This implies that DMS has a relatively long lifetime when emitted at high latitudes or when remaining in the boundary layer in the mid and low latitudes. In the warmer 21C period the vertical transport of DMS in the atmosphere becomes weaker in the mid and low latitudes which keeps DMS longer at lower altitudes, where it is less efficient oxidized compared to higher altitudes. The reduction in the vertical transport in the atmosphere is caused by an overall decrease in the temperature lapse rate in the mid and low latitudes as depicted in Figure 4.10. This explains the simulated increase in the DMS lifetime and the unproportional weak response of the DMS concentration in the atmosphere to the reduced DMS emissions in

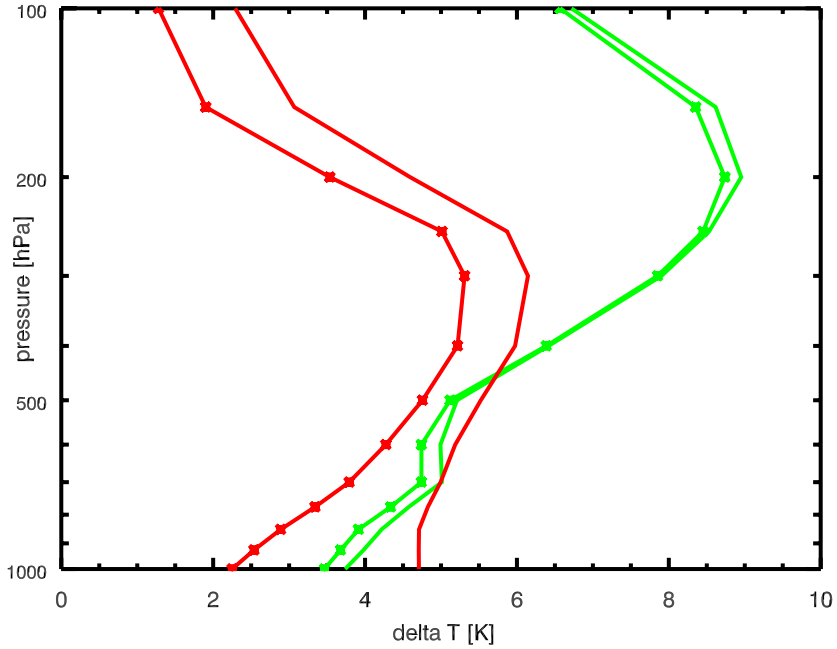

Figure 4.10: Vertical profile of the zonal mean temperature difference between the periods 1861–1890 and 2061–2090 in ° C. Green: zonal mean between 0 and 30°, Red: zonal mean between 30 and 60°. Solid lines: Northern Hemisphere, lines with bullets: Southern Hemisphere.

the mid and low latitudes.

4.3 Relationship between changes in the DMS sea surface concentration, the DMS emissions, and the DMS burden in the atmosphere

Figure 4.11 compares the zonally averaged percentage changes between the periods 19C and 21C of the DMS sea surface concentration, the DMS flux, the total DMS oxidation and the DMS burden in the atmosphere. As apparent from the global change pattern (Figure 4.6b), the zonal annual mean DMS sea surface concentration decreases almost everywhere, except at high latitudes of the Northern and Southern Hemisphere. Here the reduction in the sea ice coverage increases the insolation and leads to an enhanced primary productivity in the ocean. The strongest reduction, up to 40%, is simulated within the zonal band between 50° and 60° S. The increase in the summer MLD in this region (Figure 4.4b) together with a reduction in the shortwave radiation reduces the available light for primary productivity and leads to a decrease in the export production (Figure 4.5b) and subsequently of the DMS sea surface concentration. In the mid and low lat-

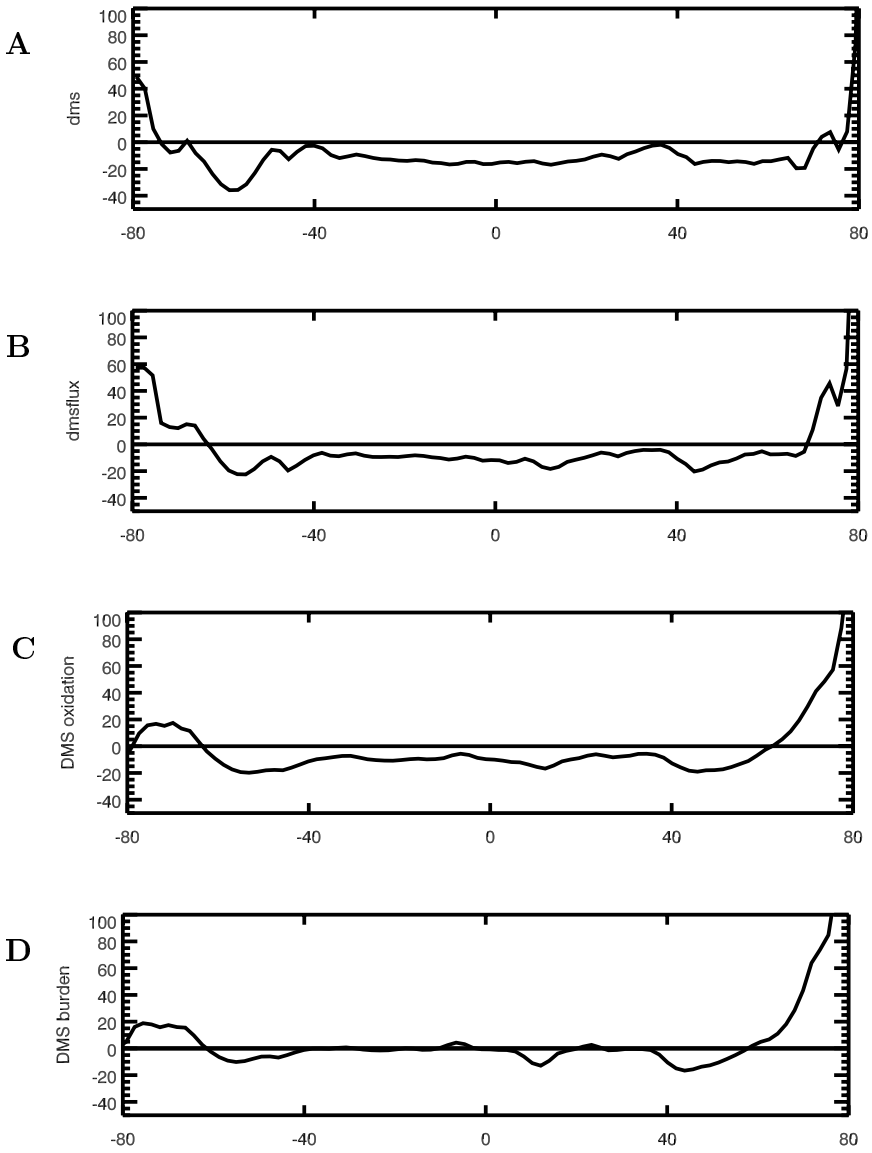

Figure 4.11: Zonal annual mean changes between the periods 1861–1890 and 2061–2090 in %. A: DMS sea surface concentration; B: DMS flux; C: vertically integrated DMS oxidation; D: DMS burden.

itudes the reduction in DMS sea surface concentrations (around -10%) is caused by the stratification-induced reduction in the maximum MLD, leading to a strong reduction in

		1861–1890	2061–2090
DMS burden	[Tg(S)]	0.077	0.075 (-3.0%)
DMS + OH	[Tg(S) yr^{-1}]	20.48	17.88 (-12.7%)
DMS + NO_3	[Tg(S) yr^{-1}]	3.97	4.09 (+3.0%)
DMS total	[Tg(S) yr^{-1}]	24.45	21.97 (-10.1%)
DMS lifetime	[d]	1.01	1.08 (+7.0%)

Table 4.6: Global mean DMS budget in the atmosphere as simulated within the aerosol model HAM. Values in parenthesis are percentage changes between the periods 1861–1890 and 2061–2090.

surface nutrient concentrations.
The large reduction in the DMS sea surface concentration between 50° and 60° S partly offsets the simulated increase in sea surface wind speed resulting in a weaker DMS flux into the atmosphere. Higher wind speeds in this region are caused by a shift of the storm track regions towards the south. As a consequence of this shift, the wind speeds are lower between 40° and 50° S leading to a decrease in the DMS flux despite almost constant DMS sea surface concentrations. The DMS flux shows a sharp increase north of 70° N. DMS sea surface concentrations are also increasing, but to a smaller extent. In summer, sea ice cover vanishes completely in the Northern Hemisphere in the 21C period (c.f.Figure 4.2). This causes an increase in biological production due to enhanced availability of light and subsequently an increase in the DMS sea surface concentration. The response of the DMS flux into the atmosphere is amplified by high surface wind speeds in this region leading to a high DMS flux in the sea ice free regions in the 21C period.
The change in the total column integrated DMS oxidation shows a much smoother latitudinal distribution than the DMS flux. The strongest reduction in the oxidation, about 20%, is located around 55° S and directly corresponds to the decreasing DMS flux. At the northern high latitudes the DMS oxidation rates increase in correspondence to the increase in the DMS flux. In the southern high latitudes, the increase in the DMS oxidation is about 20% which is much smaller than the increase in the DMS flux (+60%). This is due to the fact that the DMS flux is over ice covered regions assumed to be zero. The percentage change is therefore higher for the DMS flux than for the DMS oxidation south of 60° S.
The zonal change pattern of the DMS burden differs from that of the DMS oxidation rate in low and mid latitudes. Here the changes of the DMS burden are very small and in some regions the trend is even slightly positive, despite decreasing DMS emissions. This implies that in the 21C period DMS is less efficiently oxidized than in the 19C period, because in mid and low latitudes reduced vertical transport in the 21C period keeps DMS closer to the surface, where OH levels are lower than in the free troposphere. Thus, DMS experiences a longer lifetime in the warmer 21C period (+7%). This partly offsets the reduction in the DMS flux. However, regions with a strong reduction in the DMS flux, for example around 50° S, are accompanied by a moderate reduction in the DMS burden. The largest changes for all quantities are simulated in the northern and southern high latitudes. These areas cover only a small part of the globe and have therefore only a small

effect on the global mean changes.

4.4 Summary

Using a coupled ocean-atmosphere model including submodels for the marine biogeochemistry and the microphysical aerosol system, we modeled the temporal evolution of DMS in the ocean and in the atmosphere for the time period from 1860 until 2100 based on the IPCC SRES scenario A1B. The processes for marine DMS production and decay are included in the representation of plankton dynamics in the marine biogeochemistry model HAMOCC5 which is embedded in a global ocean general circulation model (MPI-OM). The atmospheric model ECHAM5 is extended by the microphysical aerosol model HAM. Between the periods 1861-1890 and 2061-2090 the global mean 2m temperature increases by 3.2°C. The oceanic response to global warming includes increasing sea surface temperatures, retreat of sea ice, and a general increase in ocean stratification. These changes impact on the marine biology and subsequently on the DMS production in the ocean.
Our results indicate a reduction in the global annual mean DMS sea surface concentration and the DMS flux into the atmosphere in a warmer climate. Between the periods 1861–1890 and 2061–2090 we find a reduction of around 10% for both, the DMS flux and the DMS sea surface concentration. Changes in the DMS sea surface concentrations are predominantly controlled by changes in the export production. Regionally the response and the underlying mechanisms are highly inhomogeneous:

1. At high northern and southern latitudes the DMS sea surface concentration shows an increase. This increase is caused by the retreat of sea ice which enhances the insolation in the ocean, the net primary productivity and subsequently the DMS production.

2. At low and mid latitudes the DMS sea surface concentrations show a decrease (-10 to -20%) predominantly caused by a stronger stratification of the ocean and a subsequently reduced mixing of nutrients into the euphotic zone.

3. In the Southern Ocean between 50° and 60° S we find a strong reduction in the DMS sea surface concentration (-40%) caused by an increase in the summer MLD. Phytoplankton growth in the Southern Ocean is predominantly light limited. The deeper summer MLD causes mixing of phytoplankton into regions where the conditions for photosynthesis are less favorable than in the surface levels due to reduced light availability. The increase in the summer MLD in this region is thereby caused by a shift of the storm tracks towards the south.

4. In the South East Pacific we simulate an increase in the DMS sea surface concentration. This increase is caused by an increase in the horizontal transport of nutrients into this region, owing to higher surface nutrients concentrations in the Antarctic Circumpolar Current.

5. Some regions of the North Atlantic show an increase in the DMS sea surface concentration caused by an increase in the winter MLD leading to a higher nutrient transport into the euphotic zone.

Our results do not show a distinct response of the DMS production and hence the DMS sea surface concentrations towards changes in the phytoplankton species composition. This is in contrast to the study by Bopp et al. (2004). For climate conditions equivalent to doubled present-day atmospheric CO_2 concentrations they simulate an increase in the DMS sea surface concentration in the subantarctic Pacific, caused by a retreat of diatoms and an increase in other species more efficient in producing DMS. This shift results mainly from a decrease in silicate surface concentrations. We simulate a decrease in silicate surface concentration of similar magnitude in the subantarctic Pacific (10 μmol l^{-1}) but additionally, due to the increase in the summer MLD, a decrease in the primary productivity. Therefore, even the reduced silicate surface concentration is still sufficient to supply enough nutrients for diatom growth. In contrast, the simulation of Bopp et al. (2004) shows an increase in the primary productivity in the subantarctic Pacific. They explain this increase with a longer growing season in the Southern Ocean caused by an earlier reduction in the MLD in the year. However, due to the coarse resolution of their ocean model, they cannot simulate the influence of changes in the summer MLD on the primary productivity, which leads in our simulation to a strong reduction in the primary productivity. Anyhow, our results indicate a retreat of diatoms in the Indian Ocean and in the South Atlantic. Thereby, the accompanied increase in coccolithophorids, which are more efficient DMS producers, is not large enough to overcome the general decrease in export production.
The patterns of the DMS flux into the atmosphere are spatially consistent to that of the changes in the DMS sea surface concentrations. Only in few regions the fluxes are partly offset by an increasing sea-air exchange rate. The DMS concentrations in the atmosphere are less affected by the changes in the DMS flux (-3% for the DMS burden). This is due to the fact that DMS in a warmer climate has a longer atmospheric lifetime (+7%). Reasons for that are a reduced vertical transport in the 21C period which keeps mid an low latitude DMS longer in low altitudes where OH concentrations are lower than in the free troposphere.
Although a quantitative estimate of the climate feedback of DMS is beyond the scope of this study, the results here suggest that a global warming leads to a reduction in the overall biological production in the ocean and therefore to a decrease in the DMS sea surface concentration, which is in contrast to the negative feedback proposed in the CLAW hypothesis (Charlson et al., 1987). In the CLAW hypothesis a key factor for a negative feedback is an increase in the DMS sea surface concentration in a warmer climate. However, our simulation shows the opposite, i.e. decreasing DMS sea surface concentrations in a warmer climate, for the global mean and most of the ocean surface.
Of coarse modeling, in particular modeling of biological processes, is associated with large uncertainties. In the following we will address the most uncertain parts in our simulation. First of all, the formulation of the DMS cycle in the ocean is optimized and tested by using observed present-day DMS sea surface concentrations (Kloster et al., 2006). Up to now it is not feasible to find global constraints for the DMS consumption and produc-

tion processes. However, the agreement between the simulated relative magnitude of the specific DMS production and degradation processes and observations of these processes led us conclude that the DMS parameterization within HAMOCC5 has some skills to simulate the sensitivity of DMS production and thus may be able to simulate the process correctly in a changing climate.
Another critical point in this simulation is that oxidant fields in the sulfur chemistry scheme are prescribed and kept fixed. However, chemical transport models clearly demonstrate that OH and NO_3, the main oxidants of DMS in the atmosphere, will increase in the future. Pham et al. (2005) showed that the effect of changes in the oxidant fields from 2000 to 2100 assuming the SRES A2 scenario results in a global decrease of the DMS burden by 22%, when atmospheric meteorological conditions are kept constant. However, the SRES A2 scenario is a relatively extreme scenario compared to the SRES A1B scenario applied in this study. We anticipate the SRES A1B scenario would result in smaller changes. However, this would not change our conclusion that the DMS burden is reduced in a warmer climate.

Chapter 5

Conclusions

Charlson et al. (1987) proposed a biogeochemical feedback cycle in which marine phytoplankton can influence the climate through the marine biogenic sulfur compound dimethylsulfide (DMS) often referred to as the CLAW hypothesis. In order to explain the relatively stable global mean Earth temperature over geological time scales they suggested that this biogeochemical feedback might be negative, stabilizing the Earth climate against perturbations. In a warmer climate they assume that DMS production and emissions increase, leading to a higher formation rate of sulfate aerosol particles which in turn might lead to a larger number concentration of cloud condensation nuclei (CCN). More CCNs lead to an increase in the number concentrations of cloud droplets. Therefore, clouds become brighter and longer lived and reflect more sunlight back to space. This in turn cools the Earth's surface and offsets the initiating warming effect. Despite large research efforts in the last years, it has not yet been possible to assess the strength of this feedback or even to anticipate if this feedback is negative (stabilizing) or positive (intensifying). The largest uncertainties remain in the assessment of the response of DMS sea surface concentrations to changing climatic conditions.
The aim of this study was to investigate the extent to which marine DMS production and emission is changing in a warmer climate. The first objective of this study was to:

- Establish a modeling system of the DMS cycle in the ocean and in the atmosphere which simulates realistically and dynamically consistent DMS sea surface concentrations, DMS emissions, and DMS concentrations in the atmosphere.

The simulation setup consists of a coupled atmosphere-ocean general circulation model (AOGCM), based on the atmospheric GCM ECHAM5 and the ocean GCM MPI-OM. Embedded in the ocean model is a marine biogeochemistry model (HAMOCC5) which simulates plankton dynamics and the DMS production and decay in the ocean. The simulated DMS flux from the ocean serves as a lower boundary conditions in the atmospheric model ECHAM5. The atmosphere model includes a sulfur chemistry scheme and an aerosol microphysics model (HAM) which calculate the atmospheric concentrations of DMS, SO_2 in-cloud and gas phase oxidation to SO_4^{2-}, the distribution of in-cloud formed SO_4^{2-} and the condensation of gas-phase formed SO_4^{2-} on pre-existing particles, as well

as the formation of sulfate aerosol particles. The performance of the coupled setup for present-day conditions has been evaluated with available measurements both in the ocean and in the atmosphere. To facilitate this evaluation, prescribed aerosol and aerosol precursor emissions representative for present-day conditions (year 2000) were applied.
The simulated DMS consumption and production processes in the ocean are consistent in their relative magnitude with the observations available. The simulated global annual mean DMS sea surface concentration is 1.8 nmol l^{-1}. The seasonal variations with high concentrations in the summer season of the northern and southern high latitudes generally match the observations. The DMS flux into the atmosphere amounts to 28 Tg(S) yr^{-1} resulting in a column integrated DMS burden of 0.077 Tg(S) and a lifetime of 1.0 day. DMS contributes 30% to the total sulfur source considered in the model (sulfur emissions from fossil- and bio-fuel use, wildfires and volcanoes, and sulfur from DMS oxidation). Atmospheric DMS oxidation products in the atmosphere contribute significantly to the global annual mean column integrated SO_2 and SO_4^{2-} burden (25% and 27%, respectively). For the biological active summer season of the Southern Hemisphere, the simulated atmospheric SO_4^{2-} surface concentrations in regions with a high contribution from DMS derived SO_4^{2-} are overestimated. As the DMS sea surface concentrations are in agreement with the observations, the most likely explanation is a missing chemical reaction mechanism in the atmosphere preventing the formation of SO_4^{2-} from DMS oxidation.
The generally good agreement between model and measurements indicates that the DMS cycle in the model represents the processes governing DMS sea surface concentrations, DMS emissions, and resulting atmospheric concentrations reasonably well. The DMS formulation applied in a coupled ocean-atmosphere model is a step forward in providing the tools for an assessment of the marine DMS biosphere-climate feedbacks.

The second objective of this study was to:

- Investigate the response of the DMS sea surface concentration, the DMS flux, and the DMS concentration in the atmosphere to climate change caused by increasing anthropogenic activities.

The evolution of the global DMS cycle from 1860 to 2100 has been investigated in a transient climate simulation. The results are analyzed in terms of changes in the biological production and subsequent changes in the DMS production in the ocean, DMS sea surface concentration, DMS emission, and DMS concentration in the atmosphere. The most uncertain link in the CLAW hypothesis is the response of DMS sea surface concentrations to climate change. The prognostic formulation of the DMS cycle in the ocean allows to investigate this key link.
Between the periods 1861–1890 and 2061–2090 the global mean 2m temperature increases by 3.2°C. The oceanic response to global warming includes increasing sea surface temperatures, retreat of sea ice, and a general increase in ocean stratification. These changes impact on the marine biology and subsequently on the DMS production in the ocean.
The results show that a global warming leads to a reduction in the overall biological production in the ocean and therefore to a decrease in the DMS sea surface concentration.

Consequently, a reduction of around 10% for both, the global annual mean DMS flux and the DMS sea surface concentration, is found between the periods 1861–1890 and 2061–2090. This is in contrast to the negative feedback proposed by Charlson et al. (1987) in the CLAW hypothesis. They assumed that changes in the DMS sea surface concentration in a warmer climate are predominantly controlled by the following mechanisms:

- Reduced sea ice coverage will increase the area available for gas exchange (Charlson et al., 1987).

The model results confirm this supposition. In a warmer climate the sea ice coverage is strongly reduced leading to a larger area available for DMS gas exchange. Additionally, the retreat of sea ice enhances the insolation in the ocean, the net primary productivity and subsequently the DMS production and DMS sea surface concentration. The DMS flux is increased by about 60% in the southern and northern high latitudes for the zonal annual mean. However, the high latitudes cover only a small area of the globe and have therefore a small effect on the global mean changes.

- Ecological changes can alter the abundance of phytoplankton species which efficiently produce DMS (Charlson et al., 1987).

The simulation shows a shift of species composition in the Indian Ocean and South Atlantic from diatoms towards coccolithophorids which produce DMS more efficiently. However, the increase in the DMS production is not large enough to overcome the overall reduction in the net primary production leading to a decrease in the DMS sea surface concentration and the DMS flux.

- Changes in the wind fields affect the DMS flux (Charlson et al., 1987).

The simulated changes in wind speed are small between 1861–1890 and 2061–2090. Only in the central equatorial Pacific a net increase in the DMS flux caused by higher wind speeds is simulated. In other regions changes in the DMS sea surface concentration are dominant.

- Assuming from observations that the DMS production is highest in tropical regions, increasing sea surface temperatures might enhance DMS production (Charlson et al., 1987).

The latter seems to be the most uncertain point in the CLAW hypothesis. It is observed and also reproduced in the model simulation that DMS sea surface concentrations are high in equatorial regions. The high concentrations are a result of high biological activity. Large upwelling regimes ensure a high transport of nutrients into the surface layers. These high nutrient levels allow phytoplankton to grow and to produce DMS. Thereby, the temperature itself has only a minor effect on phytoplankton growth.
The results presented here show that the dominant factors for controlling DMS sea surface concentrations under warmer climate conditions are changes in the ocean dynamics. These controlling factors were not considered in the CLAW hypothesis. The transport of nutrients into the surface layers is strongly reduced in a warmer climate due to an increase

in ocean stratification. The decrease in nutrients in the surface layers causes a reduction in the net primary productivity in regions where phytoplankton growth is predominantly limited by nutrients. Therefore, DMS sea surface concentrations and the DMS flux are reduced in large parts of the mid and low latitudes (up to -10% for the zonal annual mean between 1861-1890 and 2061-2090). The strongest reduction in DMS sea surface concentrations in a warmer climate is simulated in the Southern Ocean between 50° and 60° S (up to -40% for the zonal annual mean between 1861-1890 and 2061-2090). In the Southern Ocean phytoplankton growth is predominantly light limited. In a warmer climate, higher wind speeds persist between 50° and 60° S causing a mixing of phytoplankton into deeper levels where light conditions are less favorable for photosynthesis, thereby reducing the overall net primary productivity and the DMS production. Higher wind speeds in this region are caused by a shift of the storm tracks towards the south in a warmer climate.

In summary, changes in the ocean dynamics in a warmer climate lead to a reduction in the net marine primary production and to a decrease in DMS sea surface concentrations. Assuming that the other mechanisms in the DMS-cloud albedo feedback act as proposed in the CLAW hypothesis this feedback is positive, i.e. intensifying the initiating warming effect.

However, the DMS concentration in the atmosphere does not linearly respond to changes in the DMS emissions because it is also influenced by other controlling factors like the oxidation capacity of the atmosphere or the vertical distribution of DMS in the atmosphere. In the presented simulation the column integrated DMS burden decreases by 3%, implying a longer lifetime of DMS (+7%) in the atmosphere. These findings highlight that the DMS cycle has to be studied in the comprehensive coupled ocean-atmosphere system and can not be assessed solely in atmosphere or ocean model studies, as climatic impacts on the DMS cycle influence both the atmospheric and the oceanic part in a non linear way.

Chapter 6

Outlook

Although large progress has been made in recent years to increase the understanding of the DMS cycle in the ocean, the present knowledge of the relationship between the marine eco-system and DMS production remains incomplete. Measurements of DMS and DMS related quantities in the ocean over the last years just started to unravel the complexity of the DMS cycle in the ocean. Many factors, that still need to be identified in more detail, could be important for the role of biogenic DMS production in the climate system. The work presented here is a step forward in providing a predictive tool for DMS sea surface concentrations which allows to assess the role of DMS in the climate system. The agreement between the simulated relative magnitude of the DMS production and degradation processes and observations of these processes led to the conclusion that the DMS parameterization within the marine biogeochemistry model has some skills to simulate the DMS production also in a changing climate. However, it would be desirable to have more long-term (multi-decadal) DMS time-series measurements available in order to compare the inter-annual variability of the simulated DMS sea surface concentration against these measurements. Such a comparison would provide better insights in the predictive capability of the established modeling system.

This study shows that global annual mean DMS emissions between 1861-1890 and 2061-2090 are reduced by around 10% and the DMS burden in the atmosphere by around 3%. A quantitative estimate how these changes perturb the radiation balance of the Earth remains still unresolved. Future work will have to investigate the impact of SO_4^{2-} aerosol particles derived from DMS oxidation in the atmosphere on cloud properties (cloud optical thickness and cloud lifetime). The prognostic treatment of aerosol size distribution, composition, and mixing state in the ECHAM5-HAM model allows for an explicit simulation of cloud droplet and ice crystal number concentrations and therefore the assessment of the indirect aerosol effects. The results presented here can be used to incorporate expected changes in future DMS sea surface concentrations into climate equilibrium experiments in order to estimate the climate sensitivity of the Earth system towards these changes.

The evolving Earth system model of the Max Planck Institute for Meteorology facilitates the treatment of the relationship of the DMS cycle in the ocean and atmosphere to other physical and biogeochemical processes that have not been considered so far. The

coupling of the model system to the vegetation model JSBACH will allow a more realistic treatment of changes in dust emissions and subsequent of the oceanic deposition that are largely driven by changes in land cover. Up to now, only dust deposition changes caused by changes in the wind speed were considered which is probably an estimate on the lower end of the expected changes on multi-century scales. Variations in mineral dust depositions are expected to significantly influence the iron concentration in the sea surface and therefore impact upon the marine primary production and DMS production in the ocean. The coupling to the atmospheric chemistry model MOZART will advance the sulfur chemistry as the oxidant concentrations are calculated explicitly. This becomes especially important in climate change studies as the oxidant concentrations will change significantly with increasing temperatures and increasing anthropogenic emissions. Furthermore, the interactive treatment of the CO_2 cycle in the atmosphere, biosphere, and ocean as already applied in IPCC simulations recently performed at the Max Planck Institute for Meteorology will allow to study the impact of changes in the ocean acidification caused by increasing atmospheric CO_2 concentration on the phytoplankton speciation. It is very likely that these changes will have a strong impact on calcifying organisms, as the ocean becomes undersaturated with respect to calcium carbonate. Changes in species composition caused by an ocean acidification will have a direct impact on the DMS production in the ocean and should therefore be taken into account in future studies.

Bibliography

Albrecht, B. A.: Aerosols, cloud microphysics, and fractional cloudiness, Science, 245, 1227–1230, 1989.

Anderson, T. R., Spall, S. A., Yool, A., Cipollini, P., Challenor, P. G., and Fasham, M. J. R.: Global fields of sea surface dimethylsulfide predicted from chlorophyll, nutrients and light, J. Mar. Systems, 30, 1–20, 2001.

Andreae, M. O. and Crutzen, P. J.: Atmospheric aerosols: Biogeochemical sources and role in atmospheric chemistry, Science, 276, 1052–1058, 1997.

Andreae, M. O., Elbert, W., and Demora, S. J.: Biogenic sulfur emissions and aerosols over the tropical South-Atlantic. 3: Atmospheric dimethylsulfide, aerosols and cloud condensation nuclei, J. Geophys. Res., 100, 11 335–11 356, 1995.

Andreae, M. O., Elbert, W., Cai, Y., Andreae, T. W., and Gras, J.: Non-sea-salt sulfate, methanesulfonate, and nitrate aerosol concentrations and size distributions at Cape Grim, Tasmania, J. Geophys. Res., 104, 21 695–21 706, 1999.

Andres, R. J. and Kasgnoc, A. D.: A time-averaged inventory of subaerial volcanic sulfur emissions, J. Geophys. Res., 103, 25 251–25 261, 1998.

Ångstroem, A.: Atmospheric turbitidy, global illumination and planetary albedo of the Earth, Tellus, 14, 435–450, 1962.

Archer, D. E. and Johnson, K.: A model of the iron cycle in the ocean, Global Biogeochem. Cycles, 14, 269–279, 2000.

Archer, S. D., Smith, G. C., Nightingale, P. D., Widdicombe, C. E., Tarran, G. A., Rees, A. P., and Burkill, P. H.: Dynamics of particulate dimethylsulphoniopropionate during a lagrangian experiment in the northern North Sea, Deep-Sea Res., 49, 2979–2999, 2002.

Aumont, O., Belviso, S., and Monfray, P.: Dimethylsulfoniopropionate (DMSP) and dimethylsulfide (DMS) sea surface distributions simulated from a global three-dimensional ocean carbon cycle model, J. Geophys. Res., 107, doi:10.1029/1999JC000 111, 2002.

Aumont, O., Maier-Reimer, E., Blain, S., and Monfray, P.: An ecosystem model of the global ocean including Fe, Si, P colimitations, Global Biogeochem. Cycles, 17, doi:10.1029/2001GB001 745, 2003.

Ayers, G. P. and Gillett, R. W.: DMS and its oxidation products in the remote marine atmosphere: Implications for climate and atmospheric chemistry, J. Sea Res., 43, 275–286, 2000.

Bates, T. S., Calhoun, J. A., and Quinn, P. K.: Variations in the methanesulfonate to sulfate molar ratio in submicrometer marine aerosol-particles over the South-Pacific ocean, J. Geophys. Res., 97, 9859–9865, 1992.

Bates, T. S., Kiene, R. P., Wolfe, G. V., Matrai, P. A., Chavez, F. P., Buck, K. R., Blomquist, B. W., and Cuhel, R. L.: The cycling of sulfur in surface seawater of the northeast Pacific, J. Geophys. Res., 99, 7835–7843, 1994.

Bates, T. S., Kapustin, V. N., Quinn, P. K., Covert, D. S., Coffman, D. J., Amri, C., Durkee, P. A., Bruyn, W. J. D., and Saltzmann, E. S.: Processes controlling the distribution of aerosol particles in the lower marine boundary layer during the First Aerosol Characterization Experiment (ACE 1), J. Geophys. Res., 92, 2930–2938, 1998.

Baumann, M. E. M., Brandini, F. P., and Staubes, R.: The influence of light and temperature on carbon-specific DMS release by cultures of Phaeocystis-Antarctica and 3 antarctic Diatoms, Marine Chemistry, 45, 129–136, 1994.

Belviso, S., Bopp, L., Moulin, C., Orr, J. C., Anderson, T. R., Aumont, O., Chu, S., Elliott, S., Maltrud, M., and Simó, R.: Comparison of Global Climatological Maps of Sea Surface dimethyl sulfide, Global Biogeochem. Cycles, 18, doi:10.1029/2003GB002 193, 2004a.

Belviso, S., Moulin, C., Bopp, L., and Stefels, J.: Assessment of a global climatology of oceanic dimethylsulfide (DMS) concentrations based on SeaWIFS imagery (1998-2001), Canadian J. of Fisheries and Aquatic Sciences, 61, 804–816, 2004b.

Bengtsson, L., Hodges, K. I., and Roeckner, E.: Storm tracks and climate change, J. Clim., submitted, 2005.

Benkovitz, C. M., Scholtz, M. T., Pacyna, J., Tarrason, L., Dignon, J., Voldner, E. C., Spiro, P. A., Logan, J. A., and Graedel, T. E.: Global gridded inventories of anthropogenic emissions of sulphur and nitrogen, J. Geophys. Res., 101, 29 239–29 253, 1996.

Berglen, T. F., Berntsen, T. K., Isaksen, I. S. A., and Sundet, J. K.: A global model of the coupled sulfur/oxidant chemistry in the troposphere: The sulfur cycle, J. Geophys. Res., 109, doi:10.1029/2003JD003 948, 2004.

Berresheim, H., Eisele, F. L., Tanner, D. J., McInnes, L. M., Ramseybell, D. C., and Covert, D. S.: Atmospheric sulfur chemistry and Cloud Condensation Nuclei (CCN) concentrations over the northeastern Pacific coast, J. Geophys. Res., 98, 12 701–12 711, 1993.

Bond, T. C., Streets, D. G., Yarber, K. F., Nelson, S. M., Woo, J. H., and Klimont, Z.: A technology-based global inventory of black and organic carbon emissions from combustion, J. Geophys. Res., 109, doi:10.1029/2003JD003 697, 2004.

Bopp, L., Monfray, P., Aumont, O., Dufresne, J. L., Treut, H. L., Madec, G., Terray, L., and Orr, J. C.: Potential impact of climate change on marine export production, Global Biogeochem. Cycles, 15, 81–99, 2001.

Bopp, L., Aumont, O., Belviso, S., and Monfray, P.: Potential impact of climate change on marine dimethyl sulfide emissions, Tellus, Ser. B., 55, 11–22, 2003.

Bopp, L., Boucher, O., Aumont, O., Belviso, S., Dufresne, J. L., Pham, M., and Monfray, P.: Will marine dimethylsulfide emissions amplify or alleviate global warming? A model study, Canadian J. of Fisheries and Aquatic Sciences, 61, 826–835, 2004.

Bopp, L., Aumont, O., Cadule, P., Alvain, S., and Gehlen, M.: Response of diatoms distribution to global warming and potential implications: A global model study, Geophys. Res. Lett., p. doi:10.1029/2005GL023653, 2005.

Boucher, O. and Pham, M.: History of sulfate aerosol radiative forcings, Geophys. Res. Lett., 29, doi:10.1029/2001GL014 048, 2002.

Boucher, O., Moulin, C., Belviso, S., Aumont, O., Bopp, L., Cosme, E., von Kuhlmann, R., Lawrence, M. G., Pham, M., Reddy, M. S., Sciare, J., and Venkataraman, C.: DMS atmospheric concentrations and sulphate aerosol indirect radiative forcing: A sensitivity study to the DMS source representation and oxidation, Atmos. Chem. Phys., 3, 49–65, 2003.

Boyd, P. W.: Environmental factors controlling phytoplankton processes in the southern Ocean, J. of Phycology, 38, 844–861, 2002.

Boyd, P. W. and Doney, S. C.: Modelling regional responses by marine pelagic ecosystems to global climate change, Geophys. Res. Lett., 29, 10.1029/2001GL014 130, 2002.

Boyd, P. W., Watson, A. J., Law, C. S., Abraham, E. R., Trull, T., Murdoch, R., Bakker, D. C. E., Bowie, A. R., Buesseler, K. O., Chang, H., Charette, M., Croot, P., Downing, K., Frew, R., Gall, M., Hadfield, M., Hall, J., Harvey, M., Jameson, G., LaRoche, J., Liddicoat, M., Ling, R., Maldonado, M. T., McKay, R. M., Nodder, S., Pickmere, S., Pridmore, R., Rintoul, S., Safi, K., Sutton, P., Strzepek, R., Tanneberger, K., Turner, S., Waite, A., and Zeldis, J.: A mesoscale phytoplankton bloom in the polar Southern Ocean stimulated by iron fertilization, Nature, 407, 695–702, 2000.

Brimblecombe, P. and Shooter, D.: Photooxidation of dimethylsulfide in aqueous-solution, Marine Chemistry, 19, 343–353, 1986.

Campolongo, F., Saltelli, A., Jensen, N. R., Wilson, J., and Hjorth, J.: The role of multiphase chemistry in the oxidation of dimethylsulphide (DMS). A latitude dependent analysis, J. Atmos. Chem., 32, 327–356, 1999.

Capaldo, K. P. and Pandis, S. N.: Dimethylsulfide chemistry in the remote marine atmosphere: Evaluation and sensitivity analysis of available mechanisms, J. Geophys. Res., 102, 23 251–23 267, 1997.

Capaldo, K. P., Kasibhatla, P., and Pandis, S. N.: Is aerosol production within the remote boundary layer sufficient to maintain observed concentrations?, J. Geophys. Res., 104, 3483–3500, 1999.

Charlson, R. J., Lovelock, J. E., Andreae, M. O., and Warren., S. G.: Oceanic phytoplankton, atmospheric sulfur, cloud albedo and climate, Nature, 326, 655–661, 1987.

Chin, M., Rood, R. B., Lin, S., Müller, J. F., and Thompson, A. M.: Atmospheric sulfur cycle simulated in the global model GOCART: Model description and global properties, J. Geophys. Res., 105, 24 671–24 687, 2000.

Chu, S. P., Elliott, S., and Maltrud, M. E.: Global eddy permitting simulations of surface ocean nitrogen, iron, sulfur cycling, Chemosphere, 50, 223–235, 2003.

Clegg, N. A. and Toumi, R.: Non sea-salt sulfate formation in sea salt aerosols, J. Geophys. Res., 103, 31 095–31 102, 1998.

Coale, K., Kenneth, S., Johnson, S., Fitzwater, E., Gordon, R. M., Tanner, S., Chavez, F., Ferioli, L., Sakamoto, C., Rogers, P., Millero, F., Steinberg, P., Nightingale, P., Cooper, D., Cochlan, W., Landry, M., Constantinou, J., Rollwagen, G., Trasvina, A., and Kudela, R.: A massive phytoplankton bloom induced by an ecosystem-scale iron fertilization experiment in the equatorial Pacific Ocean, Nature, 383, 495–501, 1996.

Cofala, J., Amann, M., and Mechler, R.: Scenarios of world anthropogenic emissions of air pollutants and methane up to 2030, Tech. rep., International Institute for Applied Systems Analysis (IIASA), Laxenburg, Austria, available from: *http* : *//www.iiasa.ac.at/rains/global_emiss/global_emiss.html*, 2005.

Cox, P. M., Betts, R. A., Jones, C. D., Spall, S. A., and Totterdell, I. J.: Acceleration of global warming due to carbon-cycle feedbacks in a coupled climate model, Nature, 408, 184–187, 2000.

Cubasch, U., Meehl, G. A., Boer, G. J., Souffer, R. J., Dix, M., Noda, A., Senior, C. A., Raper, S., and Yap, K. S.: Projection of future climate change, in Climate Change 2001: The Scientific basis, Cambridge Uni. Press, pp. 527–582, J.T. Houghton, 2001.

Dacey, J. W. H. and Wakeham, S. G.: Oceanic dimethylsulfide - production during zooplankton grazing on phytoplankton, Science, 233, 1314–1316, 1986.

Denman, K., Hofmann, E., and Marchant, H.: Marine biotic response to global environmental change and feedbacks to climate, in Climate Change, pp. 483–516, J.T. Houghton, Cambridge Uni. Press, New York, 1996.

Feichter, J., Kjellstrom, E., Rodhe, H., Dentener, F., Lelieveld, J., and Roelofs, G. J.: Simulation of the tropospheric sulfur cycle in a global climate model, Atmos. Environ., 30, 1693–1707, 1996.

Fouquart, Y. and Bonnel, B.: Computations of solar heating of the Earth's atmosphere: A new parameterization. A prognostic parameterization for the subgrid-scale variability of water vapor and clouds in large-scale models and its use to diagnose cloud cover, Beitr. Phys. Atmos., 59, 35–62, 1980.

Fung, I. Y., Meyn, S. K., Tegen, I., Doney, S. C., John, J., and Bishop, J.: Iron supply and demand in the upper ocean, Global Biogeochem. Cycles, 14, 697–700, 2000.

Gabric, A., Murray, N., Stone, L., and Kohl, M.: Modeling the production of dimethylsulfide during a phytoplankton bloom, J. Geophys. Res., 98, 22 805–22 816, 1993.

Gabric, A. J., Gregg, W., Najjar, R., Erickson, D., and Matrai, P.: Modeling the biogeochemical cycle of dimethylsulfide in the upper ocean: A review., Chemosphere, 3, 377–392, 2001.

Gabric, A. J., Simó, R., Cropp, R. A., Hirst, A. C., and Dachs, J.: Modeling estimates of the global emission of dimethylsulfide under enhanced greenhouse conditions, Global Biogeochem. Cycles, 18, 10.1029/2003GB002 183, 2004.

Ganzeveld, L., Lelieveld, J., and Roelofs, G.: A dry deposition parameterization for sulfur oxides in a chemistry and general circulation model, J. Geophys. Res., 103, 5679–5694, 1998.

Gauss, M., Myhre, G., Pitari, G., Prather, M. J., Isaksen, I. S. A., Berntsen, T. K., Brasseur, G. P., Dentener, F. J., Derwent, R. G., Hauglustaine, D. A., Horowitz, L. W., Jacob, D. J., Johnson, M., Law, K. S., Mickley, L. J., Müller, J. F., Plantevin, P., Pyle, J. A., Rogers, H. L., Stevenson, D. S., Sundet, J. K., van Weele, M., and Wild, O.: Radiative forcing in the 21st century due to ozone changes in the troposphere and the lower stratosphere, J. Geophys. Res., 108, 2003.

Gent, P. R., Willebrand, J., McDougall, T. J., and McWilliams, J. C.: Parameterizing eddy-induced tracer transports in ocean circulation models, J. Phys. Oceanogr., 25, 463–474, 1995.

Gondwe, M., Krol, M., Gieskes, W., Klaassen, W., and de Baar, H.: The contribution of ocean-leaving DMS to the global atmospheric burdens of DMS, MSA, SO2, and nss SO4 =, Global Biogeochem. Cycles, 17, doi:10.1029/2002GB001 937, 2003.

Guenther, A., Hewitt, C. N., Erickson, D., Fall, R., Geron, C., Graedel, T., P. Harley, P., Klinger, L., Lerdau, M., McKay, W. A., Pierce, T., Scholes, B., Steinbrecher, R., Tallamraju, R., Taylor, J., and Zimmerman, P.: A global-model of natural volatile organic-compound emissions, J. Geophys. Res., 100, 8873–8892, 1995.

Halmer, M. M., Schmincke, H., and Graf, H. F.: The annual volcanic gas input into the atmosphere, in particular into the stratosphere: A global data set for the past 100 years, J. of Volcanology and Geothermal Res., 115, 511–528, 2002.

Harder, D. P., Worrest, R. C., Kumar, H. D., and Smith, B. C.: Effects of increased solar ultraviolet-radiation on aquatic ecosystems, AMBIO, 24, 174–180, 1995.

Hibler, W. D.: Dynamic thermodynamic sea ice model, J. Phys. Oceanogr., 9, 815–846, 1979.

Horowitz, L. W., Walters, S., Mauzerall, D. L., Emmons, L. K., Rasch, P. J., Granier, C., Tie, X. X., Lamarque, J. F., Schultz, M. G., Tyndall, G. S., Orlando, J. J., and Brasseur, G. P.: A global simulation of tropospheric ozone and related tracers: Description and evaluation of MOZART, Version 2, J. Geophys. Res., 108, doi:10.1029/2002JD002 853, 2003.

IPCC: Climate Change 2001: The Scientific basis, Cambridge Uni. Press, J.T. Houghton, 881 pp., 2001.

Johnson, C. E., Collins, W. J., Stevenson, D. S., and Derwent, R. G.: Relative roles of climate and emissions changes on future tropospheric oxidant concentrations, J. Geophys. Res., 104, 18 631–18 645, 1999.

Jones, A., Roberts., D. L., Woodage, M. J., and Johnson, C. E.: Indirect sulphate aerosol forcing in a climate model with an interactive sulphur cycle, J. Geophys. Res., 106, 20 293–20 310, 2001.

Jungclaus, J. et al.: The ocean response to increasing greenhouse gas emissions, J. Geophys. Res., in prep., 2005.

Kalnay, E., Kanamitsu, M., Kistler, R., Collins, W., Deaven, D., Gandin, L., Iredell, M., Saha, S., White, G., Woollen, J., Zhu, Y., Chelliah, M., Ebisuzaki, W., Higgins, W., Janowiak, J., Mo, K. C., Ropelewski, C., Wang, J., Leetmaa, A., Reynolds, R., Jenne, R., and Joseph, D.: The NCEP/NCAR 40-Year Reanalysis Project, Bulletin of the Meteorological Society, 77, 437–471, 1996.

Keller, M. D., Bellows, W. K., and Guillard, R. R. L.: Dimethyl sulfide production in marine phytoplankton, in Biogenic sulfur in the enviroment, edited by E. Saltzman and W. Cooper, ACS-Symposium series, pp. 167–181, New Orleans, Louisiana, 1989.

Kettle, A. J. and Andreae, M. O.: Flux of dimethylsulfide from the oceans: A comparison of updated data sets and flux models, J. Geophys. Res., 105, 26 793–26 808, 2000.

Kettle, A. J., Andreae, M. O., Amouroux, D., Andreae, T. W., Bates, T. S., Berresheim, H., Bingemer, H., Boniforti, R., Curran, M. A. J., Ditullio, G. R., Helas, G., Jones, G. B., Keller, M. D., Kiene, R. P., Leck, C., Levasseur, M., Malin, G., Maspero, M., Matrai, P., McTaggart, A. R., Mihalopoulos, N., Nguyen, B. C., Novo, A., Putaud, J. P., Rapsomanikis, S., Roberts, G., Schebeske, G., Sharma, S., Simó, R., Staubes, R., Turner, S., and Uher, G.: A global database of sea surface dimethylsulfide (DMS) measurements and a procedure to predict sea surface DMS as a function of latitude, longitude, and month, Global Biogeochem. Cycles, 13, 399–444, 1999.

Khairoutdinov, M. and Kogan, Y.: A new cloud physics parameterization in a large-eddy simulation model of marine stratocumulus, Monthly Weather Review, 128, 229–243, 2000.

Kieber, D. J., Jiao, J. F., Kiene, R. P., and Bates, T. S.: Impact of dimethylsulfide photochemistry on methyl sulfur cycling in the equatorial Pacific Ocean, J. Geophys. Res., 101, 3715–3722, 1996.

Kiehl, J. T., Schneider, T. L., Portmann, R. W., and Solomon, S.: Climate forcing due to tropospheric and stratospheric ozone, J. Geophys. Res., 104, 31 239–31 254, 1999.

Kiene, R. P.: Production of methanethiol from dimethylsulfonioproponiate in marine surface waters, Mar. Chem., 54, 69–83, 1996.

Kiene, R. P. and Bates, T. S.: Biological removal of dimethyl sulfide from sea-water, Nature, 345, 702–705, 1990.

Kiene, R. P., Linn, L. J., and Bruton, J. A.: New and important roles for DMSP in marine microbial communities, J. of Sea Res., 43, 209–224, 2000.

Kirst, G. O., Thiel, C., Wolff, H., Nothnagel, J., Wanzek, M., and Ulmke, R.: Dimethylsulfoniopropionate (DMSP) in ice-algae and its possible biological role, Marine Chemistry, 35, 381–388, 1991.

Kloster, S., Feichter, J., Maier-Reimer, E., Six, K. D., Stier, P., and Wetzel, P.: DMS cycle in the marine ocean-atmosphere system - a global model study, Biogeosciences, 3, 29–51, 2006.

Koch, D., Jacob, D., Tegen, I., Rind, D., and Chin, M.: Tropospheric sulfur simulation and sulfate direct radiative forcing in the Goddard Institute for Space Studies General Circulation Model, J. Geophys. Res., 104, 23 799–23 822, 1999.

Kwint, R. L. J. and Kramer, K. J. M.: Dimethylsulfide production by plankton communities, Marine Ecology-Progress Series, 121, 227–237, 1995.

Lin, H. and Leaitch, R.: Development of an in-cloud aerosol activation parameterization for climate modelling., in WMO workshop on measurements of cloud properties for forcast of weather, edited by W. M. Organization, pp. 328–335, Geneva, 1997.

Lin, S. J. and Rood, R. B.: Multidimensional flux-form semi-lagrangian transport schemes, Mon. Weather Rev., 124, 2046–2070, 1996.

Liss, P. S. and Merlivat, L.: Air-Sea exchange rates: Introduction and synthesis, in The role of air-sea exchange in geochemical cycling, edited by P. Buat-Menard, pp. 113–127, NATO ASI Series Series C: Mathematical and physical science, 1986.

Liss, P. S., Hatton, A. D., Malin, G., Nightingale, P. D., and Turner, S. M.: Marine sulphur emissions, Philosophical Transactions: Biological Science, 352, 159–168, 1997.

Lohmann, U. and Roeckner, E.: Design and performance of a new cloud microphysics scheme developed for the ECHAM general circulation model, Clim. Dynam., 12, 557–572, 1996.

Lohmann, U., Feichter, J., Chuang, C. C., and Penner, J. E.: Prediction of the number of cloud droplets in the ECHAM GCM, J. Geophys. Res., 104, 24 557–24 563, 1999.

Lovelock, J. E., Maggs, R. J., and Rasmusse, R. A.: Atmospheric dimethyl sulfide and natural sulfur cycle, Nature, 237, 452–453, 1972.

Maier-Reimer, E.: Geochemical cycles in an ocean circulation model: Preindustrial tracer distributions, Global Biogeochem. Cycles, 7, 645–677, 1993.

Maier-Reimer, E., Kriest, I., Segschneider, J., and Wetzel, P.: The Hamburg Ocean Carbon Cycle Model HAMOCC5.1 - Technical Description Release 1.1, Report on Earth System Science, 14, Max Planck Institute for Meteorology, Hamburg, Germany, available from http://www.mpimet.mpg.de., 2005.

Malin, G., Wilson, W. H., Bratbak, G., Liss, P. S., and Mann, N. H.: Elevated production of dimethylsulfide resulting from viral infection of cultures of Phaeocystis Pouchetii, Limnol. Oceanogr., 43, 1389–1393, 1998.

Manabe, S.: Study of global warming by GFDL climate models, AMBIO, 27, 182–186, 1998.

Marsland, S. J., Haak, H., Jungclaus, J. H., Latif, M., and Roske, F.: The Max-Planck-Institute global ocean/sea ice model with orthogonal curvilinear coordinates, Ocean Modelling, 5, 91–127, 2003.

McGillis, W. R., Dacey, J. W. H., Frew, N. M., Bock, E. J., and Nelson, R. K.: Water-air flux of dimethylsulfide, J. Geophys. Res., 105, 1187–1193, 2000.

Morcrette, J. J., Clough, S. A., Mlawer, E. J., and Iacono, M. J.: Impact of a validated radiative transfer scheme, RRTM, on the ECMWF model climate and 10-day forecasts. Technical Memorandum 252, ECMWF, Reading, UK., 1998.

Nguyen, B. C., Mihalopoulos, N., and Belviso, S.: Seasonal-variation of atmospheric dimethylsulfide at Amsterdam Island in the southern Indian-Ocean, J. Atmos. Chem., 11, 123–141, 1990.

Nightingale, P. D., Malin, G., Law, C. S., Watson, A. J., Liss, P. S., Liddicoat, M. I., Boutin, J., and Upstill-Goddard, R. C.: In situ evaluation of air-sea gas exchange parameterizations using novel conservative and volatile tracers, Global Biogeochem. Cycles, 14, 373–387, 2000.

Nordeng, T. E.: Extended versions of the convective parameterization scheme at ECMWF and their impact on the mean and transient activity of the model in the tropics. Technical Memorandum 206, ECMWF, Reading, UK., 1994.

Orr, J., Fabry, V., Aumont, O., Bopp, L., Doney, S., Feely, R., Gnanadesikan, A., Gruber, N., Ishida, A., Joos, F., Key, R., Lindsay, K., Maier-Reimer, M.-E., Matear, R., Monfray, P., Mouchet, A., Najjar, R., Plattner, G., Rodgers, K., Sabine, C., Sarmiento, J., Schlitzer, R., Slater, R., Totterdell, I., Weirig, M., Yamanaka, Y., and Yool, A.: Anthropogenic ocean acidification over the twenty-first century and its impact on calcifying organisms, Nature, 437, 681–686, 2005.

Oschlies, A.: Model-derived estimates of new production: New results point towards lower values, Deep-Sea Res., Part B, pp. 2173–2197, 2002.

Penner, J. E., Andreae, M., Annegram, H., Barrie, L., Feichter, J., Hegg, D., Jayaraman, A., Leaitch, R., Murphy, D., Nganga, J., and Pitari, G.: Aerosols, their direct and indirect effects, in Climate Change 2001: The Scientific basis, Cambridge Uni. Press, pp. 289–348, J. T. Houghton, 2001.

Pham, M., Müller, J. F., Brasseur, G. P., Granier, C., and Megie, G.: A three-dimensional study of the tropospheric sulfur cycle, J. Geophys. Res., 100, 26 061–26 092, 1995.

Pham, M., Boucher, O., and Hauglustaine, D.: Changes in atmospheric sulfur burdens and concentrations and resulting radiative forcings under IPCCSRES emission scenarios for 1990-2100, J. Geophys. Res., 110, doi:10.1029/2004JD005 125, 2005.

Putaud, J. P., Mihalopoulos, N., Nguyen, B. C., Campin, J. M., and Belviso, S.: Seasonal-variations of atmospheric sulfur-dioxide and dimethylsulfide concentrations at Amsterdam Island in the southern Indian-Ocean, J. Atmos. Chem., 15, 117–131, 1992.

Putaud, J. P., Belviso, S., Nguyen, B. C., and Mihalopoulos, N.: Dimethylsulfide, aerosols, and condensation nuclei over the tropical northeastern Atlantic-Ocean, J. Geophys. Res., 98, 14 863–14 871, 1993.

Quere, C. L., Aumont, O., Monfray, P., and Orr, J.: Propagation of climatic events on ocean stratification, marine biology, and CO_2: Case studies over the 1979-1999 period, J. Geophys. Res., 108, 2003.

Raes, F.: Entrainment of free tropospheric aerosols as a regulating mechanism for cloud condensation nuclei in the remote marine boundary layer, J. Geophys. Res., 100, 2893–2903, 1995.

Roeckner, E., Baeuml, G., Bonventura, L., Brokopf, R., Esch, M., Giorgetta, M., Hagemann, S., Kirchner, I., Kornblueh, L., Manizini, E., Rhodin, A., Schlese, U., Schulzweida, U., and Tompkins, A.: The atmospheric general circulation model ECHAM5. Part I: Model description, Report 349, Max Planck Institute for Meteorology, Hamburg, Germany, available from: http://www.mpimet.mpg.de, 2003.

Roeckner, E., Stier, P., Feichter, J., Kloster, S., Esch, M., and Fischer-Bruns, I.: Impact of carbonaceous aerosol forcing on regional climate change, Clim. Dynam., submitted, 2005.

Rotstayn, L. D. and Lohmann, U.: Simulation of the tropospheric sulfur cycle in a global model with a physically based cloud scheme, J. Geophys. Res., 107, doi:10.1029/2002JD002 128, 2002.

Saltzman, E. S., King, D. B., Holmen, K., and Leck, C.: Experimental-determination of the diffusion-coefficient of dimethylsulfide in water, J. Geophys. Res., 98, 16 481–16 486, 1993.

Sarmiento, J. L., Dunne, J., Gnanadesikan, A., Key, R. M., Matsumoto, K., and Slater, R.: A new estimate of the $CaCO_3$ to organic carbon export ratio, Global Biogeochemical Cycles, 16, doi:10.1029/2002GB001 919, 2002.

Sarmiento, J. L., Slater, R., Barbe, R., Bopp, L., Doney, S., Hirst, A., Kleypas, J., Matear, R., Mikolajewicz, W., Monfray, P., Soldatov, V., Spall, S. A., and Stouffer, R.: Response of ocean ecosystems to climate warming, Global Biogeochem. Cycles, 18, 2004.

Sato, M., Hansen, J. E., Mccormick, M. P., and Pollack, J. B.: Stratospheric aerosol optical depths, 1850-1990, J. Geophys. Res., 98, 22 987–22 994, 1993.

Sayin, H. and McKee, M. L.: Computational study of the reactions between XO (X = Cl, Br, I) and dimethyl sulfide, J. Phys. Chem., 108, 7613–7620, 2004.

Schulz, M., de Leeuw, G., and Balkanski, Y.: Sea salt aerosol source functions and emissions, in Emission of atmospheric trace compounds, edited by C. Granier, P. Artaxo, and C. Reeves, 2004.

Sciare, J., Mihalopoulos, N., and Dentener, F. J.: Interannual variability of atmospheric dimethylsulfide in the Southern Indian Ocean, J. Geophys. Res., 105, 26 369–26 377, 2000.

Seinfeld, J. H. and Pandis, S. N.: Atmospheric chemistry and physics: From air pollution to climate change, Willey Interscience, 1998.

Shaw, G. E., Benner, R. L., Cantrell, W., and Clark, A. D.: On the regulation of climate: A sulphate particle feedback loop involving deep convection, Climatic change, 39, 23–33, 1988.

Shooter, D. and Brimblecombe, P.: Dimethylsulfide oxidation in the ocean, Deep-Sea Res., Part A, 36, 577–585, 1989.

Simó, R. and Dachs, J.: Global ocean emission of dimethylsulfide predicted from biogeophysical data, Global Biogeochem. Cycles, 16, doi:10.1029/2001GB001 829, 2002.

Simó, R. and Pedrós-Alió, C.: Role of vertical mixing in controlling the oceanic production of dimethyl sulphide, Nature, 402, 396–398, 1999.

Six, K. D. and Maier-Reimer, E.: Effects of plankton dynamics on seasonal carbon fluxes in a ocean general circulation model, Global Biogeochem. Cycles, 10, 559–583, 1996.

Solanki, S. and Krivova, N.: Can solar variability explain global warming since 1970?, J. Geophys. Res., 108, 10.1029/2002JA009 753, 2003.

Spiro, P., Jacob, D., and Logan, J.: Global inventory of sulfur emissions with 1°x 1° resolution, J. Geophys. Res., 97, 6023–6036, 1992.

Stefels, J.: Physiological aspects of the production and conversion of DMSP in marine algae and higher plants, J. Sea Res., 43, 183–197, 2000.

Steinke, M., Malin, G., Archer, S. D., and Burkill, P. H.: Vertical and temporal variability of DMSP lyase activity in a coccolithophorid bloom in the northern North Sea, Deep-Sea Res., Part B, 49, 3001–3016, 2002.

Stier, P., Feichter, J., Kloster, S., Vignati, E., and Wilson, J.: Emission-induced nonlinearities in the global aerosol system - results from the ECHAM5-HAM aerosol-climate model, J. Clim., accepted, 2004.

Stier, P., Feichter, J., Kinne, S., Kloster, S., Vignati, E., Wilson, J., Ganzeveld, L., Tegen, I., Werner, M., Balkanski, Y., Schulz, M., Boucher, O., Minikin, A., and Petzold, A.: The aerosol-climate model ECHAM5-HAM, Atmos. Chem. Phys., 5, 1125–1156, 2005a.

Stier, P., Feichter, J., Roeckner, E., Kloster, S., and Esch, M.: The evolution of the global aerosol system in a transient climate simulation from 1860 to 2100, Atmos. Chem. Phys. Dissc., 5, 12 775–12 814, 2005b.

Sunda, W., Kieber, D. J., Kiene, R. P., and Huntsman, S.: An antioxidant function for DMSP and DMS in marine algae, Nature, 418, 317–320, 2002.

Sweby, P. K.: High-resolution schemes using flux limiters for hyperbolic conservation-laws, Siam Journal On Numerical Analysis, 21, 995–1011, 1984.

Tegen, I., Harrison, S. P., Kohfeld, K., Prentice, I. C., Coe, M., and Heimann, M.: Impact of vegetation and preferential source areas on global dust aerosol: Results from a model study, J. Geophys. Res., 107, 10.1029/2001JD000 963, 2002.

Tegen, I., Werner, M., Harrison, S. P., and Kohfeld, K. E.: Relative importance of climate and land use in determining present and future global soil dust emission, Geophys. Res. Lett., 31, doi:10.1029/2003GL019 216, 2004.

Tiedtke, M.: A comprehensive mass flux scheme for cumulus parameterization in large-scale models, Mon. Weather Rev., 117, 1779–1800, 1989.

Tompkins, A. M.: A prognostic parameterization for the subgrid-scale variability of water vapor and clouds in large-scale models and its use to diagnose cloud cover, J. Atmos. Sci., 59, 1917–1942, 2002.

Turner, S. M., Nightingale, P., Spokes, L., Liddicoat, M. I., and Liss, P. S.: Increased dimethyl sulphide concentrations in sea water from in situ iron enrichment, Nature, 383, 513–517, 1996.

Twomey, S.: Pollution and planetary albedo, Atmos. Environ., 8, 1251–1256, 1974.

Twomey, S.: The influence of pollution on the shortwave albedo of clouds, J. Atmos. Sci., 34, 1249–1152, 1977.

Vairavamurthy, A., Andreae, M. O., and Iverson, R. L.: Biosynthesis of dimethylsulfide and dimethylpropiothetin by Hymenomonas-Carterae in relation to sulfur source and salinity variations, Limnol. Oceanogr., 30, 59–70, 1985.

Valcke, S., Caubel, A., Declat, D., and Terray, L.: OASIS ocean atmosphere sea ice soil users's guide, Technical Report, TR/CMGC/03/69, CERFACS, Toulouse, France, 2003.

van der Werf, G. R., Randerson, J. T., Collatz, G. J., and Giglio, L.: Carbon emissions from fires in tropical and subtropical ecosystems, Global Change Biology, 9, 547–562, 2003.

Vézina, A. F.: Ecosystem modelling of the cycling of marine dimethylsulfide: A review of current approaches and of the potential for extrapolation on global scales, Canadian J. of Fisheries and Aquatic Sciences, 61, 845–856, 2004.

Vignati, E., Wilson, J., and Stier, P.: M7: An efficient size-resolved aerosol microphysics module for large-scale aerosol transport models, J. Geophys. Res., 109, 2004.

von Glasow, R. and Crutzen, P. J.: Model study of multiphase DMS oxidation with a focus on halogens, Atmos. Chem. Phys., 4, 589–608, 2004.

Wanninkhof, R.: Relationship between wind-speed and gas-exchange over the ocean, J. Geophys. Res., 97, 7373–7382, 1992.

Wanninkhof, R. and McGillis, W. R.: A cubic relationship between air-sea CO_2 exchange and wind speed, Geophys. Res. Lett., 26, 1889–1892, 1999.

Wetzel, P.: Interannual and decadal variability in the air-sea exchange of CO_2 - A model study, Report on Earth System Science, 7, Max Planck Institute for Meteorology, Hamburg, Germany, available from: http://www.mpimet.mpg.de, 2004.

Wetzel, P., Winguth, A., and Maier-Reimer, E.: Sea-To-Air CO_2 flux from 1948 to 2003: A model study, Global Biogeochem. Cycles, 19, 10.1029/2004GB002339, 2005.

Wilson, J., Cuvlier, C., and Raes, F.: A modelling study of global mixed aerosol field, J. Geophys. Res., 106, 34 081–34 108, 2001.

Yin, F. D., Grosjean, D., and Seinfeld, J. H.: Photooxidation of dimethyl sulfide and dimethyl disulfide. 1: Mechanism development, J. Atmos. Chem., 11, 309–364, 1990.

Yoch, D. C., Ansede, J. H., and Rabinowitz, K. S.: Evidence for intracellular and extracellular dimethylsulfonioproponiate (DMSP) lyases and DMSP uptake site in two species of marine bacteria, Appl. Environ. Microbiol., 63, 3182–3188, 1997.

Yoon, Y. J. and Brimblecombe, P.: Modelling the contribution of sea salt and dimethyl sulfide derived aerosol to marine CCN, Atmos. Chem. Phys., 2, 17–30, 2002.

Zemmelink, H. J., Gieskes, W. W. C., Klaassen, W., de Groot, H. W., de Baar, H. J. W., Dacey, J. W. H., Hintsa, E. J., and McGillis, W. R.: Simultaneous use of relaxed eddy accumulation and gradient flux techniques for the measurement of sea-to-air exchange of dimethyl sulphide, Atmos. Environ., 36, 5709–5717, 2002.

Acknowledgements

I would like to thank Dr. Johann Feichter and Prof. Dr. Hartmut Graßl for their supervision and steady support of my work.

Many thanks to Dr. Ernst Maier-Reimer and Dr. Katharina Six. Their profound knowledge about marine biology was always a great help.

The Max Planck Institute for Meteorology, in particular Prof. Dr. Guy Brasseur, is thanked for making it possible to write my thesis in the Atmosphere in the Earth System department. Working there was always fun.

I would like to acknowledge the support of the German DEKLIM project funded by the German Ministry for Education and Research (BMBF) and the support of the International Max Planck Research School for Earth System Modelling.

Furthermore, I would like to thank my colleagues in the Atmospheric Aerosol and Chemistry group. In particular Philip Stier is thanked for his help and many fruitful discussions and Dorothea Banse for bringing a lot of commas into my work. Many thanks to Rene Hommel and Patrick Wetzel for the encouragement during the last weeks of my Ph.D. work. I also thank Stephanie Legutke for the help with the OASIS coupler and Irene Fischer-Bruns for the significance test.

Special thanks to my family and to Focko for their love, patience, and encouragement.

MPI-Examensarbeit-Referenz:
Examensarbeit Nr. 1-82 bei Bedarf bitte anfragen:
MPI für Meteorologie, Abtlg.: PR, Bundesstr. 53, 20146 Hamburg

MPI-Report-Referenz:
MPI-Report Nr. 1-351 bei Bedarf bitte anfragen:
MPI für Meteorologie, Abtlg.: PR, Bundesstr. 53, 20146 Hamburg

---

Beginn einer neuen Veröffentlichungsreihe des MPIM, welche die vorherigen Reihen "Reports" und "Examensarbeiten" weiterführt:

„Berichte zur Erdsystemforschung" , „*Reports on Earth System Science*", ISSN 1614-1199
Sie enthält wissenschaftliche und technische Beiträge, inklusive Dissertationen.

Berichte zur Erdsystemforschung Nr.1 Juli 2004	**Simulation of Low-Frequency Climate Variability in the North Atlantic Ocean and the Arctic** Helmuth Haak
Berichte zur Erdsystemforschung Nr.2 Juli 2004	**Satellitenfernerkundung des Emissionsvermögens von Landoberflächen im Mikrowellenbereich** Claudia Wunram
Berichte zur Erdsystemforschung Nr.3 Juli 2004	**A Multi-Actor Dynamic Integrated Assessment Model (MADIAM)** Michael Weber
Berichte zur Erdsystemforschung Nr.4 November 2004	**The Impact of International Greenhouse Gas Emissions Reduction on Indonesia** Armi Susandi
Berichte zur Erdsystemforschung Nr.5 Januar 2005	**Proceedings of the first HyCARE meeting, Hamburg, 16-17 December 2004** Edited by Martin G. Schultz
Berichte zur Erdsystemforschung Nr.6 Januar 2005	**Mechanisms and Predictability of North Atlantic - European Climate** Holger Pohlmann
Berichte zur Erdsystemforschung Nr.7 November 2004	**Interannual and Decadal Variability in the Air-Sea Exchange of CO2 - a Model Study** Patrick Wetzel
Berichte zur Erdsystemforschung Nr.8 Dezember 2004	**Interannual Climate Variability in the Tropical Indian Ocean: A Study with a Hierarchy of Coupled General Circulation Models** Astrid Baquero Bernal
Berichte zur Erdsystemforschung Nr9 Februar 2005	**Towards the Assessment of the Aerosol Radiative Effects, A Global Modelling Approach** Philip Stier
Berichte zur Erdsystemforschung Nr.10 März 2005	**Validation of the hydrological cycle of ERA40** Stefan Hagemann, Klaus Arpe and Lennart Bengtsson
Berichte zur Erdsystemforschung Nr.11 Februar 2005	**Tropical Pacific/Atlantic Climate Variability and the Subtropical-Tropical Cells** Katja Lohmann

MPI-Examensarbeit-Referenz:
Examensarbeit Nr. 1-82 bei Bedarf bitte anfragen:
MPI für Meteorologie, Abtlg.: PR, Bundesstr. 53, 20146 Hamburg

MPI-Report-Referenz:
MPI-Report Nr. 1-351 bei Bedarf bitte anfragen:
MPI für Meteorologie, Abtlg.: PR, Bundesstr. 53, 20146 Hamburg

Berichte zur Erdsystemforschung Nr.12 Juli 2005	**Sea Ice Export through Fram Strait: Variability and Interactions with Climate**- Torben Königk
Berichte zur Erdsystemforschung Nr.13 August 2005	**Global oceanic heat and fresh water forcing datasets based on ERA-40 and ERA-15** Frank Röske
Berichte zur Erdsystemforschung Nr.14 August 2005	**The** HAM**burg** O**cean** C**arbon** C**ycle Model HAMOCC5.1 - Technical Description Release 1.1** Ernst Maier-Reimer, Iris Kriest, Joachim Segschneider, Patrick Wetzel
Berichte zur Erdsystemforschung Nr.15 Juli 2005	**Long-range Atmospheric Transport and Total Environmental Fate of Persistent Organic Pollutants - A Study using a General Circulation Model** Semeena Valiyaveetil Shamsudheen
Berichte zur Erdsystemforschung Nr.16 Oktober 2005	**Aerosol Indirect Effect in the Thermal Spectral Range as Seen from Satellites** Abhay Devasthale
Berichte zur Erdsystemforschung Nr.17 Dezember 2005	**Interactions between Climate and Land Cover Changes** Xuefeng Cui
Berichte zur Erdsystemforschung Nr.18 Januar 2006	**Rauchpartikel in der Atmosphäre: Modellstudien am Beispiel indonesischer Brände** Bärbel Langmann


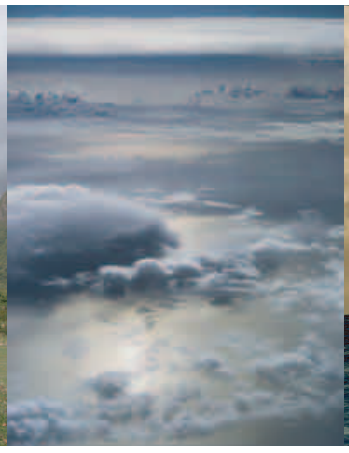


ISSN 1614-1199